

**Tandem Mass Spectrometric Analysis of Bacterial Lipid
A of *Aeromonas Salmonicida* (SJ-112)**

by:

Faisal Alarabi

**A thesis submitted to the School of Graduate Studies in partial
fulfillment of the requirements for the degree of Master of Science.**

Department of Chemistry

Memorial University of Newfoundland and Labrador

June 1, 2015

St. John's

Newfoundland and Labrador, Canada

Abstract

This study will present an interpretation of the mass spectrometry gas-phase fragmentation patterns of the extracted Lipid A that is obtained from the native LPS extracts isolated from the marine Gram-negative bacteria *Aeromonas Salmonicida* (SJ-112). It is known that the surface antigen lipopolysaccharides (LPS) SJ-112 infect various fish species (Atlantic salmon and cod) which are cultivated in aquaculture ventures. The exact molecular structure of the Lipid A has not yet been precisely established.

This thesis will present the mass spectrometric fingerprint identification and structural elucidation of the Lipid A from *A. Salmonicida*, which are carried out by using mass spectrometry techniques namely, electrospray ionization tandem mass spectrometry (ESI-MS/MS) using an FT-ICR instrument and matrix assisted laser desorption ionization tandem mass spectrometry (MALDI-MS/MS) using a TOF/TOF instrument.

The concomitant uses of high-energy (CID-MS/MS) and low-energy collision induced dissociation (CID-MS/MS) analysis were also used to elucidate the MS/MS fingerprints of this complex biomolecule and can be effectively used for any quantitative or qualitative studies.

Acknowledgments

I would like to express my special appreciation and gratitude to my supervisor Dr. Joseph Banoub for his tremendous efforts and insightful guidance. He has been always there when I needed a help or advice. He was always enthusiastic and helpful, which has greatly helped me to complete this thesis and its contents. I would like to extend my appreciation to my committee members, Dr. Paris Georghiou and Dr. Travis D. Fridgen for serving as my committee members and for their great comments during the preparation of the this thesis.

I would like to thank all my family members for supporting me and being the biggest part of this success. Special thanks and sincere appreciation to my parents for being patient waiting for me while I am abroad. They are the only reason behind everything good I have ever made.

Finally, huge thanks to the Ministry of Higher Education in the Kingdom of Saudi Arabia for the scholarship I have been granted.

Table of Contents

Abstract	i
Acknowledgements	ii
List of Figures	vi
Chapter 1 : Introduction	1
1.1 History of mass spectrometry.....	1
1.2 Mass spectrometry.....	3
1.3 Ionization techniques.....	5
1.3.1 Hard or direct ionization technique	5
1.3.2 Soft or indirect ionization techniques	6
13.2.1 MALDI	7
1.3.2.2 MALDI and Proteomics.....	9
1.3.2.3 Electrospray ionization	11
1.3.2.4 Quadrupole Analyzer	14
1.3.2.5 FT-ICR.....	15
1.3.2.6 Tandem mass spectrometry.....	19
1.3.2.7 FT-ICR-MS.....	22
1.3.2.8 Hybrid quadrupole orthogonal time-of-flight mass spectrometry (Q-ToF):	24
1.3.2.9 Time of flight (TOF) analyzer	26
1.4 Scope of the thesis.....	30
Chapter 2 : Bacterial membranes and lipopolysaccharides	31
2.1 Background:	31
2.2 Gram positive bacteria:	31
2.3 Gram negative bacteria:	33
2.4 Lipopolysaccharides:.....	34

2.4.1 The O-specific chain.....	35
2.4.2 The core oligosaccharide:.....	36
2.4.3 Lipid A:.....	37
2.5 Mass spectrometric analysis of carbohydrates:.....	39
Chapter 3 : Materials and Methods.....	41
3.1 Lipopolysaccharides:.....	41
3.1.1 Bacterial culture:.....	41
3.1.2 Lipopolysaccharide purification:.....	41
3.1.3 Lipopolysaccharide hydrolysis:.....	43
3.2 Mass spectrometric analysis of lipid A:.....	43
3.2.1 Electrospray quadrupole fourier transform ion cyclotron mass spectrometry	43
3.2.2 Electrospray quadrupole-hexapole-quadrupole mass spectrometry:.....	44
3.2.3 Matrix-assisted laser/desorption ionization time-of-flight mass spectrometry (MALDI-TOF-MS):.....	44
3.2.4 The MALDI-TOF/TOF-MS spectrometer of partial de-acylation of ester-linked to the acyl group of lipid A:.....	46
Chapter 4 : Lipid A Analysis Using FTICR-MS and Low Energy SORI-CID-FTICR-MS ⁿ	47
4.1 Background:.....	47
4.1.1 Biosynthesis of Lipid A:.....	50
4.1.2 The enzymatic pathway modification of <i>E. coli</i> and <i>Salmonella</i> Lipid A biosynthesis <i>E. coli</i> and <i>Salmonell</i> :.....	56
4.2 ESI-FTICR-MS Analysis:.....	58
4.3 CID- FT-ICR-MS/MS analysis of the heterogeneous mixture of lipid As.....	67
4.3.1 MS/MS of the precursor ions at <i>m/z</i> 1768.8732 isolated from LipA1.....	68
4.3.2 MS/MS of the precursor ions at <i>m/z</i> 1744.2209 isolated from LipA2:.....	72
4.3.3 MS/MS of the precursor ions at <i>m/z</i> 1688.2302 isolated from LipA3:.....	75
4.3.4 MS/MS of the precursor ion at <i>m/z</i> 1586.0259 isolated from LipA4 :.....	78
4.3.5 MS/MS of the precursor ion at <i>m/z</i> 1506.0586 isolated from LipA5:.....	81
4.3.6 MS/MS of the precursor ion at <i>m/z</i> 1359.8266 isolated from LipA6.....	84

4.3.7 MS/MS of the abundant precursor ion at m/z 1279.867 isolated from LipA7	87
4.3.8 CID analysis of the $[C-H]^-$ and $[Y-H]^-$ ions	90
4.3.9 Summary:	94
Chapter 5 : Analysis of Lipid A Using MALDI-TOF-MS and High Energy CID-TOF/TOF-MS/MS	95
5.1 MALDI-TOF-MS analysis of the heterogeneous mixture of lipid As	95
5.2 MALDI-CID-TOF/TOF-MS/MS analysis:	104
5.2.1 MS/MS of the precursor ions at m/z 1768.2 isolated from LipA1	104
5.2.2 MS/MS of the precursor ions at m/z 1688.0 isolated from LipA2	108
5.2.3 MS/MS of the abundant precursor ion at m/z 1585.6 LipA3	111
5.2.4 MS/MS of the abundant precursor ions at m/z 1505.7 isolated from LipA4..	114
5.2.5 MS/MS of the abundant precursor ion at m/z 1359.5 isolated from LipA5	117
5.2.6 MS/MS of the abundant precursor ion at m/z 1279.5 isolated from LipA6	120
5.3 CID analysis of the $[C-H]^-$ and $[Y-H]^-$ ions.	123
5.4 Summary:	126
Chapter 6 Conclusions	128
6.1 General Conclusion	128
Bibliography	130

List of Figures

Figure 1.1: Main processes of measuring with a mass system.	4
Figure 1.2: MALDI Ionization Process	10
Figure 1.3: The chemical structures of four commonly used matrices in MALDI-MS analysis.....	10
Figure 1.4: Schematic representation of the formation of ions during electrospray ionization.....	13
Figure 1.5: Schematic representation of a quadrupole mass analyzer showing the oscillation of ions to reach the detector.	15
Figure 1.6: Schematic diagram illustrating ion cyclotron resonance (ICR) analyzer.	16
Figure 1.7: Ion motions within an ICR cell.	18
Figure 1.8: Schematic diagram of the main components of tandem mass spectrometry (MS/MS).	20
Figure 1.9: Block diagram of scan modes of MS/MS.	22
Figure 1.10: Schematic representation of the QSTAR hybrid Qq-TOF. It is also representative of a Hybrid quadrupole orthogonal time-of-flight mass spectrometer (Courtesy from Applied Biosystems).	26
Figure 1.11: Schematic representation of the reflecting time of flight (TOF) analyzer by considering two ions with different masses ($m_A > m_B$), formed at the same time and having the same charge and the same kinetic energy. The ion which has the lower mass	28
Figure 1.12: Schematic representation of the orthogonal injection system of the reflecting TOF mass spectrometer according to Verentchikov et al. ⁷³	29
Figure 2.1: A graphic representation of gram positive and gram negative bacterial membranes. The scheme highlights the main differences between the two groups. LPS can only be found on the gram negative groups of bacteria, comprising also the internal a	34
Figure 2.2: Likely paths of fragmentation for the period of CID-MS/MS of a glycoconjugate consequent to lactose as described in the Domon & Costello Nomenclature. 109	40
Figure 4.1: Schematic structure of the E. coli K-12 cell envelop.134	49
Figure 4.2: The constitutive pathway of Kdo2-lipid A biosynthesis in E. coli	53
Figure 4.3: Covalent modifications of Kdo2-lipid A in E. coli K-12 and Salmonella. ..	57
Figure 4.4: Negative ion FT-ICR-MS of the heterogeneous mixture of native lipid As extracted from <i>Aeromonas salmonicida</i> SJ-112.	61

Figure 4.5: The seven proposed structures of the native Lipid A extract from <i>Aeromonas salmonicida</i> SJ-112.....	63
Figure 4.6: Schematic representation of the one of the possible common structures of Lipid A and the diagnostic ion of [C-H]- observed in the FT-ICR-MS spectrum.....	67
Figure 4.7: Negative ion CID MS/MS of the singly charged biphosphorylated lipid A [M-H]- ion A at m/z 1768.8732.....	70
Figure 4.8: The proposed fragmentation pathway of the selected precursor ion at m/z 1768.2056.....	71
Figure 4.9: Negative ion CID MS/MS of the singly charged monophosphorylated lipid A [M-H]- ion A at m/z 1744.2209.....	73
Figure 4.10: The proposed fragmentation pathway of the selected precursor ion at m/z 1744.2209.....	74
Figure 4.11: Negative ion CID MS/MS of the singly charged monophosphorylated Lipid A [M-H]- ion A at m/z 1688.2302.....	76
Figure 4.12: The proposed fragmentation pathway of the selected precursor ion at m/z 1688.2302.....	77
Figure 4.13: Negative ion CID MS/MS of the singly charged biphosphorylated Lipid A [M-H]- ion A at m/z 1586.0259.....	79
Figure 4.14: The proposed fragmentation pathway of the selected precursor ion at m/z 1586.0259.....	80
Figure 4.15: Negative ion CID MS/MS of the singly charged monophosphorylated Lipid A at m/z 1506.0586.....	82
Figure 4.16: The proposed fragmentation pathway of the selected precursor ion at m/z 1506.0586.....	83
Figure 4.17: Negative ion CID MS/MS of the singly charged biphosphorylated Lipid A at m/z 1359.8266.....	85
Figure 4.18: The proposed fragmentation pathway of the selected precursor ion at m/z 1359.8266.....	86
Figure 4.19: Negative ion CID MS/MS of the singly charged monophosphorylated Lipid A at m/z 1279.8676.....	88
Figure 4.20: The proposed fragmentation pathway of the selected precursor ion at m/z 1279.8676.....	89
Figure 4.21: Negative ion CID MS/MS of the singly charged monophosphorylated lipid A [C-H]- ion A at m/z 892.5778.....	92
Figure 4.22: The proposed fragmentation pathway of the selected precursor ion at m/z 892.5778.....	93
Figure 5.1: Negative ion MALDI-TOF-MS of the heterogeneous mixture of native Lipid As extracted from <i>Aeromonas salmonicida</i> SJ-112.....	97

Figure 5.2: The six proposed structures of the native Lipid A extract from <i>Aeromonas salmonicida</i> SJ-112.....	99
Figure 5.3: Schematic representation of the one of the common structure of Lipid A and the diagnostic ion of [C-H] ⁻ observed in the MALDI-TOF-TOF-MS spectrum.....	103
Figure 5.4: Negative ion CID MS/MS of the singly charged biphosphorylated lipid A [M-H] ⁻ ion A at m/z 1768.2.....	106
Figure 5.5: The proposed fragmentation pathway of the selected precursor ion at m/z 1768.2.....	107
Figure 5.6: Negative ion CID MS/MS of the singly charged monophosphorylated Lipid A [M-H] ⁻ ion A at m/z 1688.2302.....	109
Figure 5.7: The proposed fragmentation pathway of the selected precursor ion at m/z 1688.0.....	110
Figure 5.8: Negative ion CID MS/MS of the singly charged biphosphorylated Lipid A [M-H] ⁻ ion A at m/z 1585.6.....	112
Figure 5.9: The proposed fragmentation pathway of the selected precursor ion at m/z 1585.6.....	113
Figure 5.10: Negative ion CID MS/MS of the singly charged monophosphorylated Lipid A at m/z 1505.7.....	115
Figure 5.11: The proposed fragmentation pathway of the selected precursor ion at m/z 1506.0586.....	116
Figure 5.12: Negative ion CID MS/MS of the singly charged biphosphorylated lipid A at m/z 1359.5.....	118
Figure 5.13: The proposed fragmentation pathway of the selected precursor ion at m/z 1359.5.....	119
Figure 5.14: Negative ion CID MS/MS of the singly charged monophosphorylated Lipid A at m/z 1279.5.....	121
Figure 5.15: The proposed fragmentation pathway of the selected precursor ion at m/z 1279.5.....	122
Figure 5.16: Negative ion CID MS/MS of the singly charged monophosphorylated Lipid A [C-H] ⁻ ion A at m/z 892.5778.....	124
Figure 5.17: The proposed fragmentation pathway of the selected precursor ion at m/z 892.4.....	125

Chapter 1 : Introduction

1.1 History of mass spectrometry

In its earlier forms mainly at the beginning of the 20th century, the basic use of mass spectrometry was to probe some fundamental aspects of both atomic as well as molecular structure and for determining the atomic weights of elements along with the discovery of some stable isotops.¹

The birth of mass spectrometry is generally attributed to the physicist J.J. Thomson along with his discovery of the electron with the help of an electric field built inside a cathode ray tube. His success eventually led him towards development of a crude ‘mass spectrograph’ for measuring the atomic weights of elements. At the onset of World War II, various other applied benefits of mass spectrometry were observed. It was mainly used in the Manhattan project for purifying as well as assessing the enrichment of potential fissionable isotopes of uranium. Nier in this regard constructed a device on the basis of a mass spectrometer for the detection of leaks produced in the gas centrifuges for enriching ²³⁵U.^{1, 2}

This type of an instrument was mainly needed for the detection of the uranium hexafluoride which was utilized in the purification processes and was extremely corrosive. Since the demands for having higher-octane fuel for improving the performance of the fighter aircraft increased, mass spectrometers were also used for monitoring of the petroleum processing in order to increase the fuel quality. These needs

eventually drove towards a better development of a molecular ionization as well as fragmentation process to create different methods of producing more reproducible along with better diagnostic mass spectra.^{1,2}

In 1886, Eugen Goldstein experimented with positively charged gas particle streams that traveled away from the anode through channels towards the cathode, opposite to the direction of negatively charged rays.³ In 1899, Wilhelm Wien created a device with parallel electric and magnetic fields that separated the positive rays according to their charge-to-mass ratios. J.J. Thomson who was credited for the discovery of the electron and the “plum pudding” model of atoms, later improved on the work of Wien by reducing the pressure to create the mass spectrograph.⁴

Modern techniques in mass spectrometry can be traced to Arthur Jeffrey Dempster, who in 1918 established the basic design of mass spectrometers that is still used to this day.⁵ In 1919, Francis William Aston, a student of J.J. Thomson, built the first functional mass spectrometer and was able to detect isotopes of chlorine, bromine and krypton.⁶ As computing and construction techniques expanded and developed, in the 20th century the resolving power of the mass spectrometer grew exponentially. Mass spectrometers were also coupled to other separation devices, such as gas chromatographs, which improve the ability to separate mixtures of molecules molecules prior to fragmentation. Refinements continued in the sampling preparation and ionization techniques thereafter. The Nobel Prize in Physics was awarded to Hans Dehmelt and Wolfgang Paul for the development of the ion trap technique in the 1950s and 1960s.⁷ In 2002, the Nobel Prize in Chemistry

was awarded to John Bennett Fenn for the development of electrospray ionization (ESI) and Koichi Tanaka for the development of soft laser desorption (SLD).⁸ ESI and SLD allowed for the ionization of large biological macromolecules, such as proteins and are used extensively today.

1.2 Mass spectrometry

Mass spectrometry is an analytical methodology for determining the molecular mass of a chemical or biological molecule. Due to its minimal sample requirements and fast and accurate results, it is an ideal tool in most analytical chemistry and molecular biology labs. The principles behind mass spectrometry are to determine the masses of molecules and their fragments, which can be achieved when they are ionized, thus they can be separated based on their mass to charge ratio (m/z). This has important implications in identifying compounds of interests, and for characterizing or discovering new molecules.

There is a myriad of mass spectrometers available, based on the different types of configurations and the ionization source. Mass spectrometers have: The ionization source, the analyzer and the detector (**Figure 1.1**). Within the ionization source, molecules undergo ionization under low pressure and are heated to a specific temperature. It is within the ionization source where molecules undergo fragmentation and are ionized. These ions are then passed into the analyzer; the ions are separated according to their mass-to-charge ratio (m/z). Finally, the detector collects the ions,

quantifies their intensities and amplifies their signals for subsequent analysis. The process is conducted under low-pressure to minimize collision between ions and carrier gas molecules. It is at the detector, where the datum is processed and a mass spectrum is generated, which specifies the variation of ion current observed according to the ratio (m/z). Every molecule produces a characteristic spectrum or “fingerprint”.

The ionization source, the analyzer and detectors can be arranged in various configurations to create different mass spectrometers. The specific type of ionization source and analyzer will depend on the chemical and physical properties of the sample and on the quality of data desired (sensitivity, resolution and mass range).

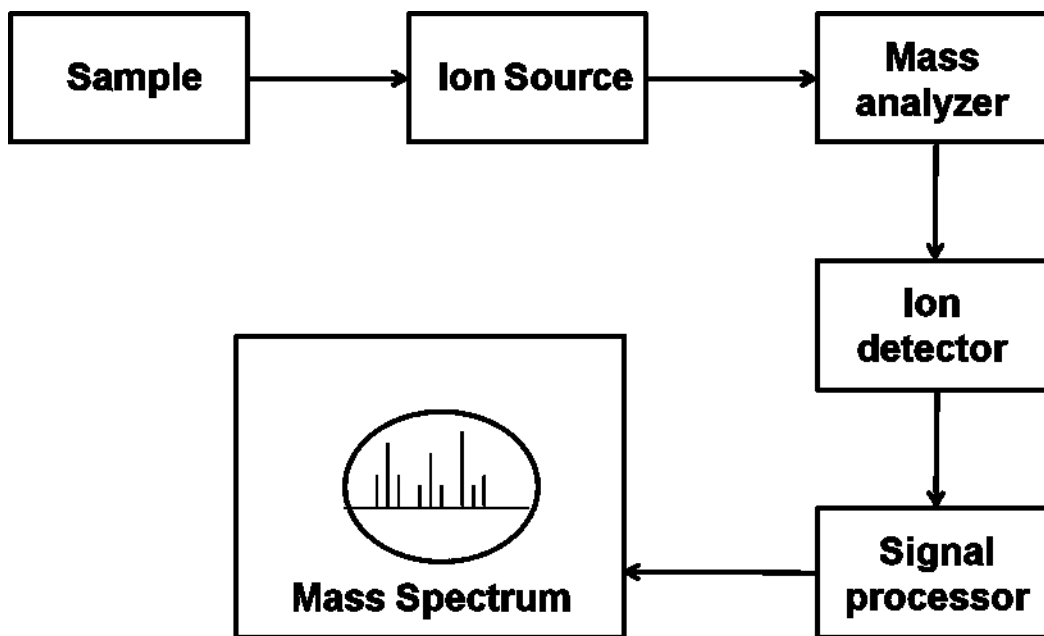
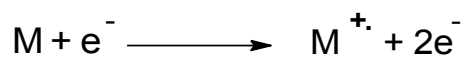


Figure 1.1: Main processes of measuring with a mass system.

1.3 Ionization techniques

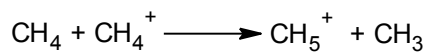
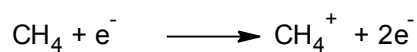
1.3.1 Hard or direct ionization technique

Electron impact ionization (EI) and chemical ionization (CI) techniques are called “hard” since they use the internal energy of the analyte to cause fragmentation. A molecule “M” is bombarded by energetic electron beams under vacuum to produce the following reaction:



In comparison, the chemical ionization method (CI), ions are formed indirectly through an intermediary reactive gas. While being considered a “softer” method than EI, this is still a hard ionization technique. The protonation of ions occurs in two stages;

The first step is the electron impact ionization of the intermediary reactive gas such as methane and the second is the protonation of the molecule M by reactive gas:



EI and CI are often chosen with compounds having small molecular masses because they can also be linked to a gas chromatography (GC) instrument whereby the sample can be first introduced in its gas phase.⁹

1.3.2 Soft or indirect ionization techniques

During “soft” ionization, a minimum amount of internal energy is given to the analyte to generate fragments. There are numerous soft ionization techniques: Fast atom bombardment (FAB),^{10, 11} liquid secondary mass spectrometry (LSIMS),¹² matrix assisted laser desorption ionization (MALDI)^{13, 14} and electrospray ionization (ESI),¹⁵ to name a few. ESI and MALDI play important roles in numerous fields such as; biotechnology, molecular biology (biological and chemical) namely the comprehensive study of all internal, and/or secreted proteins from an individual species. The Nobel Prize in Chemistry (2002) was awarded to John Fenn for ESI and Koichi Tanaka for MALDI.^{16,17} Fast atom bombardment (FAB) ionization, matrix-assisted laser desorption ionization (MALDI) and electrospray ionization (ESI) allow for single-stage direct MS analysis, and the characterization of complex biological molecules.

In addition to single-stage mass spectrometry, tandem mass spectrometry uses collision-induced dissociation, or CID-MS/MS. This is an important analytical method for the structural characterization of biomolecules, namely for the sequencing of peptides and the identification of a parent protein. Ions are fragmented in a tandem mass spectrometer by collisions with neutral gas molecules using either low or high energies; depends on tandem mass spectrometer used: Quadrupole ion trap (QIT-MS/MS), Quadrupole-Quadrupole-Quadrupole (QQQ-MS/MS), Quadrupole-Hexapole-Quadrupole (QhQ-MS/MS), Quadrupole orthogonal time-of-flight (QqToF-MS/MS), Fourier

transform ion cyclotron resonance (FT-ICR-MS/MS) and MALDI-Tof-Tof-MS/MS.¹⁸⁻

24

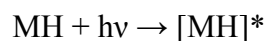
13.2.1 MALDI

MALDI is a soft ionization technique that is useful for the analysis of large biomolecules. This methodology is compatible with biomolecules in tissues because of its high sensitivity, high tolerance for salts and other contaminants, and a wide mass range with little fragmentation. For example, the structural characterization of vitellogenin protein and a fish biomarker have been done using MALDI in tandem.^{25,26}

MALDI was first introduced in the year 1988 by Hillenkamp along with Karas and since then, it has become a useful analytical tool mainly for peptides, proteins, and many other biomolecules such as oligonucleotides, carbohydrates, lipids and natural products.²⁷ Some of the basic advantages includes its efficient along with a directed energy transfer during the overall process of matrix-assisted laser-induced desorption which provides high yields of the ion of the intact analyte. In addition, it also allows for highly accurate measurements of analytes as well as sub-picomole sensitivities.²⁸

MALDI mass spectrometer is often combined with other analytical instruments or separation techniques. For example, the analysis of rough-type lipopolysaccharides combined with thin-layer chromatography and MALDI mass spectrometry, another example for the detection of affinity of purified cross-linked peptides by MALDI-TOF MS combined with chemical crosslinking of proteins.^{29,30} MALDI is an important tool for the study of DNA,³¹ glycoconjugates,³² and lipids.³³

In MALDI, the matrix and sample mixture are placed on a stainless steel plate, and after evaporation of the solvent, the matrix will then co-crystallize with the analyte. The laser commonly used is the nitrogen laser (337 nm). Common matrices used are; 2,5-dihydroxybenzoic acid (DHB),³⁴ sinapinic acid (SA), α -cyano-4-hydroxycinnamic acid (CHCA) and 2,4,6-trihydroxyacetophenone (THAP) which is used for proteins and peptides.³⁵⁻³⁸ The sample is dissolved in an appropriate matrix that has a strong absorption at the wavelength of the laser used. As such, the absorbed laser energy can lead to ionization of the analytes. The resulting ions are then desorbed by proton-transfer between the photoexcited matrix and the analyte (Figure 1.2). During laser irradiation ($h\nu$), the molecules of the matrix (MH) are excited according the following equation:



The energy is transferred to the analyte which is ejected into the gas phase. The ionization process seems to be occurring in gas phase according to two different phenomena; 1) A proton-transfer mechanism resulting from an acid/base reaction; 2) A proton-transfer when the matrix ions collide with the target molecule (analyte) in the gas phase.³⁸ Hence, the matrix plays a critical role by absorbing the laser light energy and eventually causing the indirect vaporization of the analyte. The matrix also acts as a proton donor as well as an acceptor and serves to ionize analyte both in the positive and in the negative ionization modes, respectively.

1.3.2.2 MALDI and Proteomics

Traditional characterizing techniques for proteins involved using gel electrophoresis, and Western Blotting. MALDI MS has emerged as a revolutionary tool in molecular biology due to its superior sensitivity, precision, accuracy, and throughput. The use of tandem mass spectrometry, where peptide fragments can be further fragmented via collision induced dissociation to its composite amino acids.

This allows for high throughput sequencing and structural/ functional analysis of classes of proteins versus the one protein at a time approach.³⁹ In terms of beneficial applications, entire signaling pathways or more importantly, aberrant ones in cancer cell lines can be determined, potentially leading to novel therapeutic options.⁴⁰ Other clinical applications include studying neuropsychiatric disorders where mouse lines have been developed to mimic cerebral spinal fluid (CSF).⁴⁰ Diseases such as Alzheimer's have protein structural abnormalities and thus understanding these protein structures and function can give an overall insight to the progression of this disease.⁴¹

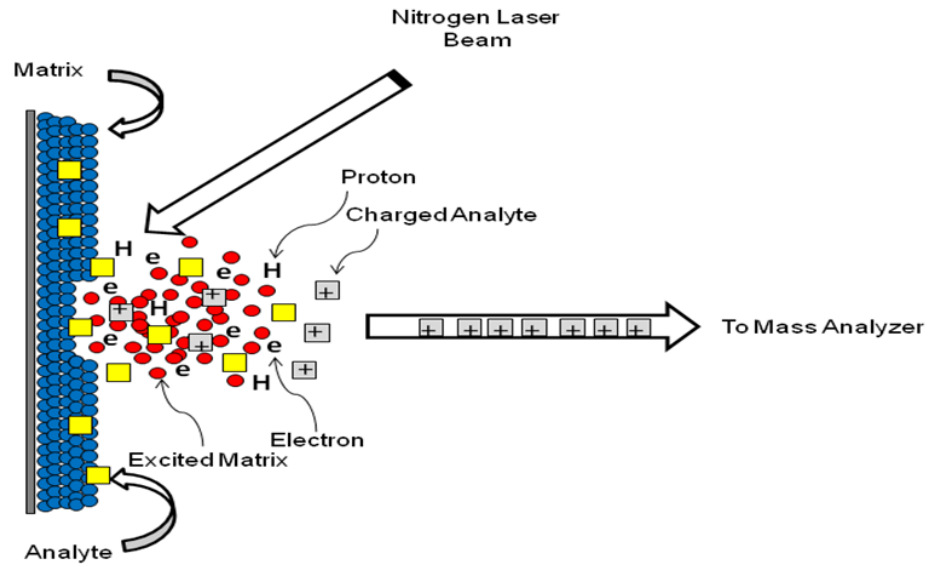


Figure 1.2: MALDI Ionization Process

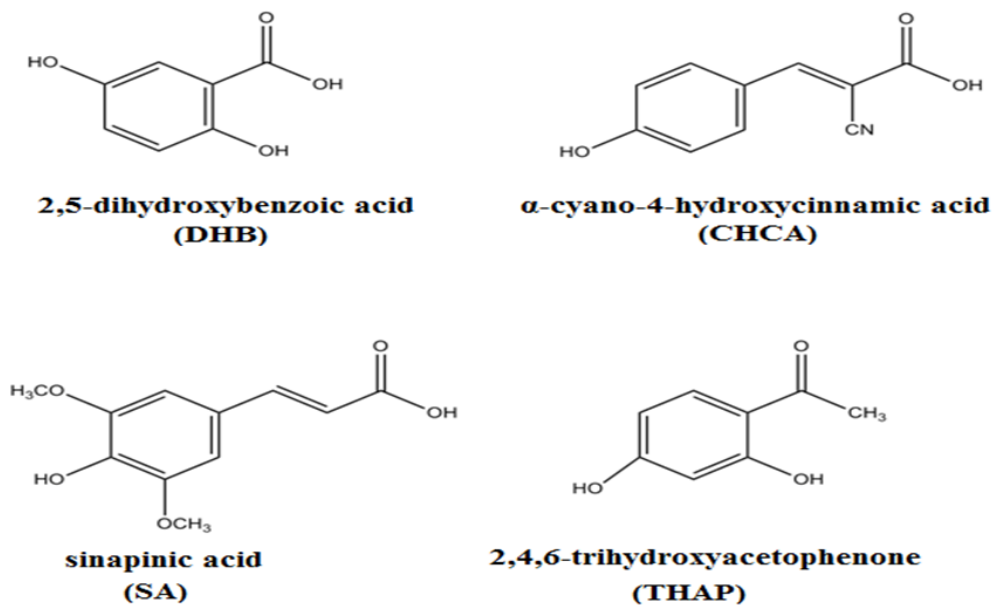


Figure 1.3: The chemical structures of four commonly used matrices in MALDI-MS analysis.

1.3.2.3 Electrospray ionization

ESI is a soft ionization method used for determining the molecular masses of peptides, and many other biological macromolecules. Electrospray is basically a method in which a liquid is dispersed into smaller charged droplets after applying a high potential electric charge between the liquid present in a thin capillary as well as in the counter electrode.⁴² The charging of the main analytes usually takes place in their liquid phase, but the ions are subsequently transferred into the gas phase. The charging of these analytes can mainly occur in different ways: the analytes might already be charged in the solution, with the help of adduct formation, gas-phase ionisation as well as electrochemical ionisation.⁴²

The first recorded description of electrospray was basically a short description of a minor experiment specifically with the static electricity. In the year 1745, the German scientist G. M. Bose wrote about his own observations and around the same time another scientist named L'abbé J carried out his experimentations.⁴²

The foremost purpose of this particular technique is to evaluate the various polar as well as the non-polar compounds, thereby dissolving the sample in a solvent which is polar organic (be it either basic or acidic in nature), and instilling it through a capillary into the resource (maintaining the appropriate atmospheric pressure). It is to be made sure that the application of 2-6 kV is necessary at the brim of the tube or capillary so that it can produce charged droplets.

There are two mechanisms that describe how the droplets are produced, see **(Figure 1.4)**.²⁴ The first mechanism of ESI ion formation is called the ion evaporation method and is believed to favour ions with relatively low m/z values. Under this condition, the droplets break down and their size is continuously being diminished while moving inside the source. Eventually, the repulsive forces among the ions on the surface of the shrinking droplets become very high. As a result of the surface tension of the solvent from these forces, ions will desorb into the gas-phase. The second theory is the charge residue model, which is predicted to be dominant in the case of ions with very high m/z . The evaporation of the solvent is continuous and is accompanied by droplet fragmentation so that a single ion (probably multiply charged) is formed at the end of this process.²⁵

This specific technique also involves the migration of the ions with the help of an electric field, which is eventually dried by the application of nitrogen gas. By using this technique, an emphasis is also laid on the fact that in order to generate ions in the specific gas phase, a gas nebulizer is provided to conduct the electrospray process.⁴³

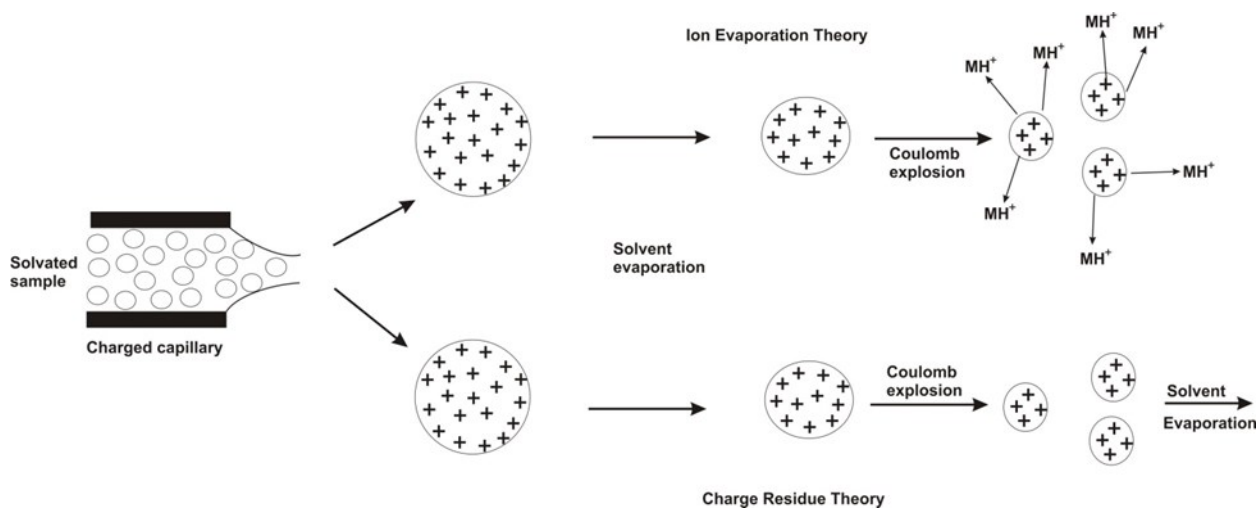


Figure 1.4: Schematic representation of the formation of ions during electrospray ionization.

Mass analyzers

The mass analyzer is basically the main component of the mass spectrometer and it takes the ionized masses and eventually separates them on the basis of their charge to mass ratios. After this, the outputs are produced from the detector where they are efficiently detected and later converted in the form of a digital output. In this part of this introduction the various types of mass analyzers will be described in more detail:

1.3.2.4 Quadrupole Analyzer

Being a type of mass analyzer, the quadrupole analyzer makes use of an electric field in order to separate gas phase ions. Consisting of four parallel poles or rods, the quadrupole analyser is designed in such a way that opposite voltage polarity is applied to the adjacent poles. It is ensured that the voltage that is applied to each pole or rod is formed from the totaling of a constant DC voltage (U) along with a changing radio frequency.⁴⁴ It is the electric force that is generated from the ions which leads to the oscillation of ions in the area that lies in between the four poles. However, it is also to ensure that the measurement of the orbit's radius remains constant.

The purpose of using the Quadrupole Analyzer is its effectiveness in attaining good quality reproducibility along with providing comparatively low and small cost systems. The movement of the ions is directly proportional to that of the Quadrupole's voltage, the ion's mass, and radio frequency. Ions are found to continue to move around the area that exists between the rods. However, there is no notable change in the length of the rods until the ions form a steady velocity being created when the ions tend to enter the quadrupole. The ions, however, travel through a probable voltage, before getting an entry into the analyser. The probability and the potential of the voltage is determined and formed by a ring electrode so that it provides a steady amount of velocity to the ions, with the help of which they can form a slant structure in relation to the Quadrupole centre.^{45, 46}

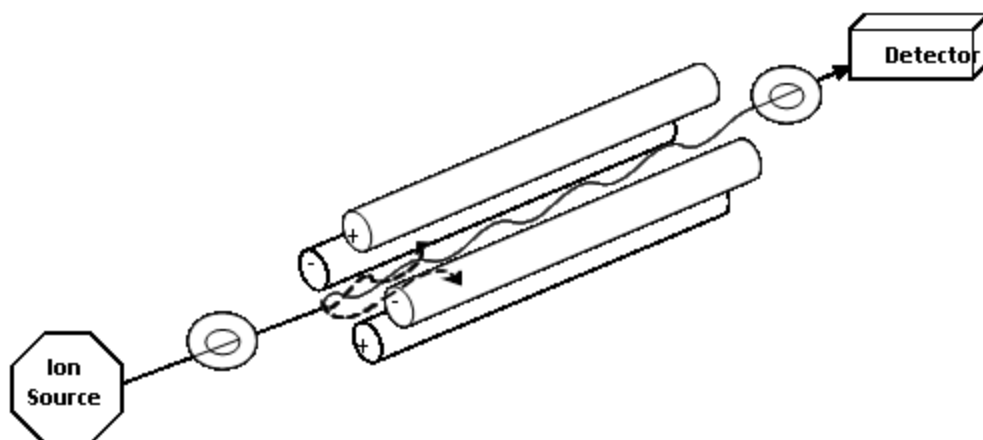


Figure 1.5: Schematic representation of a quadrupole mass analyzer showing the oscillation of ions to reach the detector.

1.3.2.5 FT-ICR

The massive interest mainly in the Fourier-transform ion cyclotron resonance mass spectrometry (FT-ICR-MS) has increased since its successful introduction in 1974 by Comisarow and Marshall.⁴⁷ This technique basically consists of three core components including a superconductive magnet along with an ultrahigh vacuum, as well as an analyzer cell (ICR) (**Figure 1.6**). The core of FT-ICR-MS is the cell analyzer which measures the mass-to-charge (m/z) ratio of the ion mainly on the basis of its frequency. In addition to this, the ICR cell is also made up of three opposite pairs of plates which form various shapes such as cubic, orthorhombic, cylindrical, etc.), and are hence named as either trapping plate (having one pair), an excitation or the detection plates (having 2 pairs) that are parallel to the surrounding magnetic field.⁴⁷

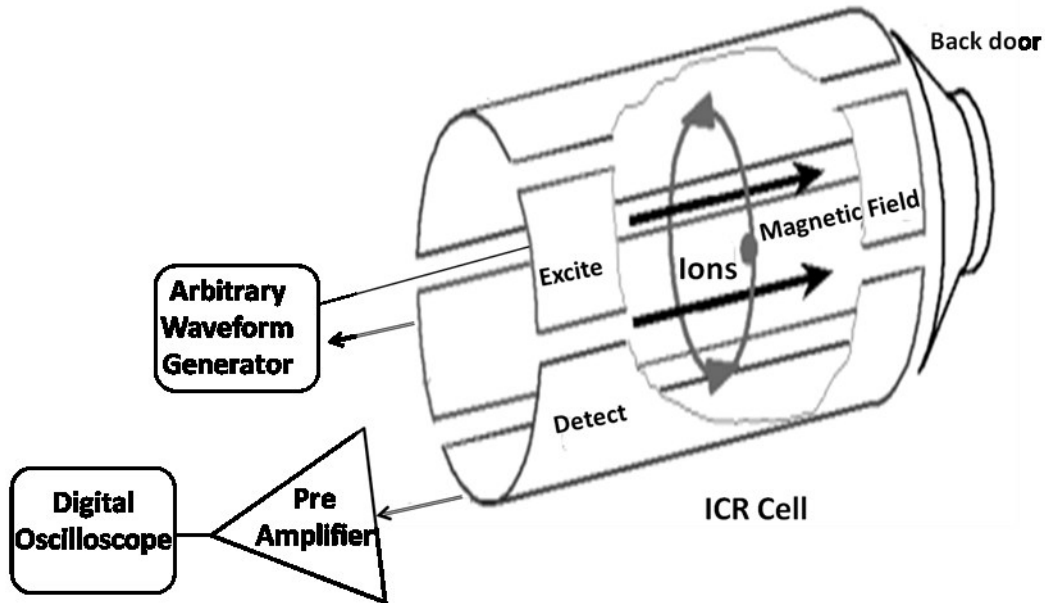


Figure 1.6: Schematic diagram illustrating ion cyclotron resonance (ICR) analyzer.

After the ions are generated in the ionization source, they eventually pass into the ICR cell. After this, they undergo some harmonic oscillations mainly in the electric field existing between the trapping plates for creation of a trapping motion. Due to the strength of the magnetic field, the ions eventually undergo a comparatively stable cyclic motion, specifically in a plane which lies perpendicular to the surrounding magnetic field, in order to obtain a cyclotron motion through the force, called as a “Lorentz force”. Cyclotron motion is typically represented by ω_c which is the cyclotron frequency since each ion rotates with a specific frequency. All three motions usually lead towards a complex and complicated ion movement mainly in the analyzer cell (**Figure 1.7**).⁴⁸

The ions basically undergo two different forces present in the cell and these can be expressed as:

$$\text{Centripetal force } F = qB/m \quad (1)$$

$$\text{Centrifugal force } F = mv^2/r$$

Ions could also be stabilized on the trajectory whenever the balances of two forces occur:

$$qvB = mv^2/r \quad \text{or} \quad qB = mv/r \quad (2)$$

here, q denotes ion charge, m is mass of the ion and B is the magnetic strength of the field.

Ions usually complete a circular trajectory which can be represented by $2\pi r$ having a frequency v :

$$v = \omega/2\pi r \quad (3)$$

Hence, the angular velocity ω becomes equal to:

$$\omega_c = 2\pi v = v/r = qB/m \quad (4)$$

Since ω_c is directly proportional to the m/q , the smaller the mass-to-charge ratio is, the greater would be the cyclotron frequency.^{48,49}

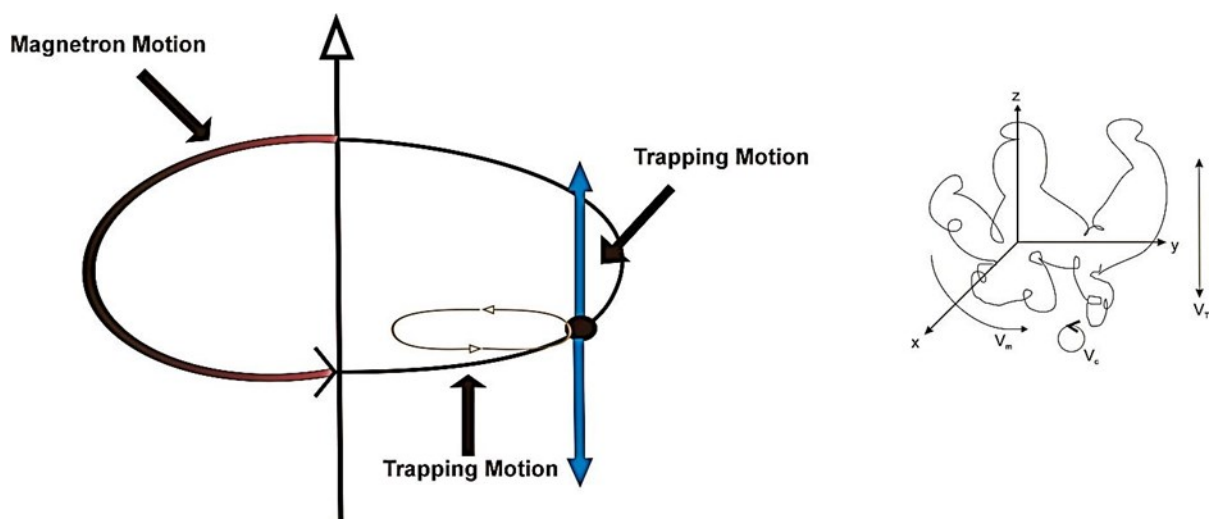


Figure 1.7: Ion motions within an ICR cell.

Because ions have inherent kinetic energy while moving in the ICR cell, they get more excited mainly under the magnetic field and also even at room temperature. Ions, however are not detectable on various detection plates since they get excited even at the room temperature. Under such conditions, ions become statistically distributed in the entire cell due to their varied velocities provided by the different energies for the ions having similar m/q ratios. Hence, these ions should be excited mainly as “ion packets” for a much larger radius for obtaining of a measurable signal via supplying relative sinusoidal voltage to all of the excitation plates. This is basically a simplified explanation of how the ions could be generated in the existing ICR cell.⁵⁰

1.3.2.6 Tandem mass spectrometry

Tandem mass spectrometry is a very powerful technique which involves multiple steps instead of a single step involved in traditional mass spectrometry, which allows the ions or fragments to be carefully analyzed, and also provided much useful structural information. The core components are shown in Figure 1.8. Ions, or their fragments being produced in the softer ionization source, generally first pass to the mass analyzer for ensuring that the ions having specific m/z are chosen. Such ions, which are known as the *precursor ions*, are basically processed under strong gas collision and also by a highly intense laser beam for production of ions known as the *product ions*. Such ions are subsequently analyzed in the next (second) mass analyzer and are carefully detected with the help of an ion detector.⁵¹⁻⁵³

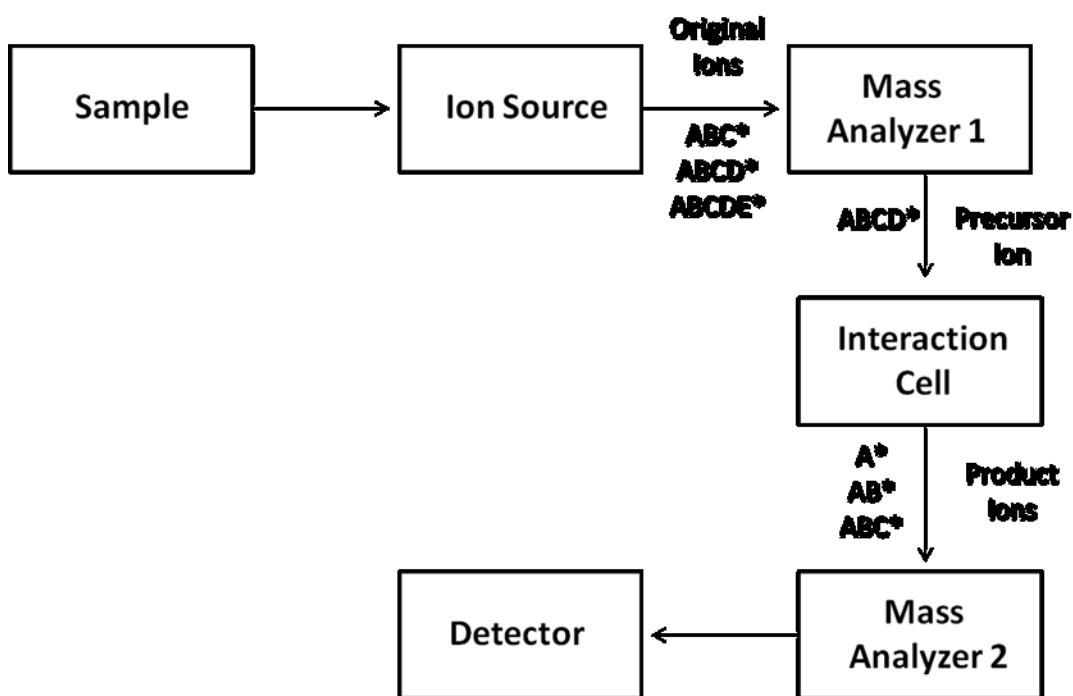


Figure 1.8: Schematic diagram of the main components of tandem mass spectrometry (MS/MS).

Different types of spectra can also be identified with the help of different MS/MS experiments, as shown in Figure 1.9. In this regard, the product ion scanning is considered as one of the four major scanning experiments which could be successfully performed. The product ion can be isolated in the second mass analyzer. Subsequently, it could be analyzed in the very first mass analyzer for obtaining the precursor ion. In addition, the precursor ion could also help in scanning and this could possibly be obtained by simply isolating it mainly in the very first step which is followed by fragmentation which are then further scanned in the second mass analyzer. Furthermore, a natural loss scan might be obtained in the first mass analyzer mainly for all the masses,

and also in the second mass analyzer. The second mass analyzer however, should be present at a set offset from the initial first one in order to make sure that this doesn't occur in the time tandem instruments. This type of scan is usually more beneficial for the closely related compounds, which more often result in similar product ions. Lastly, both of these mass analyzers can also be measured simultaneously as a set of already selected analyte masses that give either a selected ion monitoring scan (SIM) and/or multiple reaction monitoring (MRM) scans, which measures the transitions of a m/z protonated molecule $\rightarrow m/z$ product ions.⁵⁴

In addition, ion decomposition can also be obtained in the tandem mass spectrometry with the help of four major mechanisms involving (a) collisions of the ions with the gas which can be either helium, nitrogen, or argon; (b) strong interactions that take place between ions mainly with the electrons; (c) interactions of the ions with the persistent photons simply by using infrared multiphoton dissociation (IRMPD) and (d) lastly, interactions between the ions and the surrounding surfaces.⁵⁵⁻⁵⁸

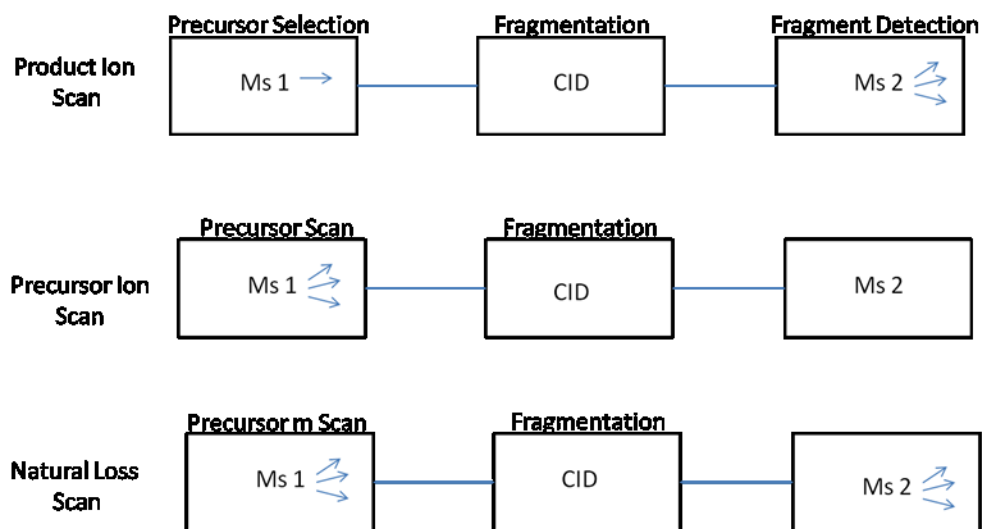


Figure 1.9: Block diagram of scan modes of MS/MS.

1.3.2.7 FT-ICR-MS

The MS/MS experiment performed in the FT-ICR is basically analogous to the Quadrupole ion trap (QIT) experiment; but is more limited, mainly in terms of obtaining product ion spectra. Generally speaking, FT-ICR is aimed in scanning various functions for the MS/MS operation which are quite similar to the ones used in a QIT. Firstly, a quench pulse is carefully applied for ejecting a residual ion in the preceding experiment. After this, an ionization pulse must be applied. Followed by this, the precursor ion is then isolated mainly with a resonant excitation signal consisting of different frequencies, except for the single one which is directly related to a precursor ion.⁵⁹ After careful mass selection, a collision gas is applied into the entire ICR cell, causing the trapped ions to collide actively and to obtain a much bigger orbit.

The CID products are basically mass analyzed as usual and by this, it means excitation of all the products to various orbits of large radii as well as detection of their entire image current. The FT-ICR is known to have some unique distinction which in addition to the SORI-CID, both fast as well as slow ion-activation procedures could be performed.^{60,61} In addition, interactions of the ions mainly with electrons can also be used for electron capture dissociation (ECD), as well as electron transfer dissociation (ETD).

ECD, is generally employed in Fourier transform ion cyclotron resonance mass spectrometers (FT-ICR) because of the need of having several milliseconds interactions to occur between both the ions, along with the electron, and also because of the fact that the efficiency of ECD is highest for lower-energy electrons (around <1 eV) which are quite difficult to provide mainly in quadrupole ion traps having strong RF potentials affecting the movement of the electrons in the trap. In addition, the stabilization of every captured electron is much faster than the electron emission that is typically present on the time-scale of 10^{-14} s, hence bond dissociation usually occurs at a faster rate when compared to the frequency of a typical bond vibration.^{62, 63}

On the other hand, electron transfer dissociation (ETD) is solely based on the ion-ion reactions which occurred in a quadrupole ion trap mainly between an electron-rich species. In both these ECD and ETD, the concluding result is successful acquisition of the electron having a charge-state reduction of both the ion as well as the subsequent fragmentation. In both of these two methods, the overall chance of a direct bond cleavage

occurrence can only be observed with none, and in some cases, minimal energy redistribution, along with randomization away from the major reacting site. Because of this, a stronger backbone of N-C_α peptide bonds is cleaved which form *c* and *z*-ions that are complementary to both *b* and *y* ions which are normally produced in the lower-energy CID. In addition to this, the interactions between ions and photons mainly with the help of infrared multiphoton dissociation (IRMPD) as well as ion spectroscopy can also be applied to all the trapped ions in either the ion trap or in the FT-ICR analyzers.⁶⁴⁻⁶⁶

1.3.2.8 Hybrid quadrupole orthogonal time-of-flight mass spectrometry (Q-ToF)

The Q-ToF instrument was initially described in the year 1996 mainly as a means to combine the scanning abilities of both the quadrupole as well as the ToF analyzer's resolving power.⁶⁷ It can also provide some informative, simple, high-quality and one-stage MS as well as tandem MS/MS spectra. A diagrammatic representation is shown in Figure 1.10 for the Q-Star instrument which was carefully manufactured by *Applied Biosystems*. The figure shows a mass spectrometer composed of three different quadrupoles directly linked to a ToF analyzer that is aligned geometrically in the orthogonal configuration mainly with respect to existing quadrupoles; thus, the name was formulated as Q-ToF orthogonal mass spectrometry. In addition to this, the very first along with the third quadrupoles are always operating in the rf-only mode.⁶⁸

A second quadrupole as the main analyzer, rather than the ToF, is used just for tuning of the instrument, since this ToF is more effective and more efficient for this specific purpose. Because of the critical role of the second along with the third

quadrupoles mainly during MS/MS analysis, both these instruments are typically referred to as QqToF mass spectrometers. The first “Q” usually refers to the mass-resolving quadrupole while the second “q” clearly indicates the collision cell.

One of the biggest advantages of QqToF instrumentation noted up till now is its capability to be interfaced with ESI or MALDI needing little manipulation of the entire configuration. The main association of MALDI is known to have more importance mainly because of the fact that conventional MALDI-ToF fails in performing MS/MS experiments. Hence, due to the existing limitation of quadrupole mainly in terms of its mass range, there exists; however, some difficulties specifically in the orthogonal injection of much larger and singly charged ions in the ToF. Despite this, other common advantages of QqToF instruments basically include the ease of its operation, high mass accuracy as well as high resolution, and also up to an 100-fold increase in its overall sensitivity, when compared to that of the triple quadrupole.⁶⁹ QqQ instruments nevertheless are still being favored mainly for both quantitative studies and also for the precursor ion scans involving the “parent” ion of a certain fragment which could be identified.

QSTAR XL - Schematics

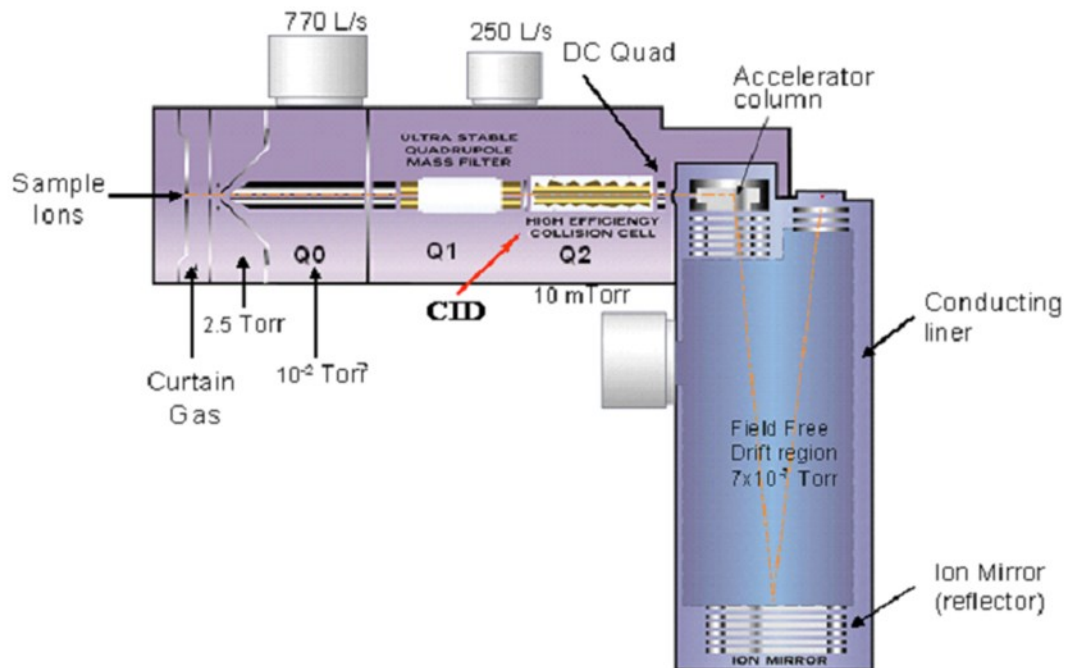


Figure 1.10: Schematic representation of the QSTAR hybrid Qq-TOF. It is also representative of a Hybrid quadrupole orthogonal time-of-flight mass spectrometer (Courtesy from Applied Biosystems).

1.3.2.9 Time of flight (TOF) analyzer

A TOF analyzer was basically first described by Stephens in 1946 and it is considered as the simplest form of mass analyzer.⁷⁰ At the ending of the 20th century, both Brown as well as Lennon focused and also managed to redevelop this technique.⁷¹ The ions which were formed in the source were mainly accelerated on the basis of their voltage V_s , and also travelled through the analyzer (d) for reaching the detector without using any other acceleration source or process. In addition, whenever the ion leaves the

main source mainly with a mass m along with a total charge $q = Ze$, it would ultimately have an additional kinetic energy (E_c). As a result, the ions would reach to the detector. The correlation mainly between both the mass/charge ratio as well as the time of flight can be expressed as: $E_c = 1/2mv^2 = qV_s$. The equation could also be reduced to a much simpler form; (t_f): $m/z = K t_f^2$ and here K represent the calibration factor. Hence, the calibration factor existing between both t and m/z is mainly a function of all of the prevailing experimental conditions. The biggest advantage of this analyzer is its capability of analyzing a high mass range of different molecules; but the major drawback associated with is its lower resolution. In order to overcome this major drawback, an electrostatic ion mirror is introduced (ion mirror reflectron) which increases both the resolution power and hence, accuracy in measurement of the mass (**Figure 1.11**).⁷²

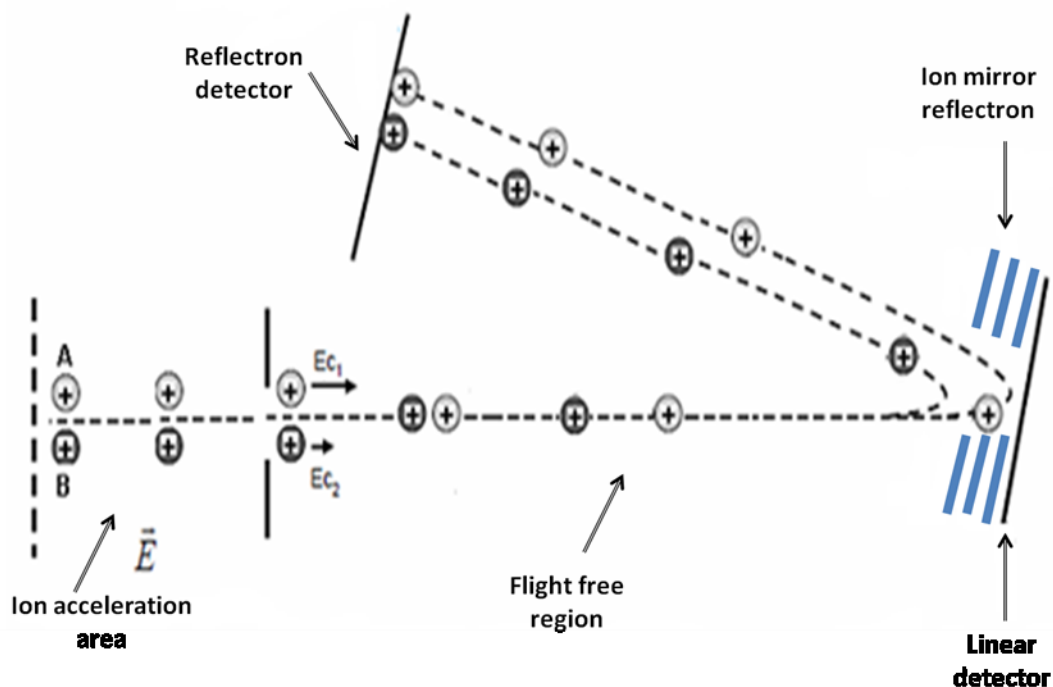


Figure 1.11: Schematic representation of the reflecting time of flight (TOF) analyzer by considering two ions with different masses ($m_A > m_B$), formed at the same time and having the same charge and the same kinetic energy. The ion which has the lower mas

Analyzers like TOF are more preferable than quadrupole and are also mostly adopted for pulsed ionization procedures such as MALDI. In addition, the laser shot would determine the initiating time mainly for the time measurement, specifically during which the ions can reach to the detector. It is not suitable nevertheless to combine both ESI along with TOF. In the Figure 1.12, the ions are initially injected with the help of continued, as well as pulsed ionization. Followed by this, the ions continuously arrive in the major source mainly within the Y axis. They are, after this accelerated and also

pulsed mainly with the help of a pusher present within the Z axis that would eventually accelerate the ions in order reach similar levels of energy and to give the measurement of TOF.⁷³

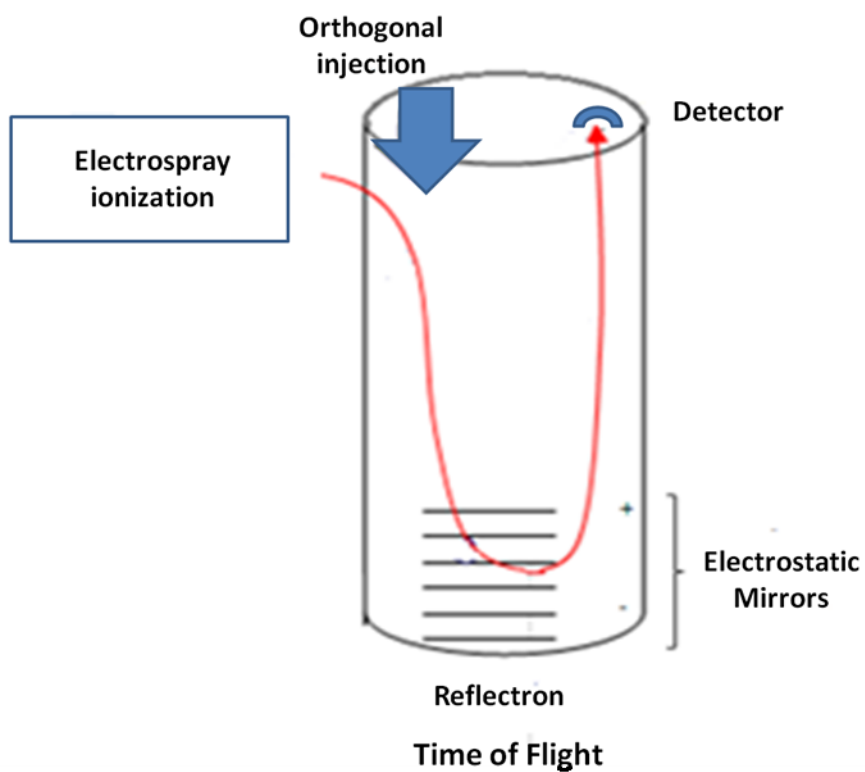


Figure 1.12: Schematic representation of the orthogonal injection system of the reflecting TOF mass spectrometer according to Verentchikov *et al.*⁷³

1.4 Scope of the thesis

In this work, tandem mass spectrometry was used to investigate the Gram negative bacteria by analyzing Lipid A. A brief introduction into the mass spectrometry has been presented within this chapter. In chapter 2, a detailed discussion about bacterial membranes and lipopolysaccharides will be given. In Chapter 3, the experimental system and apparatus such as the lipopolysaccharide purification, the lipopolysaccharide hydrolysis, and mass spectrometers will be described. In Chapter 4 and 5, the experimental results will be shown followed by a detailed discussion of each result. Finally, in chapter 6, we will summarize the work presented herein and provide concluding remarks about the findings of this work.

Chapter 2 : Bacterial membranes and lipopolysaccharides

2.1 Background

Hans C. J. Gram is the Danish bacteriologist who became famous for inventing a staining methodology that could be used to differentiate bacterial microorganisms and categorize them under two main categories.⁷⁴ The methodology acquired its name from its inventor, and this was through classifying bacteria as either Gram-positive, that is forming a violet color, and Gram-negative which forms a red color. The staining properties of different bacteria are different mainly as a result of the structure and how the surface membrane is composed. All bacteria contain cells wall that protect the inner environment from the outside, and makes it secure to transport substances from the inside to the outside surroundings, and from the outside back to the interior of the cell.

2.2 Gram positive bacteria

Gram positive bacteria are comprised of an internal phospholipid bilayer, peptidoglycans, polysaccharides and proteins in its cell wall.⁷⁵ These types of bacteria produce a violet color after gram staining due to the capacity of the multilayered peptidoglycan to maintain the crystal violet stain after decolourization with the solvent has taken place, furthermore the layer is of a thicker texture with these bacteria than is the case in gram negative bacteria. Peptidoglycan, or murein, which is a natural polymer, comprises of sugars and amino acids and is an essential component of the bacterial envelope. It is important for the membrane's mechanical integrity.⁷⁶ If its formation is

hindered by the antimicrobial agent, for instance, penicillin, then cell growth is inhibited.^{77, 78} The bacterial membrane is also comprised of polysaccharides, which either appear in connection to peptidoglycans, or can appear separately within the membrane. The ones that appear in connection to peptidoglycans can be classified under two categories, which include namely teichuronic acids and teichoic acids.^{79,80} Lipoteichoic acids and lipoglycans are other examples of polysaccharides.^{75, 81} These carbohydrates are structurally diverse, with numerous functions, which include attaching to proteins and metals, and supplying phosphate moieties.⁸²

Most research, qualitative and quantitative, on these biological glycoconjugates employ mass spectrometry. One example is ESI-MS/MS which was linked with high-performance anion-exchange liquid chromatography in a study that involved neutral and acidic sugars that were isolated from certain bacteria, such as bacilli, grown in locations that were phosphate-restricted.⁸³ The researchers were able to use this system effectively to confirm the structure and conduct selective quantification of the carbohydrates. In the same way, MALDI-TOF was used in a recent study to assess the influence that acyl chains have on the role of lipoteichoic acid, and validate the deacylation process of pneumococcal lipoteichoic acid.⁸⁴ Even though mass spectrometry has been successfully used to study polysugars isolated from gram positive bacteria, it is more valued when studying the molecular structure of lipopolysaccharides that are linked to gram negative bacterial membranes.

2.3 Gram negative bacteria

Gram negative and gram positive are differentiated by the inner and outer portions that are found in the former, along with a coat of lipopolysaccharides (LPSs), which is the outermost component of gram negative bacterial membranes. The inner and outer membranes are made up of phospholipids, which are largely glycerolphospholipids and proteins. There is the peptidoglycan layer found inside the gelatinous material, which is referred to as periplasm and divides the two layers. The peptidoglycan layer is not capable of maintaining gram staining, and actually the gram procedure tends to dissolve the external membrane and in part destroy the peptidoglycans and does not retain the initial dye color.⁸⁵ The external leaflet of the outer membrane is mostly made up of the amphiphilic LPS moieties. These have a lipid portion (Lipid A) inserted inside the membrane environment. Figure 2.1 shows how the gram positive and negative envelope structures are built up.

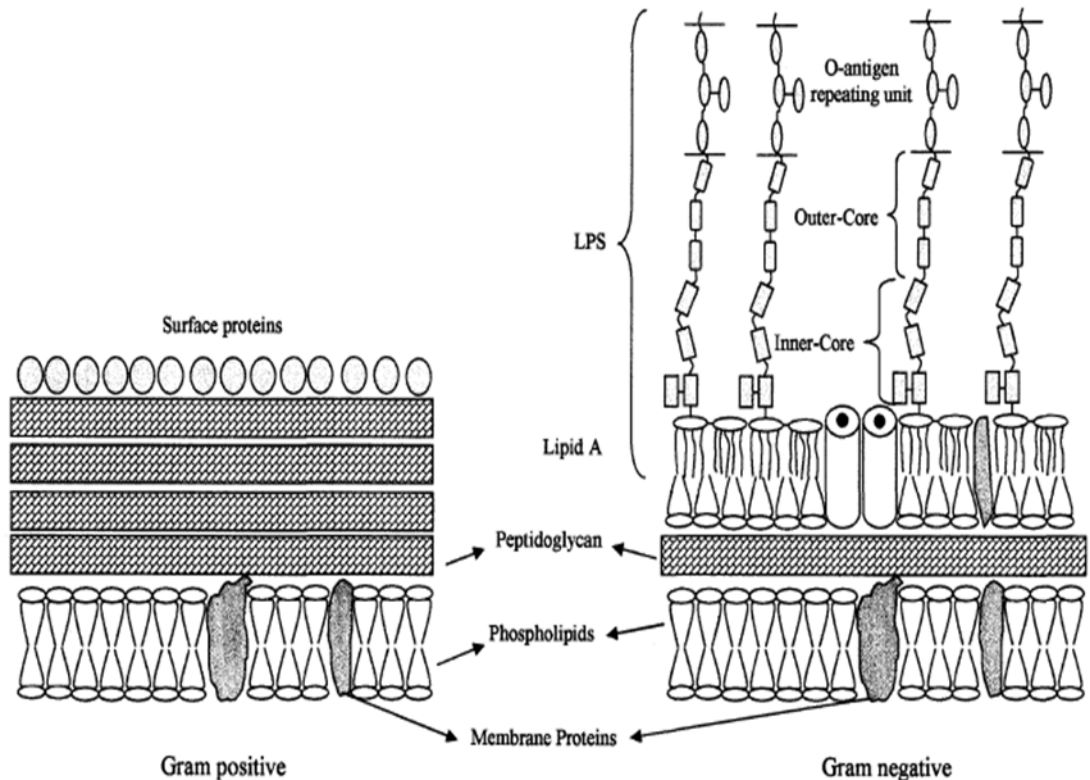


Figure 2.1: A graphic representation of gram positive and gram negative bacterial membranes. The scheme highlights the main differences between the two groups. LPS can only be found on the gram negative groups of bacteria, comprising also the internal and external membranes.⁴⁵

2.4 Lipopolysaccharides:

Lipopolysaccharides (LPSs) refer to the amphiphilic macromolecule parts found in the outer leaflet of gram-negative bacteria's external membranes. They are regarded as the virulence aspect of the human and animal disease-causing bacteria. LPS are usually made up of two parts, which include a polysaccharide and Lipid A. The polysaccharide portion comprises of O-antigen (O-chain) and the core oligosaccharides. These are attached to the membrane through the Lipid A. The oligosaccharide antigen has a

covalent association with the core oligosaccharide, which is then associated covalently with the Lipid A. LPS causes endotoxic shock, and is also responsible for their pyrogenic activity of gram negative bacteria. Moreover, LPSs are also capable of triggering and complimenting macrophages.^{86,87}

On the other hand, LPS contains endotoxic properties that are contained majorly within the Lipid A portion. Hence, the major attributes of Lipid A are to present immense toxic properties. Its structure is liable for the biological activities of endotoxins that play a role in the diverse cells of the immune system.⁸⁸

2.4.1 The O-specific chain

The O-specific chain has replicating oligosaccharides of 50 units, with diverse structure and composition among several genera and bacterial serotypes. In addition, the oligosaccharide units comprise of up to eight sugar residues that arise in smooth LPS types, rather than the rough types of LPS without this practicality.⁸⁹ The rough LPS have units of the O-antigen associated with the core oligosaccharide. This is then linked to the glycosylate in Lipid A. The O-antigen is responsible for the divergence in the structure of Lipid A for diverse types of bacteria. The O-chains are the basis for differentiating the various bacteria types, and are therefore used to determine the special aspects of each bacteria serotype. With regard to the pathogenic factor of gram-negative bacteria, the O-chain is the host, and the infection is what protects the central integrity from its environment. This feature is caused by various glycoside links, substitution of sugars and

the genetic ability to give the O-chain its distinctive structure that contains linear or branched connections.⁹⁰

The O-chains contribute to the O-antigenic properties that create the links between species-specific antibodies. They are also important for the protection of several antibiotics which is evident in the relative sensitivity of the rough strains as opposed to the smooth types of bacteria. The O-chains of LPSs such as *Actinobacillus pleuropneumoniae* along with other types of LPS are some of the contributors of linkage to mammalian tissues, hence facilitating infection. The major linkage in lung tissues is the LPS of *A. pleuropneumoniae*. Certain O-chains are able to stick to a mineral surface, for instance the *Shewanella algae* LPS, which was the first bacterial polysaccharide that was discovered comprising of a malic acid residue.⁹¹

2.4.2 The core oligosaccharide:

Core oligosaccharides fall under two categories, which include; the outer core, comprising of hexoses (largely glucose), galactose, and *N*-acetyl-D-glucosamine, and the inner oligosaccharide core that is comprised of precise residues attributes of LPS, including L-glycero-D-manno-heptose (LD-Hep) and 3-deoxy-D-manno-octulosonic acid (Kdo) that is connected to the O-6` position of lipid A through an α -ketosidic association. Kdo is a distinctive and definite 8-carbon sugar that can be found in the LPS of various Gram-negative bacteria.⁹²

Kdo is comparable to the sugars in the LPS component, since it is capable of substitution with reactive groups, for instance phosphate, or phosphoethanolamine. The

LPS internal core also contains L-glycero-D-manno-heptose (Hep), a distinctive 7-carbon sugar. There are, however, some bacteria that do not have any Hep residues.

Three species of the genus *proteus* (*vulgaris*, *penneri*, and *mirabilis*), have been found to have the internal core of most of the strains containing Kdo-I with its residue substituted at C-8 position by 4-amino-4-deoxy- β -L-arabinose. This is a portion of the core that is similar to those of other species, while the outer cores tend to be significantly different. Some of their remarkable components include a Kdo with a link to Hep, and the α -amino group of L-lysine and 2-glycylamino-2-deoxy-D-glucose. There is also GalNAc glycosidically in its open-chain form with a link to a cyclic acetal GaIN.⁹³

2.4.3 Lipid A:

Lipid A is a hydrophobic link of lipopolysaccharide (LPS), a glucosamine disaccharide that contains around seven acyl chains. Its structure has a bisphosphorylated β -(1 \rightarrow 6)-with a link to a D-glucosamine disaccharide backbone. Esters and amides are the linking backbone elements with fatty acids that are positioned at O-3 and O-3' for the esters and then N-2 and N-2' for the amide. This occurs in the hydroxylated type of these unusual fatty acids, having a 3-OH group. This then esterifies through other residues of fatty acids.^{94, 95} Recognizing the numerous species of Lipid A is determined by the amount and length of fatty acids presenting the Lipid A. A Lipid A is the Lipid A fraction is inherently heterogeneous, and this is as a result of the diverse levels of phosphorylation and acylation, the type of acyl residues and the way they are dispensed. As a result, the

structure of lipid A changes, and the changes contribute to the pathogenesis of various diseases.⁹⁶

Even though Lipid A fatty acids typically are comprised of 10-16 carbon atoms, there is evidence of other abnormal chains. For instance, a 20-carbon chain that is found in certain isolates, which are linked to the lipid A isolate of *Chlamydia*. How long the fatty acids are determines how toxic Lipid A is. The most toxic types include those that have C₁₂, C₁₂ (OH), C₁₄, and C₁₄ (OH).⁹⁷ Fatty acids that are unsaturated are hard to detect, and where they exist, they tend to combine with the saturated ones.^{98, 99} Some of the LPS intrinsic extracts, such as lipid A are complex combinations of glycoforms, with a structural relationship. This exists due to the existence of a number of biosynthetic pathways and degradation that occurs throughout the isolation process. Through mass spectrometry, these mixtures can be studied and the precise molecular structure of every element demonstrated.¹⁰⁰ This can differ, based on the factors that affect growth, for example, temperature.¹⁰¹ Furthermore, these multifaceted biological glyco-mixtures are potential candidates for qualitative and quantitative analysis *via* capillary electrophoresis coupled with mass spectrometry (CE-MS).¹⁰² Apart from the fatty acids, the existence of phosphate and occasional pyrophosphate group substitutions, existence is usually at locations of C-1 of the reducing glucosamine residue, along with the C-4' of the non-reducing end.¹⁰³ Substitution can subsequently take place between these phosphate groups and phosphoryl-ethanolamine, ethanolamine, or at times neutralized by means of an additional substituent, for instance arabinosamine.^{104, 105} The studies of Lipid A structure, whereby spectrometry is applied, play a significant role, especially when

analyzing biological activity. An example of this is that lipid A is usually regarded as a pro-inflammatory agent. On the other hand, effective assessment has shown that certain synthetic analogues are antagonistic aspects against *Escherichia Coli* Lipid A.¹⁰⁶

2.5 Mass spectrometric analysis of carbohydrates

Mass spectrometry analysis of carbohydrates makes it possible to gather structural information regarding their components for purposes of structural and post-translational adjustment. The polymeric chains of carbohydrates are comprised of sugar units connected through glycosidic linkages by analogy with peptide bonds formed by amide linkages in proteins.¹⁰⁷ MS and MS/MS analysis have indicated that besides the breaking of glycoside bonds there are also a possibilities for inner-sugar cleavages to take place, which create analytical fragment ions. This absenting created an opportunity for studies on the structures of carbohydrate chains.¹⁰⁸

Domon and Costello were the first to illustrate the CID analysis of the protonated molecules of complex glycoconjugates. They proposed a systematic nomenclature for carbohydrate fragmentation of complex glycoproteins when carrying out FAB-MS/MS analysis.¹⁰⁹

When the reducing end is Glc (glucose) and the non-reducing unit is Gal (galactose), potential fragmentations are demonstrated through the simple disaccharide lactose as shown in Figure 2.2. This figure shows units that result from the indicated cleavages. Ions formed from the non-reducing end are named D A, B, and C. A is connected to inner sugar fragments. The fragments that branch from the reducing end are

named Z, Y, and X. X relates to the inner-sugar fragments. Similarly, A, B, C, Z, Y, and X letters may also be classified depending on the precise location of the sugar residue. Purposely, the non-reducing end begins with the number 1 where there are A, B, and C ions, while, the reducing end begin from 1 for the Z and Y ions. Nevertheless, the Y_0 ion is usually given the number 0 in case it is the reducing end group's aglycone.

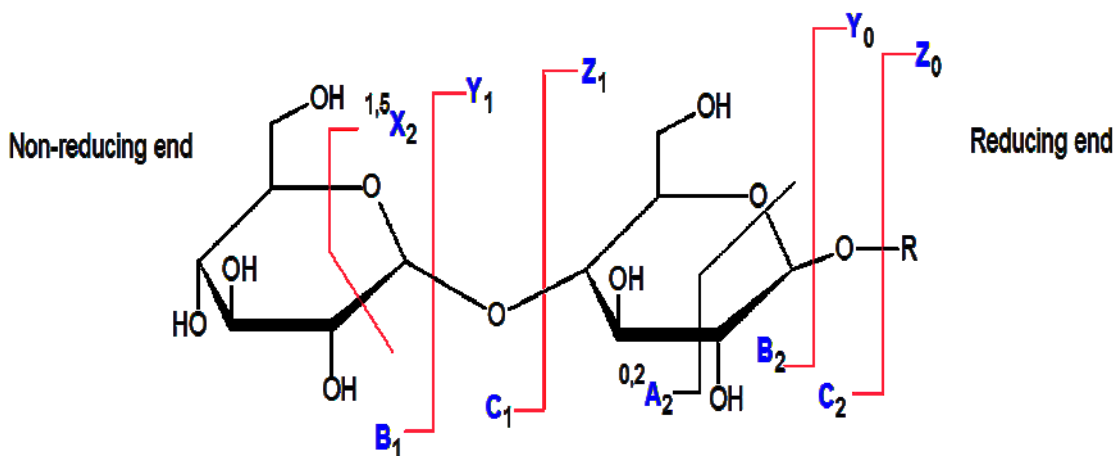


Figure 2.2: Likely paths of fragmentation for the period of CID-MS/MS of a glycoconjugate consequent to lactose as described in the Domon & Costello Nomenclature.¹⁰⁹

Chapter 3 : Materials and Methods

3.1 Lipopolysaccharides:

3.1.1 Bacterial culture:

T.P.T Evelyn (Department of Fisheries and Oceans, Nanaimo, British Columbia, Canada) provided a rough mutant strain of the *Aeromonas Salmonicida* bacteria, isolated from the Sockeye salmon. It was then given the numeric code description (Strain SJ-112, rough mutant, of the collection of the Northwest Atlantic Fisheries Centre, St. John's, NL, Canada). Between the stationary and late phase, the organisms were cultured within Trypticase Soy Broth, glucose was not added (Baltimore Biological Laboratories Inc.). The culture grew at 25°C for 20 hours. Aeration was set at 20-1/min in an MF-128S fermenter. The bacteria were killed by adding formalin at a 0.3% aqueous concentration. The process was conducted under room temperature with agitation for 16 hours. The centrifuge was set at 20,000 rpm to collect cells. A Sorvall SS-34 rotor was used for the centrifugation. Sodium chloride aqueous (0.15 M) was used to wash the cells which were finally stored at temperatures of -50° after being lyophilized. The cells stored at -50°C until the time they would be needed.

3.1.2 Lipopolysaccharide purification

The hot-phenol technique was used for the extraction of LPS.¹⁰¹ After extraction, the lipopolysaccharides were freeze-dried. Ten grams of the stored cells were suspended in 175 ml deionized water. The mixture was then heated up to 70° C.¹⁰¹ An additional

175 of aqueous 90% phenol was also added. The mixture was then stirred continuously for 20 mins at the same temperature. Ice was used to cool the mixture after the 20 minutes. The mixture was then centrifuged a second time using the Sorvall SS-34 rotor. This time the centrifuge is set at 3500 rpm. Aspiration was used to isolate the aqueous layer. The process was repeated two more times. The layers were then combined and water was used to dialyze in order to get rid of any phenol traces. Evaporation was used to reduce the volume of water in the mixture. Finally, the mixture was set on the centrifuge for three hours at a speed of 39,000 rpm. This process led to the suspension of the lipopolysaccharide pellet in water. The process of centrifuging the mixture was repeated two more times, as a result the lipopolysaccharide were lyophilized. Affi-prep beads (Bio-Rad Laboratories, Richmond, CA, USA) were then used for purification of the LPS isolates. Phosphate-buffered saline (15 ml) at 7.4 pH was used to suspend 15mg of LPS. Polymyxin beads were then mixed with the LPS solution. The beads were washed using sodium hydroxide first and afterwards also washed in distilled water. The LPS mixture was incubated for a whole night. The orbital shaker was set at 1500 rpm in order to agitate the mixture during the incubation duration.

The LPS mixture was then centrifuged for 10 minutes at 2500 rpm before the collection of the supernatant. Aqueous solution of sodium hydroxide (15 ml and 5 ml, 0.1 M) was used to wash the beads. After combining the supernatants, water was used to dialyse the LPS. Finally, the LPS was lyophilized.

3.1.3 Lipopolysaccharide hydrolysis

Aqueous 1% acetic acid at a temperature of 100°C was used to hydrolyze 100 mg of LPS for duration of 90 minutes. The mixture was then centrifuged for 30 minutes at 3000 rpm. This centrifugation process resulted in Lipid A precipitation. The aqueous media contained the polysaccharide. Water was used to wash Lipid A after removal. Chromatography (using Sephadex G-50) was used to recover the main oligosaccharide from the supernatant. Differential refraction (Water Associates) was used to visualize the fractions.

3.2 Mass spectrometric analysis of lipid A

3.2.1 Electrospray quadrupole fourier transform ion cyclotron mass spectrometry

An Apex Qe 7.0 Bruker Fourier Transform Ion Cyclotron Mass Spectrometer (FT-ICR-MS) was used to perform the mass spectrometry. The FT-ICR MS contains four segments. These include the ICR cell, ion transfer optics, a quadrupole region, and the gas phase ion phase. Electrospray ionization is used to initially generate gas phase ions from the solution. Afterwards, the ion are pushed through a quadrupole filter into a collision cell. Minimizing the flow of Ar gas and introducing a solvent past the separation of the cell and solvent reservoir produces the solvated ions.

Methanol and chloroform in ratio of 1:1 with 0.1% TMA/ Milli-Q water was used to dilute Lipid A. The mixture was then underivatized in the negative ion mode. The conditions that were used are: 8.00 l/min dry gas, 40 volt skimmer, 1.7 volt quadrupole,

scan beginning at m/z 500 then stopping at m/z 2000, the accumulation time was 200000 μs .

3.2.2 Electrospray quadrupole-hexapole-quadrupole mass spectrometry

A Micromass Quattro II mass spectrometer was used to record the ESI mass spectrum. The device had a mega flow source that had the ability to analyze ions at m/z 4000. A Compaq PII personal computer (266 MHz, with Windows NT 4, service pack 3) was installed with the MASSLYNX 3.2.0 Mass Spectrometry Data System application. The software application was important in acquiring and processing data. The ESI source temperature as set at a steady 75°C . The capillary of the ESI was operating at 3.0 kV. During this operation, the high power lens was operating at 0.40. A 25 volt cone voltage was used to record the ESI-MS.

3.2.3 Matrix-assisted laser/desorption ionization time-of-flight mass spectrometry (MALDI-TOF-MS)

The α -cyano-4-hydroxycinnamic acid matrix that was employed had a 1:2:2 water, acetonitrile, methanol concentration of 5 mg/ml. The ratio of the mixture was 1:2:2. The concentration of the Lipid A that was used was 2 mg/ml in a mixture of methanol and chloroform. The volume ratio of the mixture was 1:1. The sample that was prepared contained the same volumes of a solution of α -cyano-4-hydroxycinnamic acid and a solution of Lipid A. After the two solutions had been mixed, 1 μl was used for spotting the MALDI plate. After the spot had crystalized and dried it was loaded into a MALDI-MS instrument.

It was possible to isolate Lipid A mass spectra from the bacterium in the negative ion mode. This experiment used a MALDI-TOF/TOF-MS spectrometer (MALDI 4800, Applied Bioscience). The mass of the data that was acquired ranged between 600 and 2000 m/z . A 337 nm nitrogen laser had been used in the MALDI-TOF/TOF-MS equipment. The spectra were observed as 600 different laser shots. The accelerating voltage had been set at 25 kV. The guide wire that was used for focusing had a comparative potential of 0.18%. The intensity of the laser that was used in the experiment was 4200. The mass accuracy of the instrument was quite high at 5 ppm. The resolution was between 15000 and 25000 (FWHM). The ratio of signal (minimum) to noise had been set at 35.

The same instrument was used in conducting the collision dissociation MS (CID-MS/MS). A collision cell with high CID was employed in inducing the scans of product ion of the masses that had been selected. A TOF analyzer was used to analyze the product ions that resulted. Air was used as the collision gas in achieving analyses of mass spectrometry. The collision energy was set at 1 KV. The potential corresponds to the difference of the floating cell potential (7KV) and the accelerating voltage of 8KV.

3.2.4 The MALDI-TOF/TOF-MS spectrometer of partial de-acylation of ester-linked to the acyl group of lipid A

By using sodium methoxide in methanol, it was possible to partially liberate the ester fatty acid from the bacterium Lipid A. Dry ice was then used for neutralization. Afterwards a MALDI-TOF/TOF-MS spectrometer was used to analyze the sample that was collected. The conditions were as in the previous experiment. The same instrument was used to conduct collision dissociation at high energy (CID-MS/MS). A collision cell at high CID was used to induce the scans of product ions of the masses that had been selected.

High-energy collision dissociation MS/MS (CID-MS/MS) experiments were conducted using the same instrument. Product ion scans of selected masses were induced by a high CID collision cell. A TOF analyzer was used to analyze the product ions that resulted. Nitrogen was used as the collision gas. The collision energy was set at 1 KV. The potential corresponds to the difference of the floating cell potential (7 KV) and the accelerating voltage of 8 KV. The pressure of nitrogen gas (collision gas) was increased in order to enhance sodium ion dissociation.

Chapter 4 : Lipid A Analysis Using FTICR-MS and Low Energy SORI-CID-FTICR-MSⁿ

4.1 Background:

In recent times, LPS has elicited interest in diverse research. Since LPS forms an essential component of the outer membranes of Gram negative bacteria cells. Research has already determined that derivatives of LPS carry significant potential for the development of bacterial vaccines.^{110, 111}

It has been established that Lipid A can become an adjuvant for the treatment of immune illnesses,¹¹²⁻¹¹⁴ and has also been recommended as a possible anticancer agent.¹¹⁵⁻¹¹⁷ In order for Lipid A to be used for therapeutic purposes however, its exact structure has first to be determined. Different analytical methods such as nuclear magnetic resonance spectroscopy, X-ray diffraction and Fourier transform spectroscopy, have been important in determining the chemical composition of moieties of Lipid A.¹¹⁸⁻¹²² Early mass spectrometry techniques were also applied to establish the chemical structure of extracts of Lipid A.¹²³⁻¹²⁵ Recently, ESI-MS and MALDI-MS have also been applied for the same purpose.¹²⁶⁻¹²⁸

Extracts of Lipid A are composed of mixtures that have different Lipid A constituents. The mixtures of major and minor component are due to the incomplete biosynthesis of Lipid A. The differences in the mixture are with regard to the lengths of

the fatty acid chains and the substitution and saturation of the phosphate groups by glycosyl groups and ethalumine groups.^{127, 129, 130}

Today, both FT-ICR and MALDI-TOF-TOF mass spectrometries are applied in differentiating and elucidating the structure of the major components of Lipid A from *A. salmonicida* bacterium. The analyses have also been important in illustrating the fragmentation patterns of the Lipid A. In the future, the data can be important to researchers needing to determine the structures of other lipid As, and in conducting studies on the formulations of the compound. .

The majority of the Gram-negative bacteria can synthesize lipid A in order to synthesize extra cellular monolayer characteristic of the outer membrane (OM) (Figure 4.1). As well, the Lipid A biosynthetic pathway occurs from either a constitutive (conserved) or from some variable (modification) components. The constitutive backbone of lipid A is mainly synthesized from various intracellular enzymes present virtually in every Gram-negative bacteria and are not highly subjected to regulation. On the other hand, the backbone of variable lipid A is mainly synthesized from various extra-cytoplasmic enzymes that may vary from one organism to another.¹³³

The advanced biochemical modifications specifically in case of lipid A are basically formed with several enzymes located in the outer membrane, or even on the periplasmic surface of the inner membranes.¹³⁴ Furthermore, these enzymes can also be induced because of some changes taking place in the various bacterial growth conditions,

namely pH changes, divalent cation concentrations as well as presence of some anti-microbial peptides.

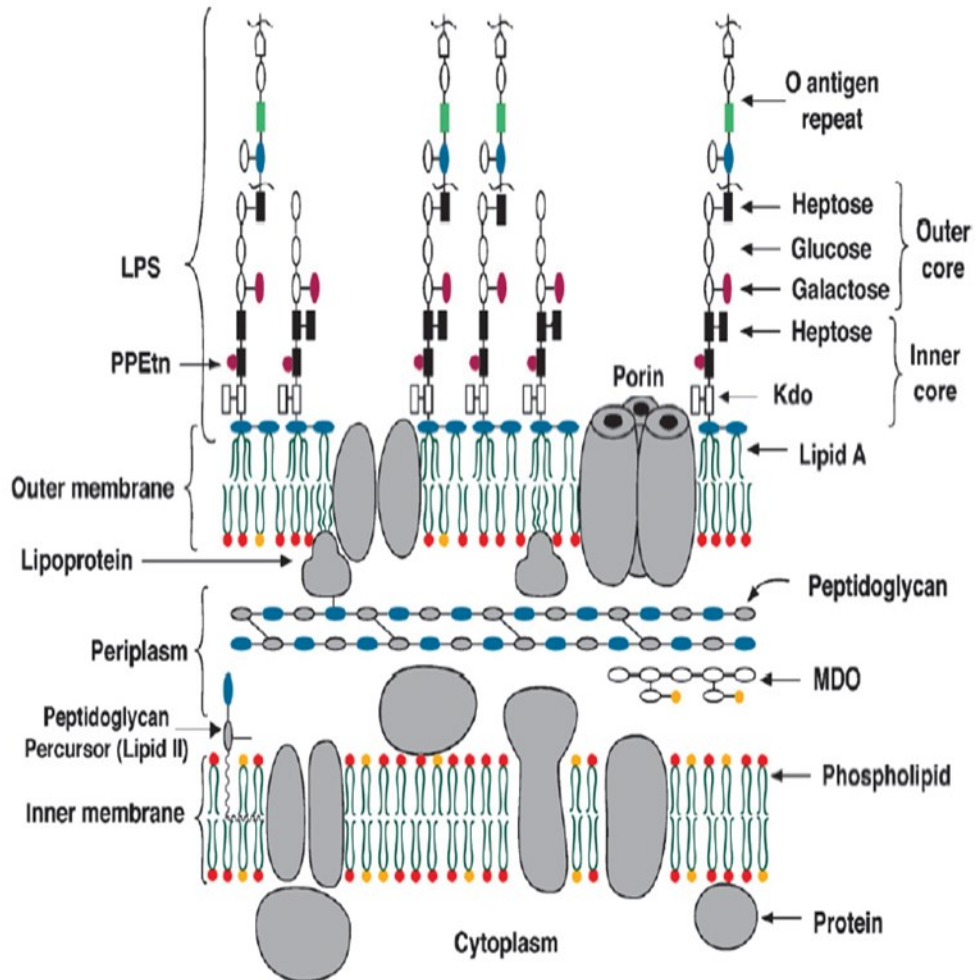


Figure 4.1: Schematic structure of the *E. coli* K-12 cell envelop.¹³⁴

4.1.1 Biosynthesis of Lipid A:

There are around nine enzymes associated with the constitutive Lipid A pathway.¹⁴⁹ In addition to this, only a single-copy of the genes that encode these enzymes are present, which are mainly conserved in almost every Gram-negative bacteria such as *E. coli*. Despite this, for a simple organism such as *Sphingomonas*, it has been shown the organism was basically formed during the biosynthesis of specific bioactive sphingolipids rather than Lipid A.¹³⁵⁻¹³⁷ In addition to this, 2,3-diacetylglucosamine 1-phosphate (labeled a LpX) mainly facilitates the overall systematic determination of this highly constitutive pathway associated with lipid A biosynthesis.

In this regard, Figure 4.2 mainly represents the entire constitutive pathway for the biosynthesis of Lipid A mainly in which LpxA, C as well as D are basically the soluble proteins, and in addition to this, both LpxB along with LpxH are mainly the peripheral membrane proteins whose chemically structures are not reported yet.¹³⁸

The first step in the entire Lipid A biosynthesis mainly occurs after the fatty acylation by the thioester *R*-3-hydroxymyristoyl acyl carrier protein (denoted by ACP), which is catalyzed through LpxA, occurs on the specific uridine diphosphate *N*-acetylglucosamine (UDP-GlcNAc), (Figure 4.2).¹²³ The *E. coli* LpxA basically functions as a highly precise β -hydrocarbon scaffold connecting the C14 hydroxyacyl to the hydroxyl groups of the uridine diphosphate *N*-acetylglucosamine (UDP-GlcNAc). This acylation has been shown to be faster by two order magnitude even when compared to

C12 to C16 chains. Furthermore, the equilibrium constant (0.01 units) mainly for the UDP-GlcNAc acylation by LpxA mechanism is unfavorable.^{139, 140}

Additionally, it was shown that LpxC is mainly a Zn²⁺-dependent enzyme greatly conserved for almost every Gram-negative bacteria.¹⁴¹ It also possesses no sequence similarity when compared to either deacetylases or amidases and can efficiently play an important role as the target for a wide range of antibiotics. Even more recently, LpxC was revealed to slow down and to tightly bind inhibitors having lower nM affinity (known also as *N*-aroyl-L-threonine hydroxamates).

The next step in the Lipid A biosynthesis occurs when the second important *R*-hydroxymyristate chain is next added up monoacylated uridine diphosphate *N*-acetylglucosamine (UDP-GlcNAc) through LpxD for formation of UDP-2,3-diacyl-GlcN.

Furthermore, the integral membrane proteins including LpxK, LdtA, LpxL, as well as LpxM actively catalyze five steps which take place at the end of constitutive pathway. It was shown that only a single segment of membrane-spanning appears for every protein mainly at its *N*-terminus. When considering the active sites then, these were presumed for facing the inner membrane's cytoplasmic surface. After this, LpxK mainly phosphorylates the 4'-position for the formation of intermediate Lipid A, labeled as IV_A, which can then serve as the endotoxin antagonist specifically in different human cells; whereas, endotoxin is mainly an agonist in mice.¹⁴²

This overall variable pharmacology of Lipid A was identified due to the existence of Lipid A receptor specifically of the mammalian innate immune system that was called as the TLR4 or MD2 complex.¹⁴³ One should also note that the much labile nucleotide CMP-Kdo that is derived from arabinose 5-phosphate was also Kdo donor.¹⁴⁴

At the end, Lipid A biosynthesis mainly involves the addition of another secondary laurate as well as myristate chains mainly by LpxL along with LpxM displaying specific sequence similarity to one another and are greatly linked to the lysophosphatidic acid acyltransferases.¹⁴⁵

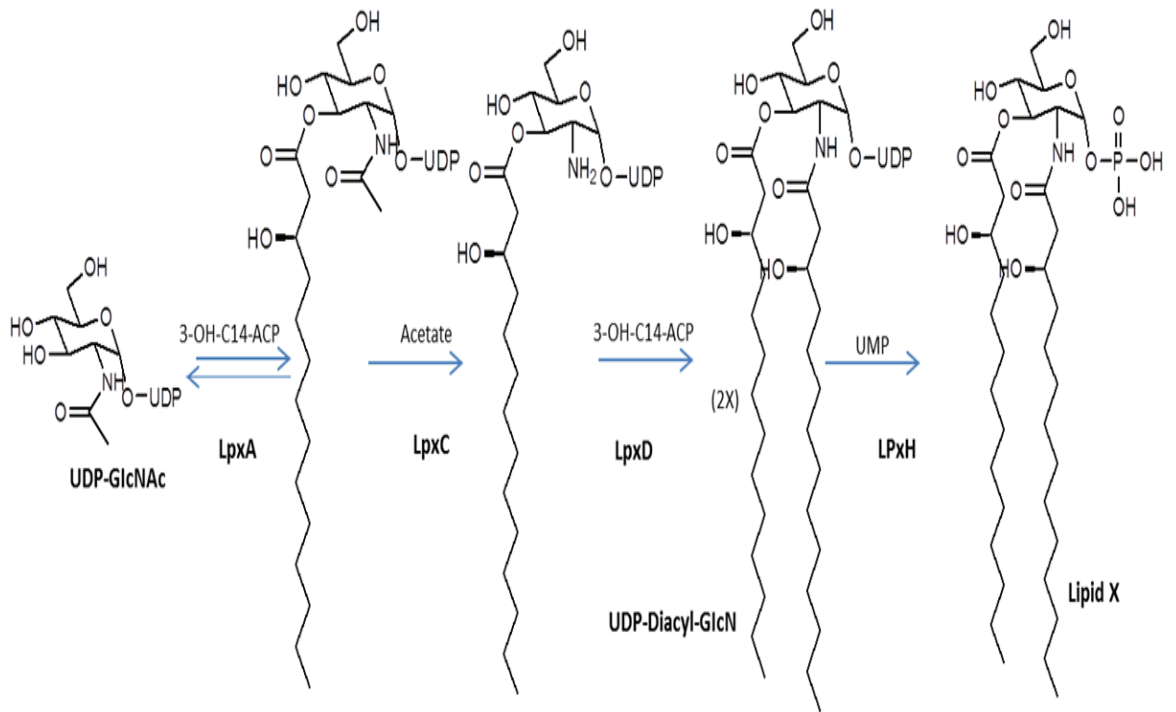


Figure 4.2: The constitutive pathway of Kdo2-lipid A biosynthesis in *E. coli*

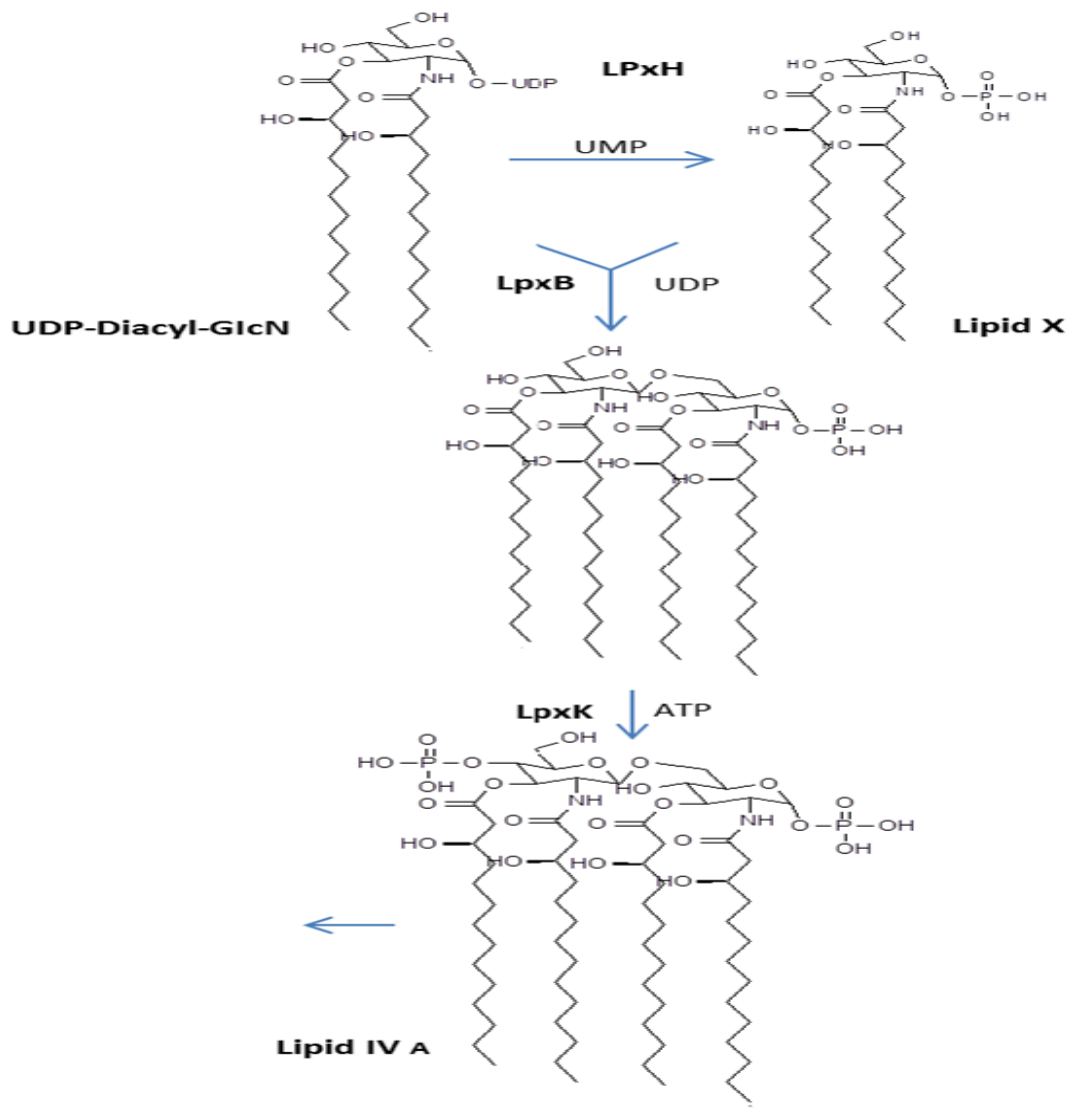


Figure 4.2, continued: The constitutive pathway of Kdo₂-lipid A biosynthesis in *E. coli*

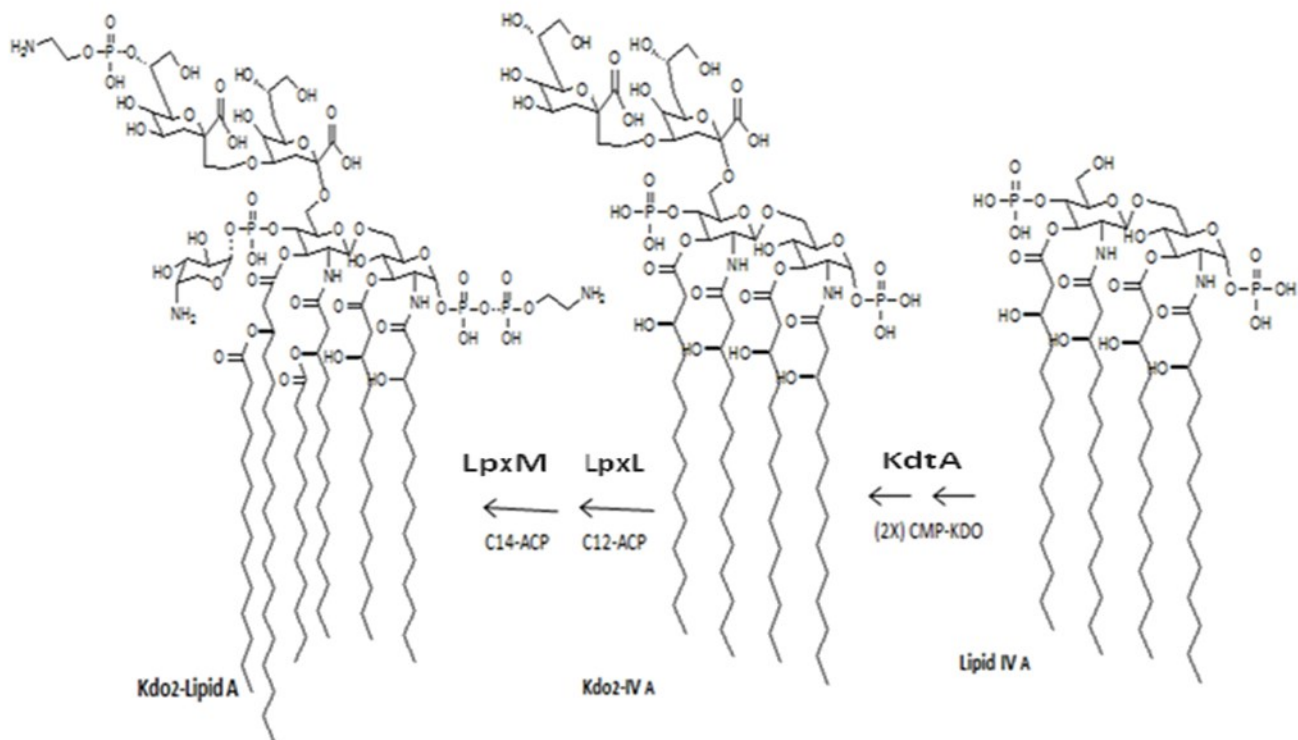


Figure 4.2, continued: The constitutive pathway of Kdo2-lipid A biosynthesis in *E. coli*

4.1.2 The enzymatic pathway modification of *E. coli* and *Salmonella* Lipid A biosynthesis *E. coli* and *Salmonell*:

It has been shown that Lipid As in case of both *E. coli* K-12 along with *S. typhimurium* can further be modified with the help of some enzymes such as phosphoethanolamine, palmitate as well as L-Ara4N, and an example of these structures is illustrated in Figure 4.3.¹⁴⁶ *S. typhimurium* contains two selective deacylases along with a dioxygenase and these can further modify enzymes that are regulated specifically in the presence of changes taking place in their overall growth conditions.¹⁴⁷

The attachment of the L-Ara4N with the help of enzyme ArnT can be further induced in response to inactivation by the PmrA transcription factor because of exposure of bacterial cells to either mild acidic or to the constitutive mutations occurring in *pmrA*. Furthermore, the biosynthesis along with the mechanism of attaching it to the Lipid A has been determined.¹³⁵ The first step in this biosynthesis is principally the oxidative decarboxylation specifically of UDP-glucuronic acid done by C-terminal domain specific to ArnA for formation of the UDP-4-ketopentose. After this step, some considerable quantities of UDP-L-Ara4N was obtained after when UDP-4-ketopentose was actively transaminated with the help of ArnB and followed by this, it was mainly formed by systematic formylation of the N-terminal domain for formation of ArnA. ArnA along with ArnB are basically the soluble proteins and in addition to this, their associated structures are mainly identified by using X-ray studies.¹⁴⁸

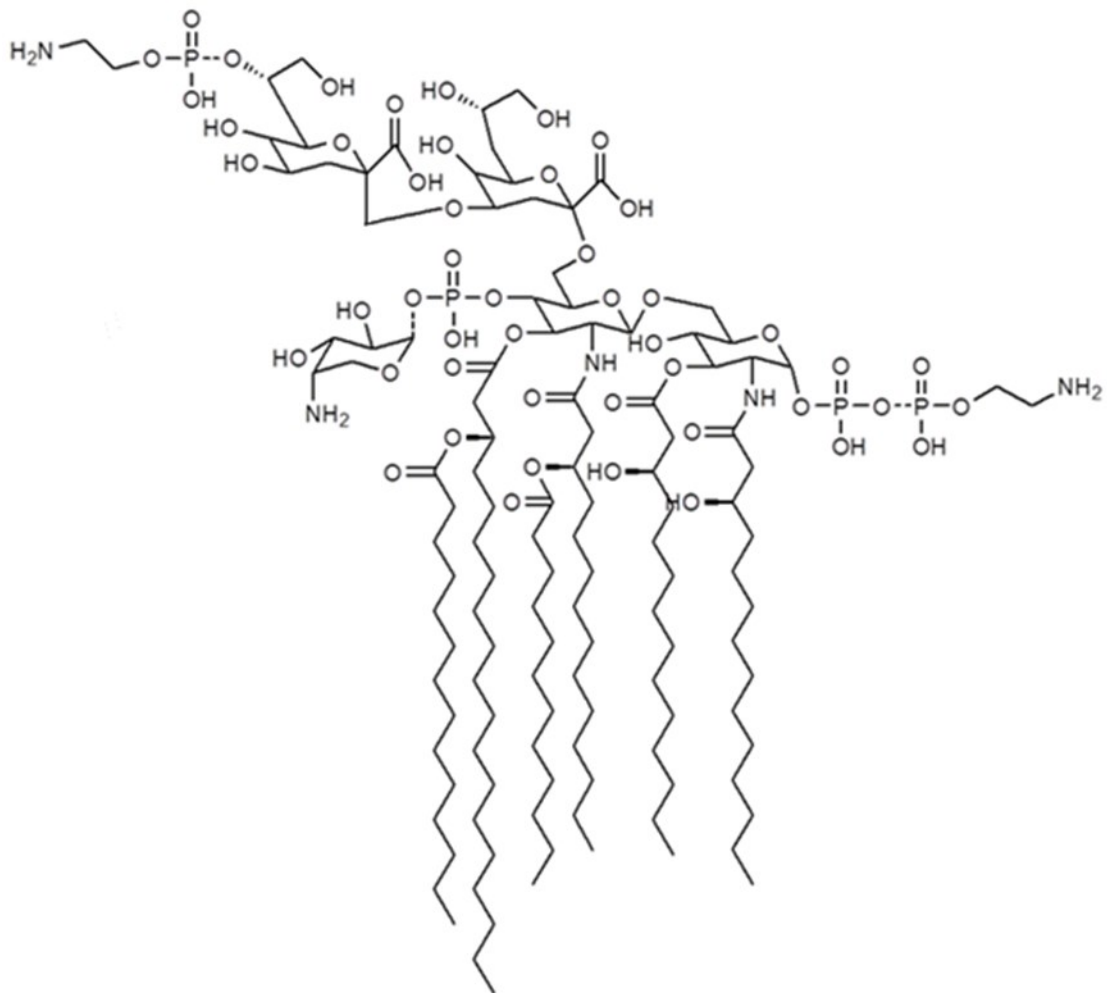


Figure 4.3: Covalent modifications of Kdo2-lipid A in *E. coli* K-12 and *Salmonella*.

It is extremely important to note and understand that these Lipid A extracts are typically formed as a specific micro-heterogeneous mixture that is further composed of a significant Lipid A component as well as other minor products. Thus, this heterogeneity can typically result from either complete or incomplete Lipid A biosynthesis and is

known to differ mainly in the overall composition of length of fatty acid, saturation as well as substitution of the phosphate with the help of ethanolamine as well as various glycosyl groups.⁹⁷

In this specific chapter, MALDI- ionization in a TOF/TOF tandem mass spectrometer is used for differentiating as well as elucidating the molecular structure of the major constituents of the native isolated Lipid As from *Aeromonas salmonicida* SJ-112.

Furthermore, CID-MS/MS analysis revealed the major routes of gas-phase fragmentation of different constituents associated with incomplete biosynthesis of Lipid A mixture. The structural identification data about this biological compound could be used for further evaluation of Lipid A and also for performing different quantitative studies

4.2 ESI-FTICR-MS Analysis

ESI-FT-ICRMS (negative ion mode) obtained for Lipid A of *Aeromonas salmonicida* SJ-112 displayed an incomplete biosynthesis as illustrated by the multiple molecular ions shown in Figure 4.5. The ESI-FTICR-MS showed *inter alia* seven different deprotonated molecules having related structures of the Lipid A. The fragment ions were tentatively assigned as the following: LipA1 at m/z 1768.2056, lipA2 at m/z 1744.2209, LipA3 at m/z 1688.2356; and four most abundant ions LipA4 at m/z 1586.0259, LipidA5r at m/z 1506.0586, Lipid A6 at m/z 1359.8266 and Lipid A7at m/z 1279.8676.

As a result, the lower intensity fragment ion LipA1 at m/z 1768.1491 was assigned to the deprotonated molecules of the biphosphorylated Lipid A moiety bearing a phosphate group on each sugar and containing two units of the branched 14:0(3-(*R*)-*O*-12:0) fatty acid and 2 units of (*R*)-14:(3-OH) fatty acid. At this point of time, the exact positions of these fatty acids on O-3, O-3', N-2, N-2' are not known.

The monophosphorylated Lipid A was also observed as major ions at m/z 1744.2209 for lipA2 and at m/z 1688.2365 for LipA3 both carrying four (*R*)-14:0 (3-OH) (primary fatty acid) located on the N-2, O-3, N-2', and O-3' positions of the Lipid A disaccharide. However, for the fragment ions at m/z 1744.2209; it contained an extra 16:0 branched fatty acid at 14:0(3-(*R*)-*O*-12:0) and one 12:0 branched fatty acid at 14:0(3-(*R*)-*O*-12:0)..

For the deprotonated molecule of LipA1 at m/z 1768.1491, we proposed that the N-2' was acylated with one branched 14:0(3-(*R*)-*O*-12:0) fatty acid at from N-2' position and another branched 14:0(3-(*R*)-*O*-12:0) fatty acid at the N-2 position.

For the deprotonated molecule LipA3 at m/z 1688.2209, we suggested that the two branched 14:0(3-(*R*)-*O*-12:0) fatty acids were located on the N-2' and N-2 positions. When this tentative structure is compared to the fragment ion at m/z 1768.1491, it suggests that LipA1 has lost its HPO_3 at the reducing or the non-reducing sugar group to form LipA3.

On the other hand for the deprotonated molecule LipA2, it was proposed that the fragment ion at m/z 1744.2209 contained two branched 14:0(3-(*R*)-*O*-12:0) fatty acid at the N-2' and at the N-2 positions, (Figure 4.5).

In addition, two most abundant ions at m/z 1586.0259 LipA4 and at m/z 1359.8266 LipA6 were tentatively attributed to the biphosphorylated lipid A forms for the deprotonated molecule LipA4 m/z 1586.0259 carrying four (*R*)-14:0(OH) (primary fatty acid) on the N-2, O-3, N-2' and O-3' positions of the lipid A disaccharide, and one branched 14:0(3-(*R*)-*O*-12:0 at N-2'. Furthermore, the deprotonated molecule at m/z 1359.8266 for LipA6 was attributed to contain the biphosphorylated lipid A carrying three (*R*)-14:0(OH) fatty acid located on either the N-2, O-3 and N-2' positions of the lipid A disaccharide; one branched 14:0(3-(*R*)-*O*-12:0) fatty acid located on N-2' position, (Figure 4.5). It should be noted that the mass difference of 228 Da between the fragment ions at m/z 1586.0259 for LipA4 and at m/z 1359.8266 for LipA6 indicated the elimination of a C14-acid at the O-3 position from the ions at m/z 1586.0259 LipA4.

Moreover, two most abundant fragment ions at m/z 1506.0586 and m/z 1279.8676 were assigned to LipA5 and to LipA7 respectively. These ions were tentatively attributed to the mono-phosphorylated pentaacylated forms for the deprotonated molecule LipA5 at m/z 1506.0586 carrying four (*R*)-14:0(OH) (primary fatty acid) on either of the N-2, O-3, N-2' and O-3' positions of the lipid A disaccharide, one branched 14:0(3-(*R*)-*O*-12:0 fatty acid at position of at N-2 position at m/z 1506.0511. The deprotonated molecule LipA7 at m/z 1279.8676 was attributed to the mono-

phosphorylated tetraacylated forms carrying three (*R*)-14:0 (OH) (primary fatty acid) on either the N-2, O-3 and N-2' positions of the lipid A disaccharide; one branched 14:0(3-*R*)-*O*-12:0) fatty acid on position at N-2' position, (Figure 4.5). It should be noted that the mass difference of 228 Da between the ions LipA5 at m/z 1506.0511 and the ions LipA7 at m/z 1279.8676 indicated the elimination of a C14-acid at the O-3' position from the ions at m/z 1506.0511 for LipA5.

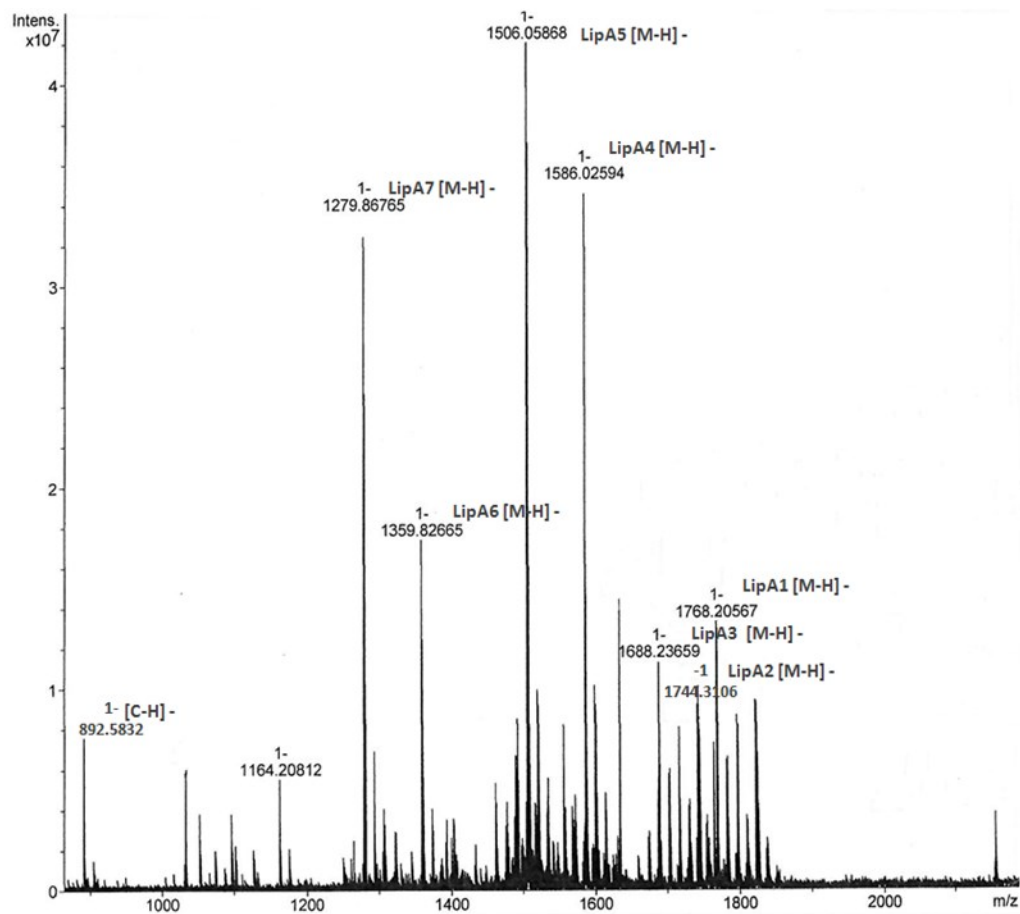


Figure 4.4: Negative ion FT-ICR-MS of the heterogeneous mixture of native lipid As extracted from *Aeromonas salmonicida* SJ-112.

The proposed structures of the biphosphorylated, monophosphorylated Lipid A and its distinctive fragment ions observed in the FT-ICRMS are illustrated in Figure 4.4.

It should be noted, that at this stage of this study, the positions of the esterified fatty acids were tentatively assigned and that there were many other possible structures for this Lipid A.

The theoretical structure shown in Figure 4.5 corresponds to a biphosphorylated Lipid A with a theoretical $[M-H]^-$ at m/z 1586.0586 LipA4 and at m/z 1359.8266 LipA6 respectively and a monophosphorylated Lipid A with a theoretical $[M-H]^-$ at m/z 1506.0586 LipA5 and at m/z 1279.8676 LipA7 respectively.

The fragment ions at lower m/z values and their intensities were tentatively assigned as different mono-phosphorylated species containing one D-GlcN devoid of 14:0 acid and 14:0(3-OH) acid m/z 892.5934, 14:0(3-OH) acid and 12:0(OH) ketene m/z 708.2501. These lower fragment ions of lower m/z value ions are explained by the partial degradation of Lipid A during work-up and acid liability of some acylchains and phosphate group at O-1 position during the acid hydrolysis.

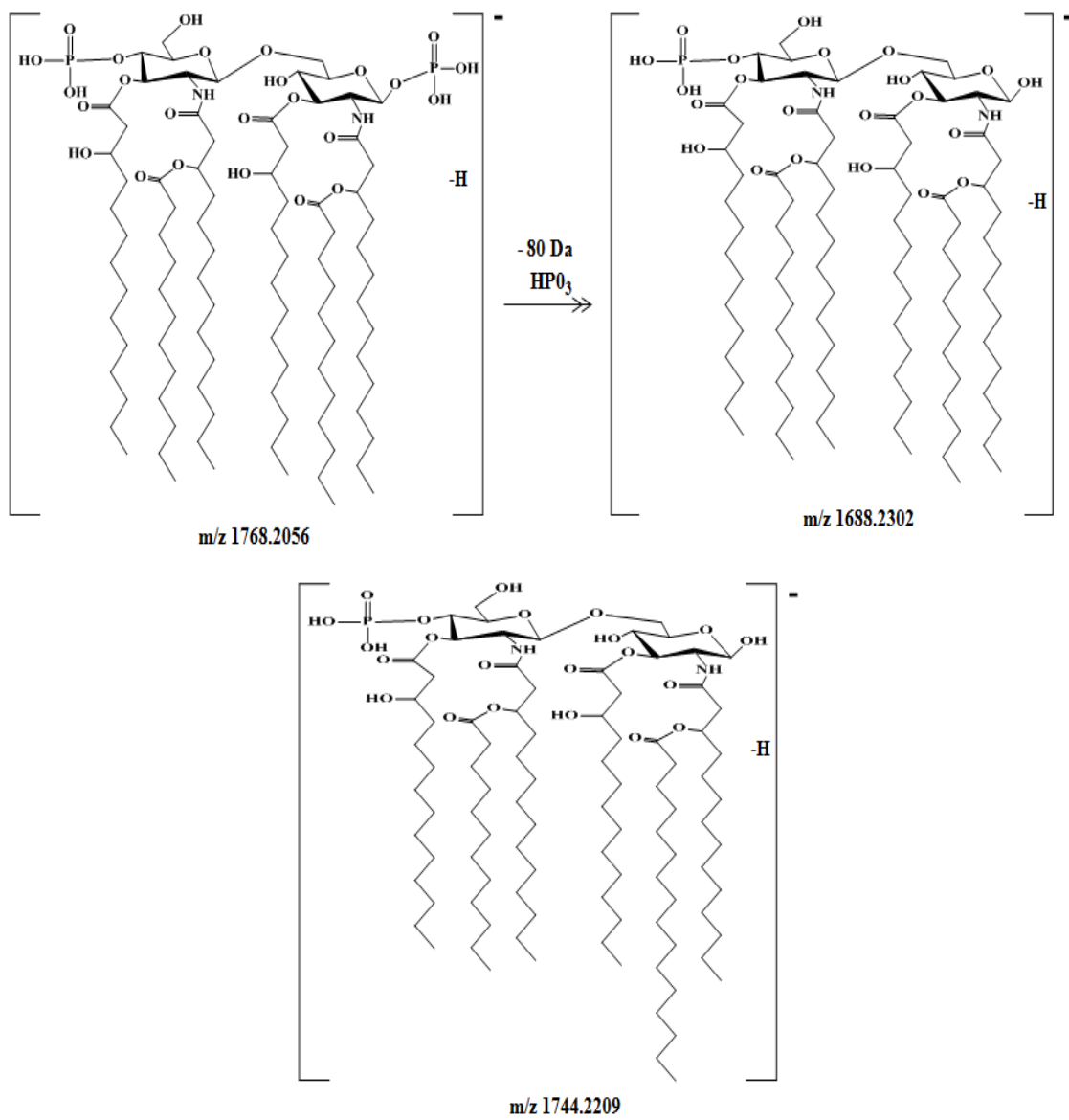


Figure 4.5: The seven proposed structures of the native Lipid A extract from *Aeromonas salmonicida* SJ-112.

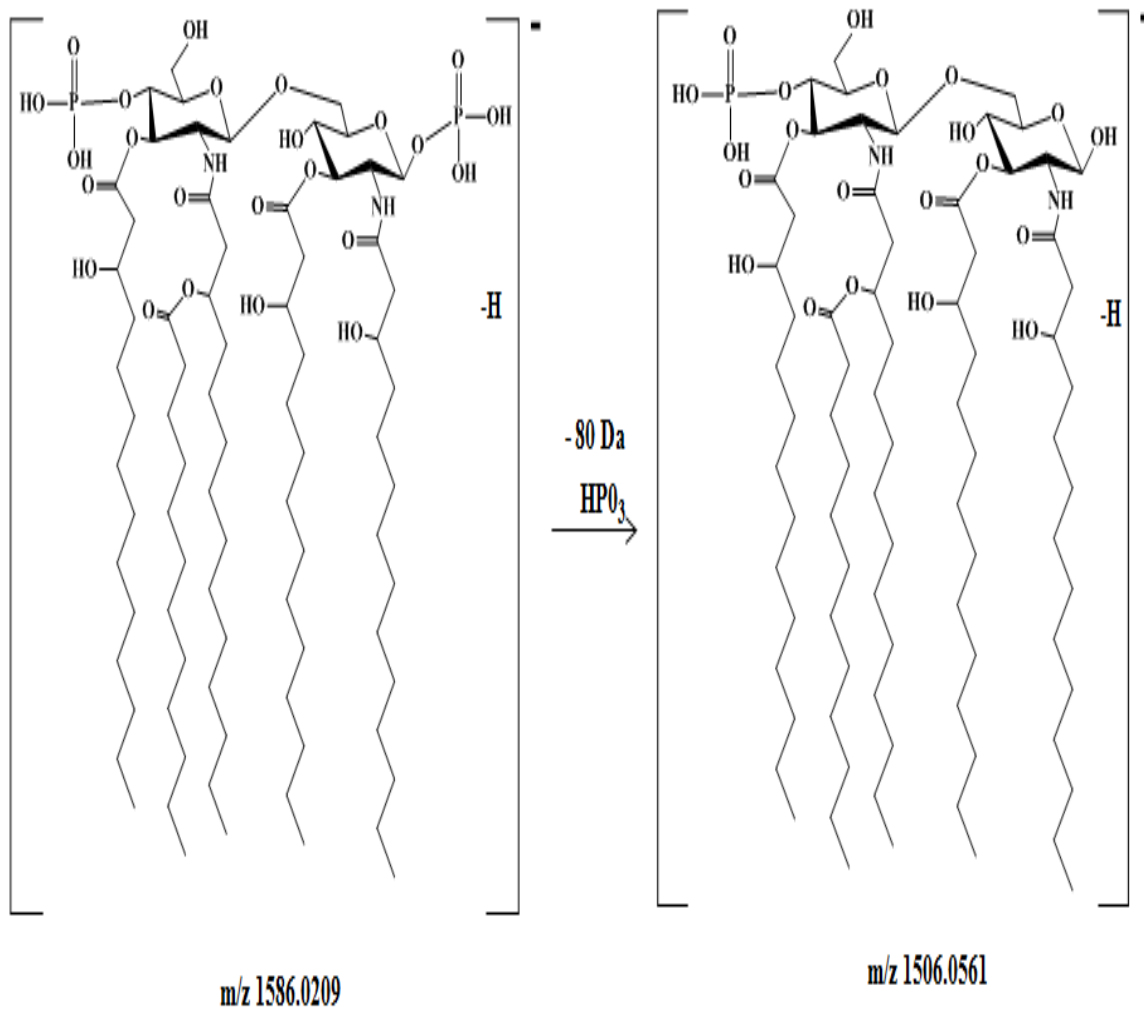


Figure 4.5, continued: The seven proposed structures of the native Lipid A extract from *Aeromonas salmonicida* SJ-112.

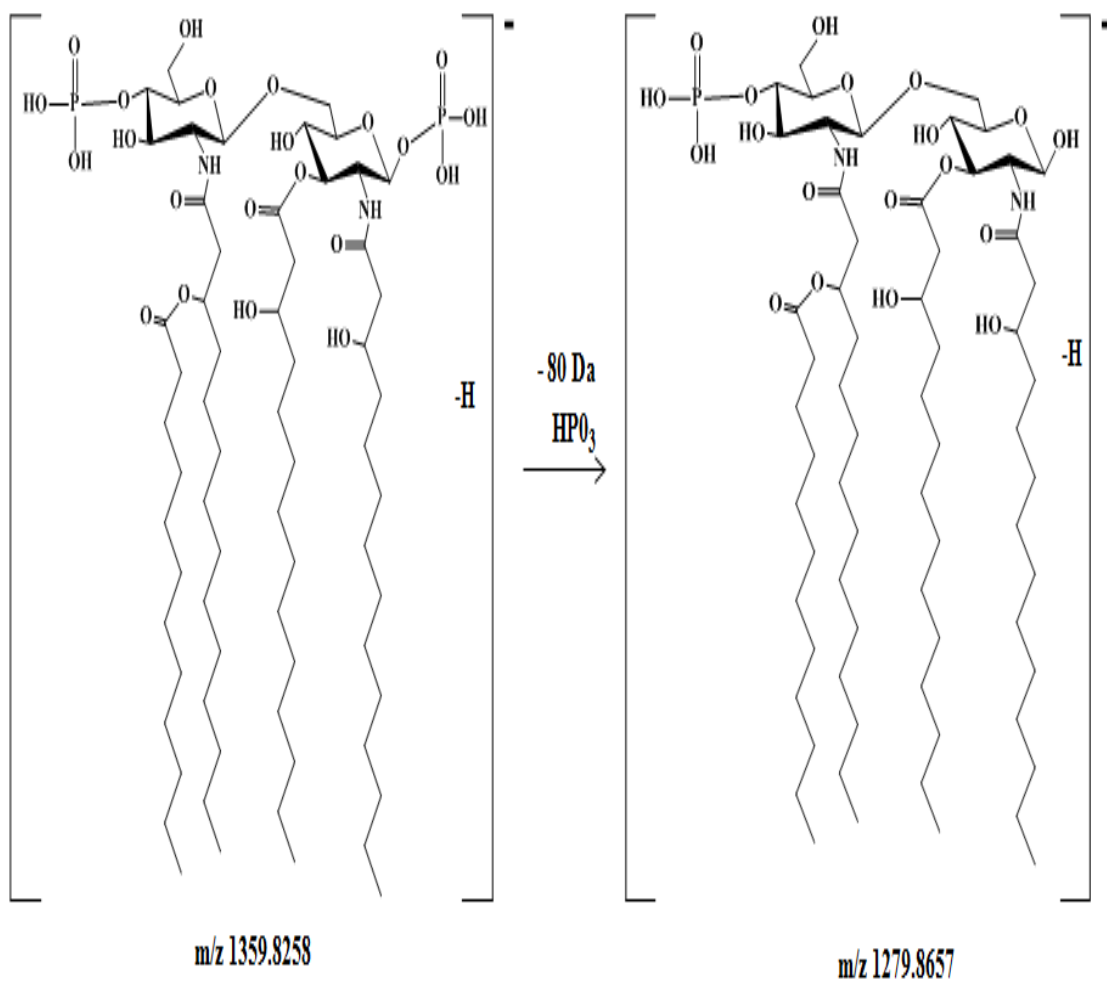


Figure 4.5, continued: The seven proposed structures of the native Lipid A extract from *Aeromonas salmonicida* SJ-112.

It is important to note that some of these low value m/z ions can be also explained by their gas-phase fragmentation in the conventional ESI-MS scan. Accordingly, it was noted that the glycosidic bond cleavages could be induced by the conventional ESI-MS

cone fragmentation, hence providing useful structural information and sugar sequencing of complex carbohydrates. In the ESI-MS medium m/z values, a distinctive ion, at m/z 892.5975 was observed and it was assigned as the $[C-H]^-$ ion, which is shown in Figure 4.6. This fragment ion represents the non-reducing GlcN residue formed during the biosynthesis of the complete Lipid A.¹³¹

The assignment of the ions observed in the simple one-stage high-resolution MS analysis is based on the exact molecular masses only, and additional evidence is required to validate these assignments. Therefore, without further confirmation, it would be impossible to suggest various constitutional isomer structures for this Lipid A mixture. For example, all the proposed ion structures shown in Figure 4.4 could also be correct if, instead, the fatty acid acylation on the disaccharide backbone were reversed.

For this reason, the use of tandem mass spectrometry permitted the identification of the diagnostic product ions and also confirmed the proposed molecular structures. Indeed, the structures shown in Figure 4.4 were confirmed with a detailed MS/MS analysis of selected molecular anions, as described in the following sections. As a result, the different proposed structures of the deprotonated molecules attributed to LipA1 to LipA7, which were obtained in the conventional single stage MS, have now been tentatively confirmed.

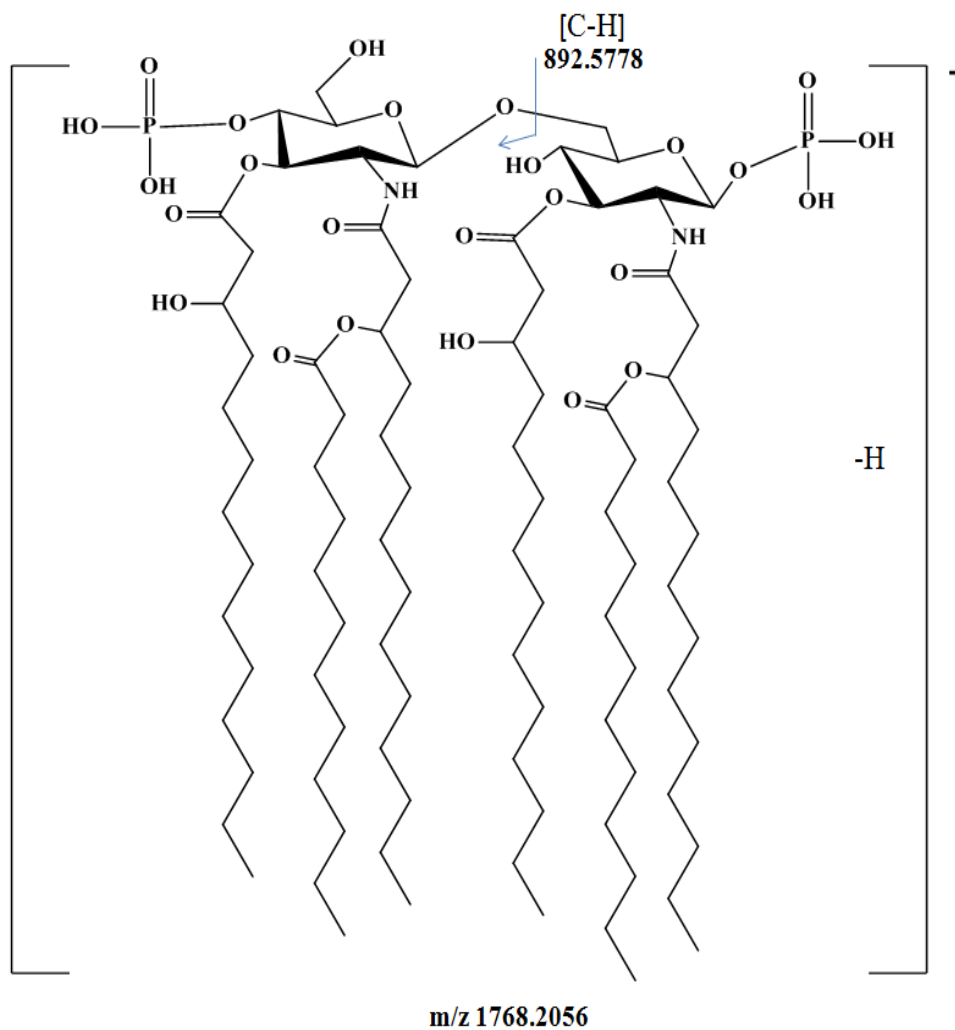


Figure 4.6: Schematic representation of the one of the possible common structures of Lipid A and the diagnostic ion of [C-H]⁻ observed in the FT-ICR-MS spectrum.

4.3 CID- FT-ICR-MS/MS analysis of the heterogeneous mixture of lipid As

The distribution of the fatty acids was determined for the Lipid A isolated from *Aeromonas salmonicida* SJ-112 by multiple-stage ESI-MS² CID. The detected product ions were interpreted according to the rules described previously in the ESI-CID-MS²

studies of Lipid A.¹³² ESI-MS² of the precursor ions at m/z 1768.8732 for LipA1 (Figure 4.7), m/z 1744.2209 for LipA2 (Figure 4.9), m/z 1688.2356 for LipA3 (Figure 4.11), m/z 1586.0586 for LipA4 (Figure 4.13), m/z 1506.0511 for LipA5 (Figure 4.15), m/z 1359.8266 for LipA6 (Figure 4.17), and m/z 1279.8676 for LipA7 (Figure 4.19) were performed to determine the distribution of fatty acids on the disaccharide Lipid A backbone. Moreover, to determine the exact location of the phosphate group at m/z 892.5778 (Figure 4.21) similar CID-MS² experiments were performed.

4.3.1 MS/MS of the precursor ions at m/z 1768.8732 isolated from LipA1

The location of the fatty acid acyl group distributions was determined by performing by MS/MS of the ion at m/z 1768.8732 for LipA1 observed in the ESI-MS of Lipid A preparations from *Aeromonas salmonicida* SJ-112 (Figure 4.7). On the basis of the chemical structure proposed for this Lipid A constituents and after MS/MS analysis, this ion was assigned to the biphosphorylated, hexa-acylated Lipid A form, containing two GlcN residues, two P groups, four (*R*)-14:0(3-OH) groups on the N-2, O-3, N-2', and O-3' positions, and two 12:0 fatty acids on the 14:0(3-(*R*)-O-12:0) at the N-2 and N-2' position.

The most abundant product ion at m/z 1243.34909 was formed by the by the consecutive elimination of the C14 (3OH) acid from the C-3' of the non-reducing GLcN' residue (244 Da), the loss of C12:0 Ketene (200 Da) from the branched 14:0(3-(*R*)-O-

14:0) present on the N-2 position and elimination of HPO₃ (80 Da) from the reducing GlcN residue of the precursor ion at *m/z* 1768.8732.

The product ion at *m/z* 1035.74947 was formed by the consecutive losses of two molecules of 14:0 fatty acid (-488 Da) of the C-3 and C-3' positions of both GlcN residues, followed by elimination of a C12:0 acid from 14:0(3-(R)-O-14:0) branched fatty acid from the N-2 position and elimination of HPO₃ of the reducing GlcN, sugar group of the precursor ion at *m/z* 1768.8732.

It is interesting to note that the ^{0,4}X₁ product ion was identified at *m/z* 708.6617. This product ion results from the X-cleavage at the 0.4 positions of the cyclic pyranose ring of the reducing GlcN residue, followed by the elimination of the 14:0 fatty acid from the C-3 position. This product ion is diagnostic for the presence of the branched 14:0(3-(R)-O-14:0) present on the N-2' position of the non-reducing GlcN residue, containing a phosphate group on the C-4' position (Figures 4.8).

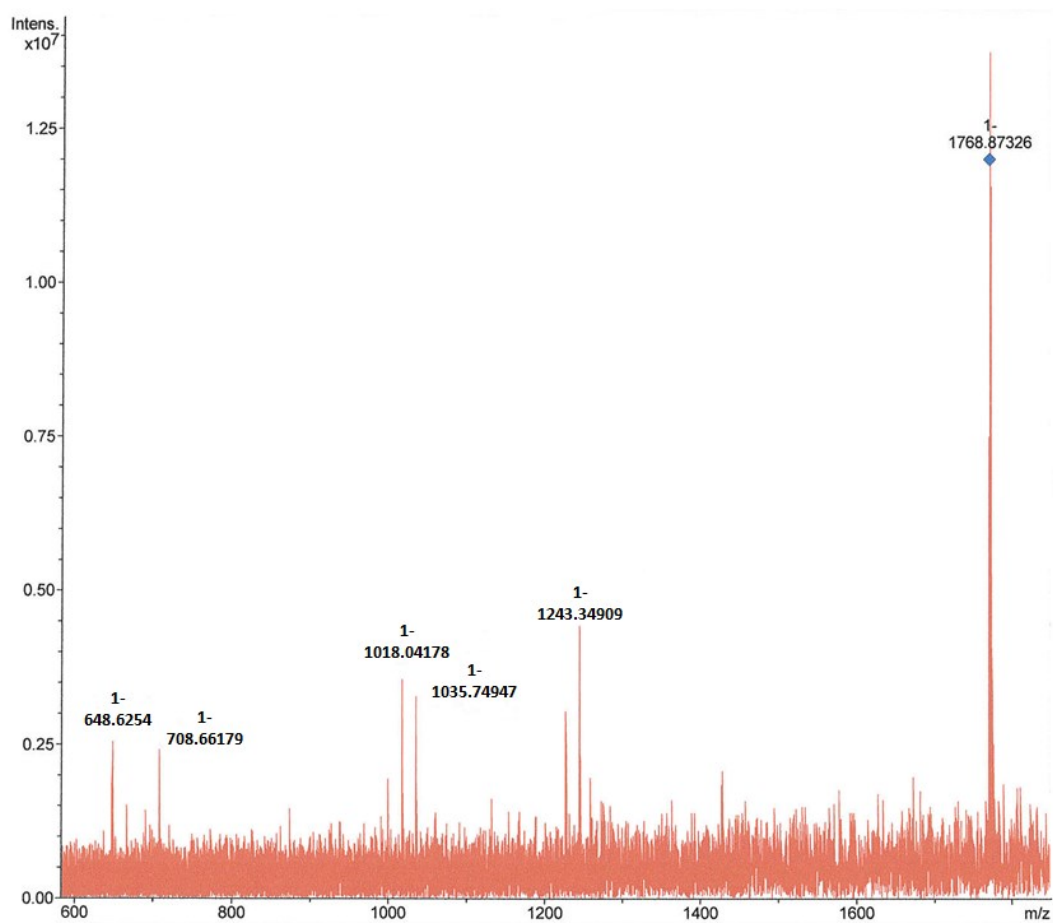


Figure 4.7: Negative ion CID MS/MS of the singly charged biphosphorylated lipid A [M-H]⁻ ion A at m/z 1768.8732.

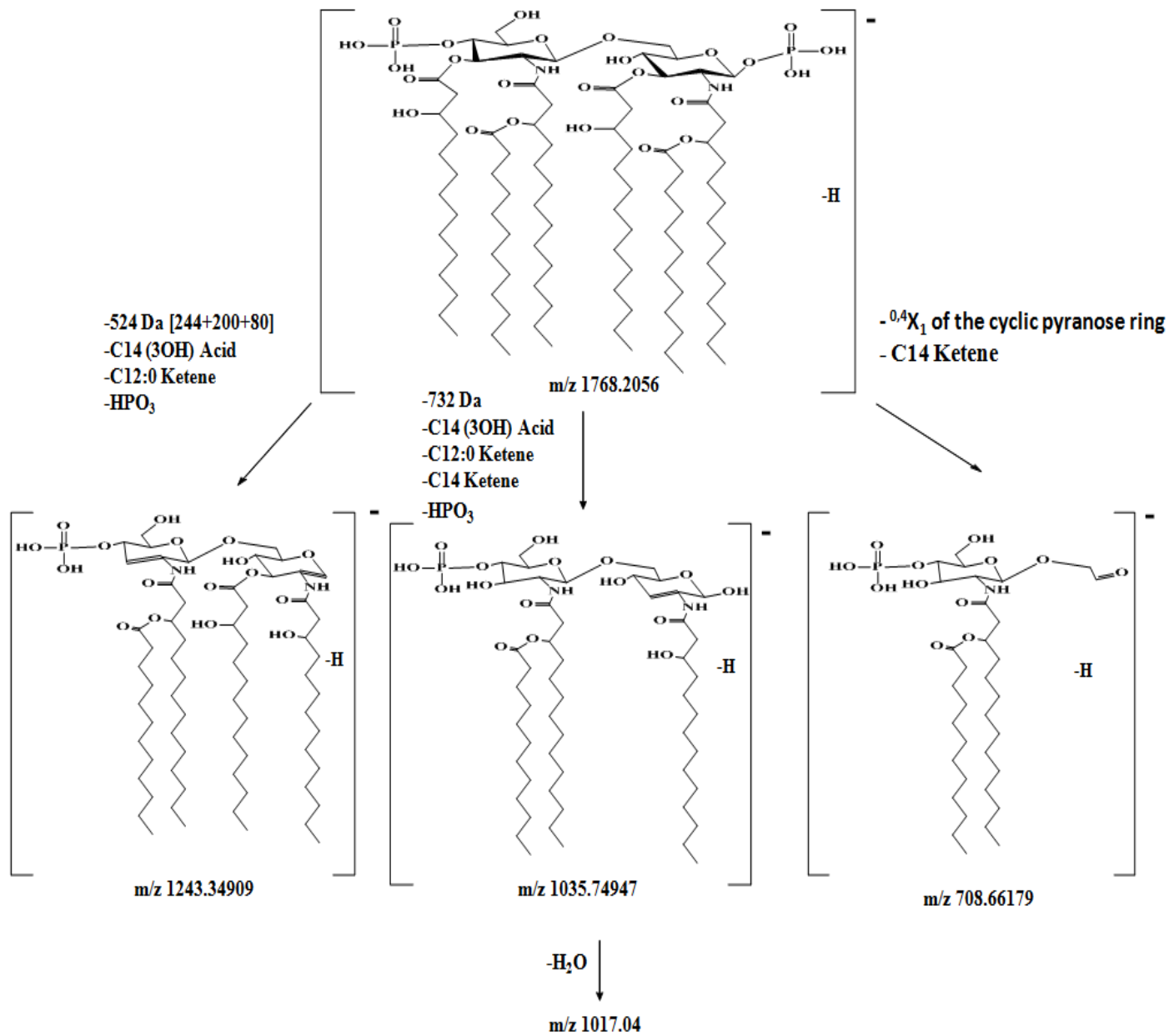


Figure 4.8: The proposed fragmentation pathway of the selected precursor ion at m/z 1768.2056

4.3.2 MS/MS of the precursor ions at m/z 1744.2209 isolated from LipA2

The CID analysis of the precursor ion at m/z 1744.2209 for LipA2 gave the product ions at m/z 1488.0378, 1243.8355, and 1035.6495 (Figure 4.9). It should be noticed that the product ions at m/z 1243.8355 and at m/z 1035.6495 m/z were also observed in the MS/MS of the precursor ion at m/z 1768.8732 for LipiA1. In contrast, the product ion at m/z 1488.0378 was formed only by the precursor ion at m/z 1744.2209 LipA2 and it indicates the elimination of a 16:0 ketene (-256 Da), present from either the reducing end or non-reducing end from the N-2 and N-2' positions of the disaccharide backbone of the Lipid A (Figures 4.10). The presence of this unique precursor at m/z 1744.2209 indicated the presence of a C16:0 fatty acid present on the branched fatty acid 14:0(3-(R)-O-16:0) present on C-N2 and confirmed the presence of an aberrant incomplete biosynthesis of Lipid A.

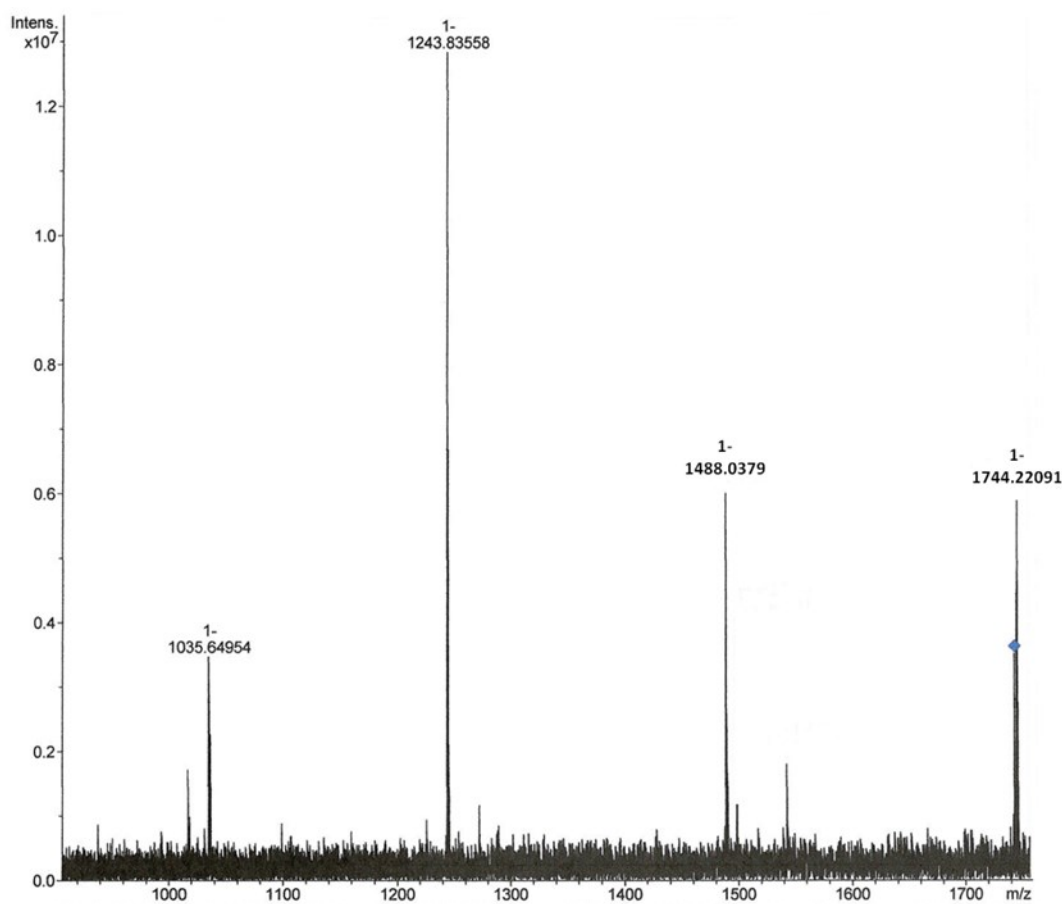


Figure 4.9: Negative ion CID MS/MS of the singly charged monophosphorylated lipid A [M-H]⁻ ion A at m/z 1744.2209.

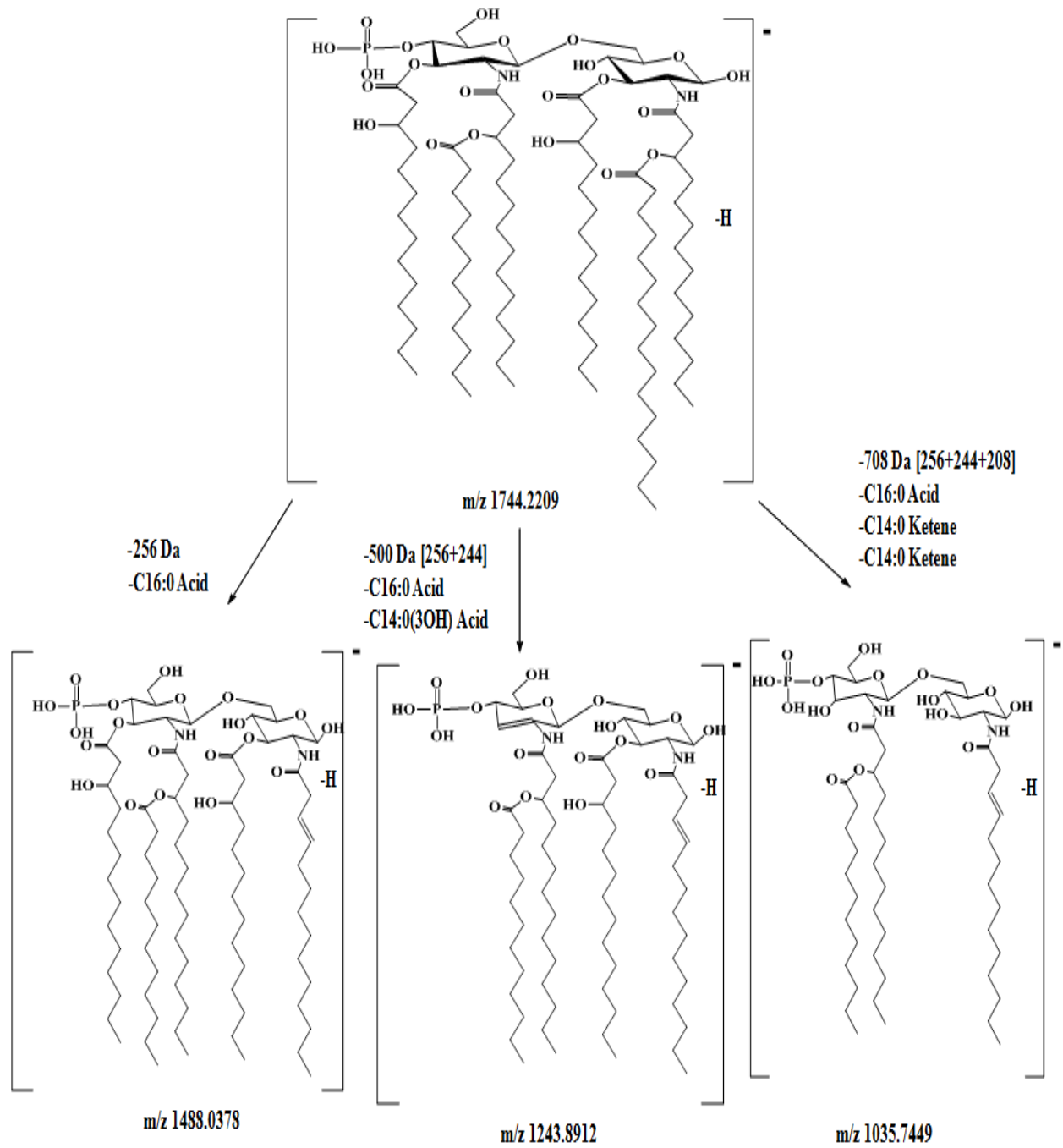


Figure 4.10: The proposed fragmentation pathway of the selected precursor ion at m/z 1744.2209.

4.3.3 MS/MS of the precursor ions at m/z 1688.2302 isolated from LipA3

Furthermore, the CID analysis of the precursor ion at m/z 1688.2302 for LipA3 gave product ions at m/z 1488.0378, 1444.5755, 1243.8355, 1035.6495, and at m/z 708.6815 (Figure 4.11). These product ions, except for m/z 1444.5755, were also observed in the MS2 of the precursor ion at m/z 1768.8732 for LipiA1 and at 1744.2209 for LipA2. For the product ion at m/z 1444.5755, the mass difference between the ions at m/z 1688.2302 for LipA3 and at m/z 1444.5755 (-244 Da), indicates the elimination of 14:0 fatty acid from the 14:0(3-(R)-O-14:0) from the O-3 or O-3' position (Figures 4.12). It is very important to note that the product ion at m/z 708.6815 gave an excellent support to our proposed structure at the precursor ion at m/z 1768.8732 LipiA1 and at 1688.2302 LipA3.

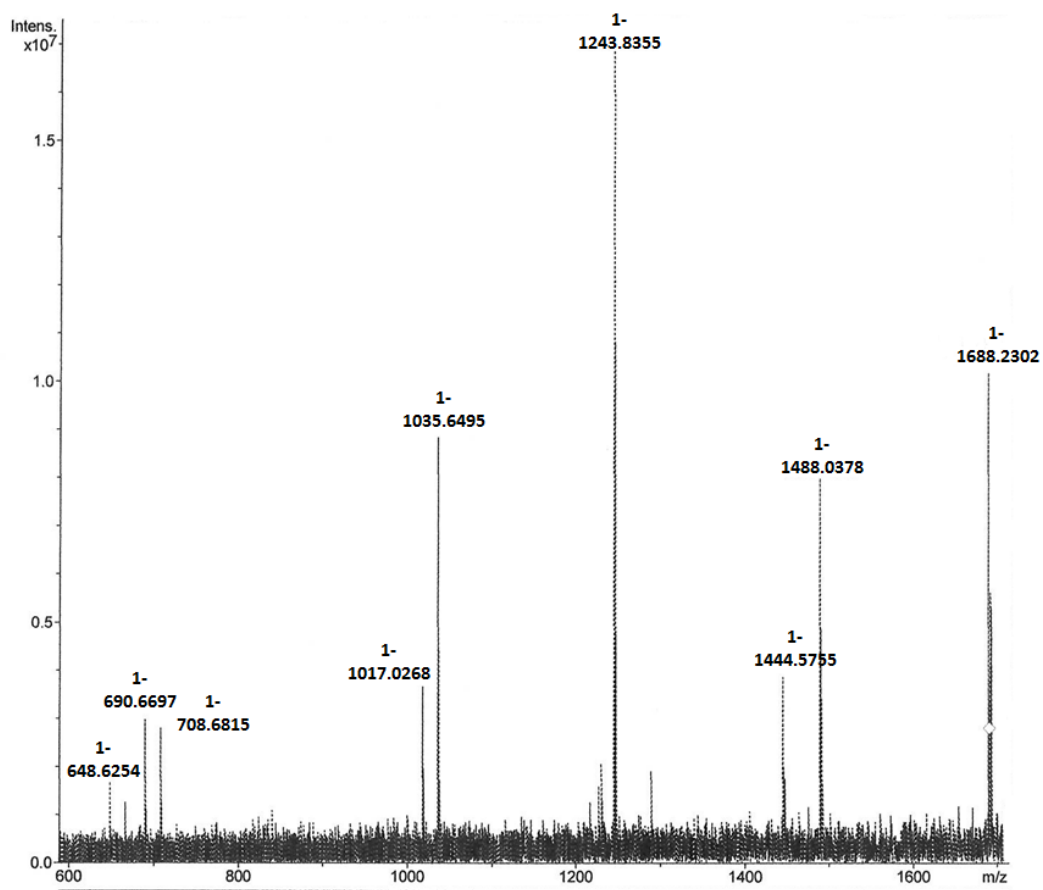


Figure 4.11: Negative ion CID MS/MS of the singly charged monophosphorylated Lipid A [M-H]⁻ ion A at m/z 1688.2302.

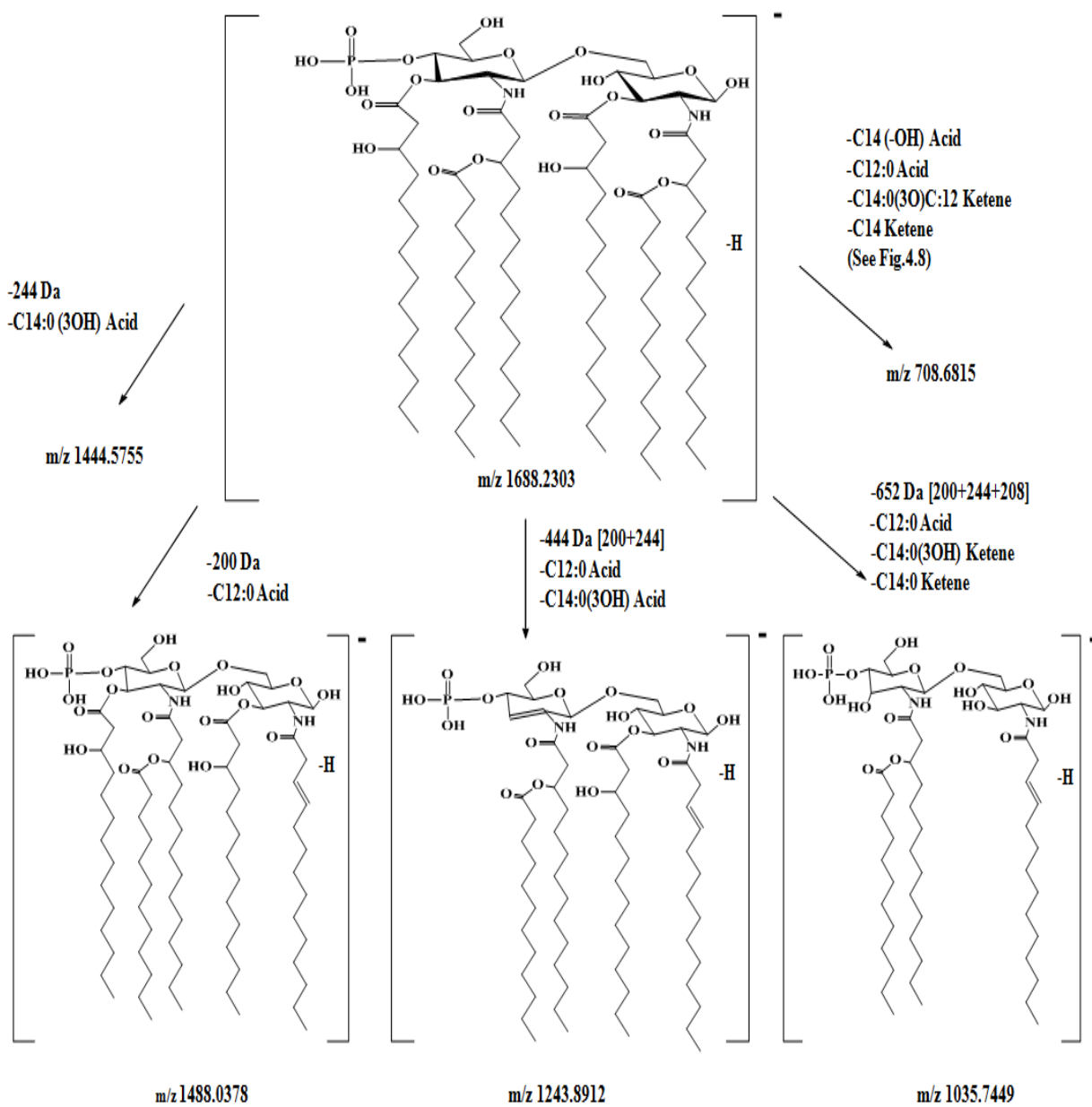


Figure 4.12: The proposed fragmentation pathway of the selected precursor ion at m/z 1688.2302

4.3.4 MS/MS of the precursor ion at m/z 1586.0259 isolated from LipA4

To determine the possible structures of the most abundant ions shown in the ESI-MS, the precursor ion at m/z 1586.0259 for LipA4 was subjected to a MS² experiment, and as shown in Figure 4.13; it gave the product ions at m/z 1488.0742, 1341.8129, and 1243.8798 (Figure 4.13). The product ions at m/z 1488.0742 indicated the elimination of H₂PO₄ from the non-reducing sugar group and from m/z 1586.0259 the precursor ion. The product ions at m/z 1341.8129 indicated the loss of a 14:0 fatty acid from the 14:0(3-(*R*)-*O*-14:0) from the O-3' position from the precursor ion at m/z 1586.0259. Also, the elimination of a 14:0 fatty acid from the 14:0(3-(*R*)-*O*-14:0) at the O-3' position, and a H₂PO₄ from the non-reducing sugar group was appeared as a product ion at m/z 1243.8798 (Figures 4.14).

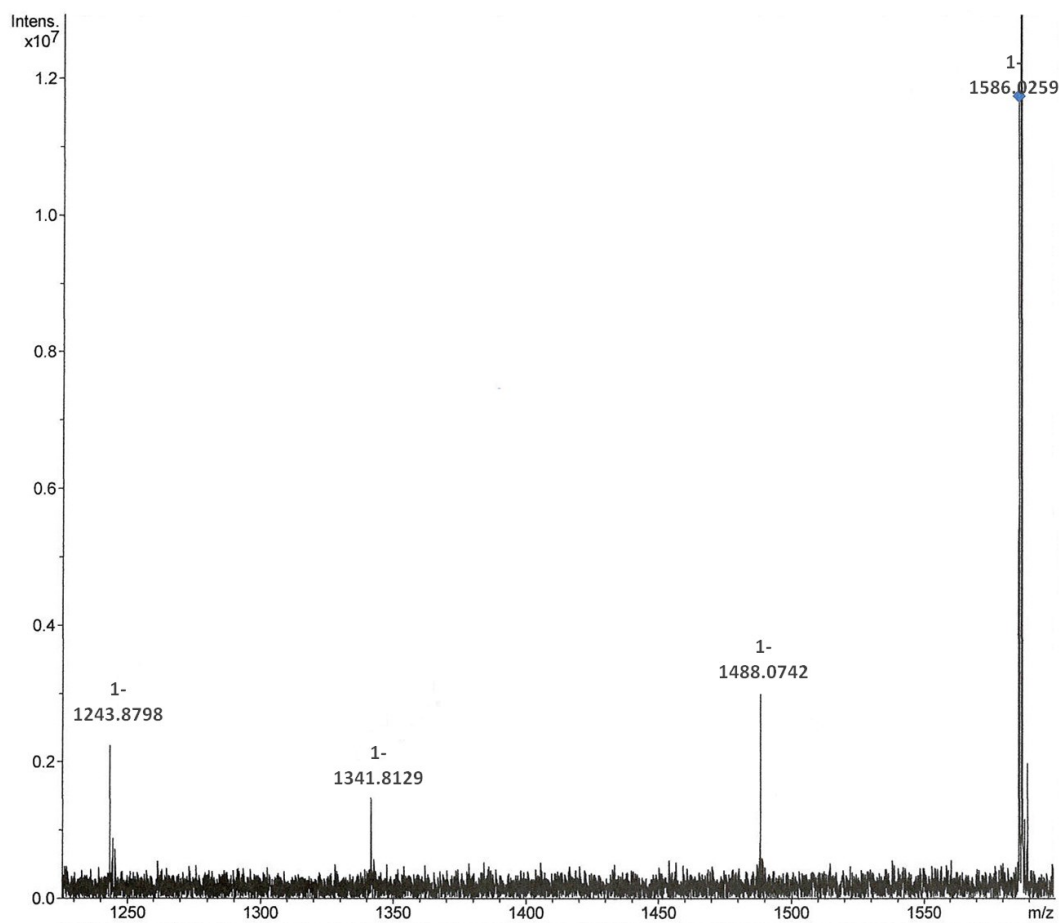


Figure 4.13: Negative ion CID MS/MS of the singly charged biphosphorylated Lipid A [M-H]⁻ ion A at m/z 1586.0259.

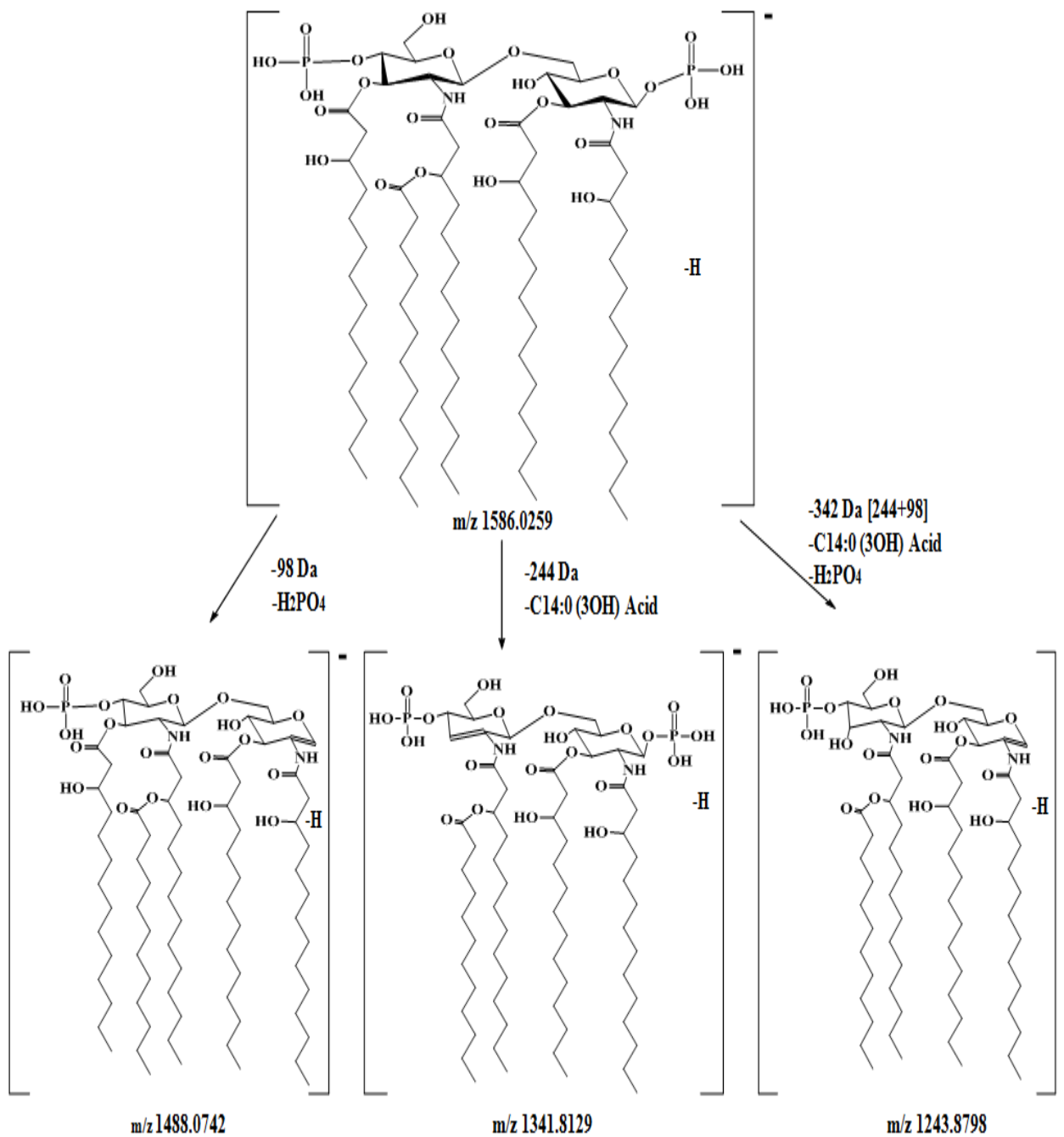


Figure 4.14: The proposed fragmentation pathway of the selected precursor ion at m/z 1586.0259.

4.3.5 MS/MS of the precursor ion at m/z 1506.0586 isolated from LipA5

The CID analysis of the second most abundant precursor ion at m/z 1506.0586 for LipA5 (Figure 4.15) gave the product ions at m/z 1261.8542, 1305.9065, and 1035.6546 (Figure 4.16). The m/z 1261.8542 product ion indicated elimination of the 14:0(3-OH) acid from the O-3' position (-244 Da difference) from the precursor ion at m/z 1506.0586. This elimination could in fact occur from either at the O-3 and O-3' positions located respectively in the reducing end, or non-reducing end of the lipid A disaccharide backbone. The mass difference (-200 Da) between the ions at m/z 1506.0586 for LipA5 and at m/z 1305.9065, indicated the elimination of a 12:0(OH) acid. Also, the elimination of a 14:0 fatty acid from the 14:0(3-(*R*)-O-14:0) at the O-3' position, a 14:0 ketene from the O-3 position acid appeared in the product ion at m/z 1035.6546 (Figure 4.16).

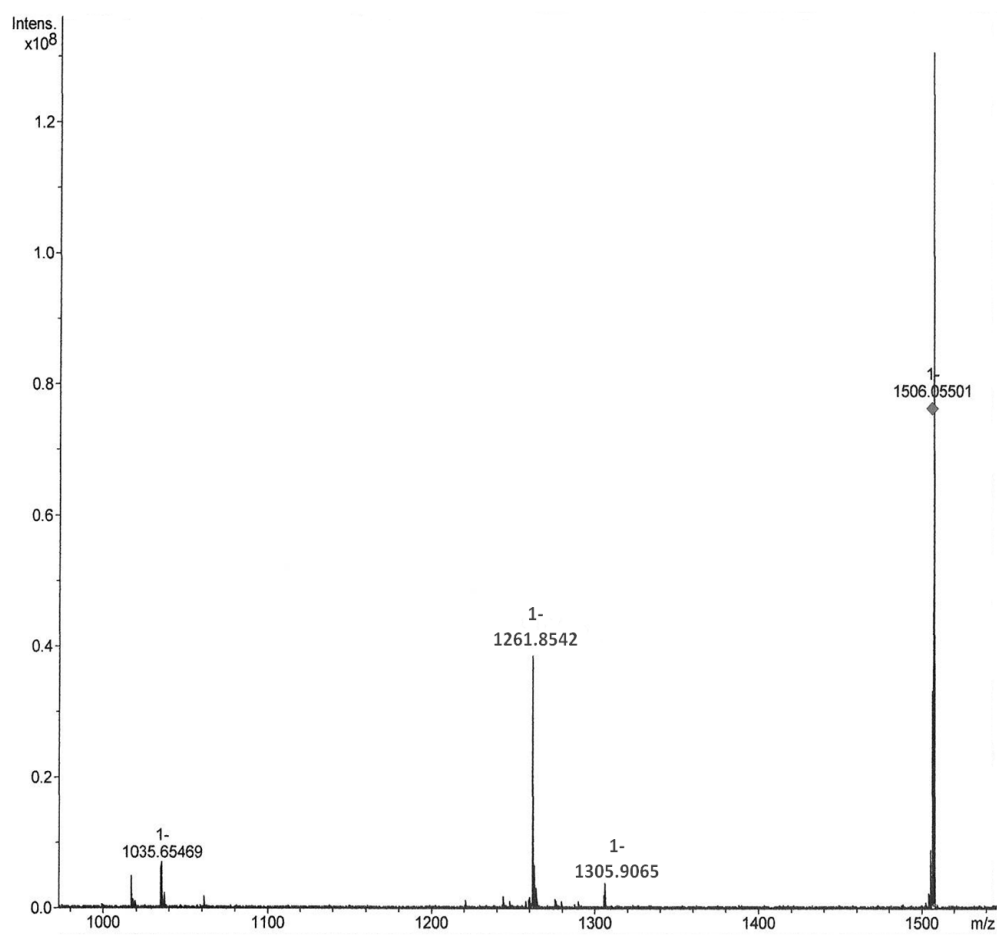


Figure 4.15: Negative ion CID MS/MS of the singly charged monophosphorylated Lipid A at m/z 1506.0586.

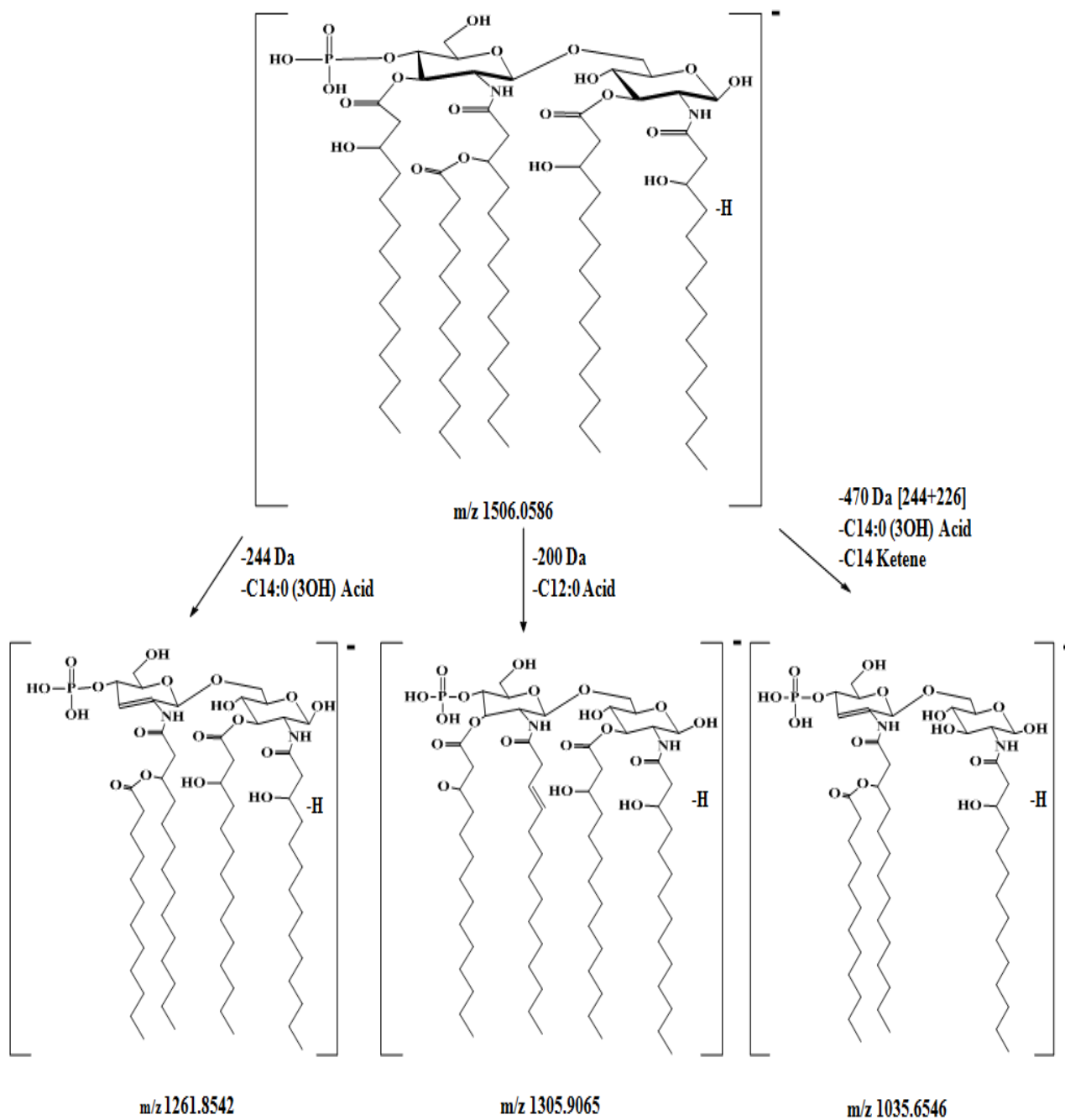


Figure 4.16: The proposed fragmentation pathway of the selected precursor ion at m/z 1506.0586.

4.3.6 MS/MS of the precursor ion at m/z 1359.8266 isolated from LipA6

The CID analysis of the third most abundant precursor ion at m/z 1359.8266 for LipA6 (Figure 4.17) gave the product ions at m/z 1261.6628, 1115.9844, 1017.6426, 1035.6735, 919.7743, and 817.8521. The product ion of m/z 1261.6628 indicated the elimination of the H_2PO_4 from the non-reducing sugar group (-98 Da differences) from the precursor ion at m/z 1359.8266 LipA6. The mass difference (-244 Da) between the ions at m/z 1359.8266 LipA6 and 1115.9844, indicated the elimination of 14:0(3-OH) acid from the O-3' position. Also, the elimination of a 14:0 fatty acid from the 14:0(3-(*R*)-O-14:0) at the O-3' position, a H_2PO_4 from the non-reducing sugar group appeared in the product ion at m/z 1017.6426. For the product ion at m/z 1035.6735, the elimination of 14:0 ketene from the O-3' position from the precursor ion at m/z 1035.6735 was observed. The loss of H_2PO_4 from the reducing sugar group from the precursor ion at m/z 1017.6426 to give the precursor ion at m/z 919.7743 was also observed. The product ion of m/z 817.8521 showed the elimination of a 12:0 acid from the branched fatty acid at the N-2 position from the precursor ion at m/z 1017.6426 (Figure 4.18). As a result of this elimination, m/z 1359.8266 for LipA6 was assigned to the biphosphorylated, tetra-acylated lipid A form containing two phosphate group, three 14:0(3-OH) located at the N-2, O-3, N-2' positions, and one 12:0 fatty acid located on the 14:0(3-(*R*)-O-12:0) group at the N-2' position

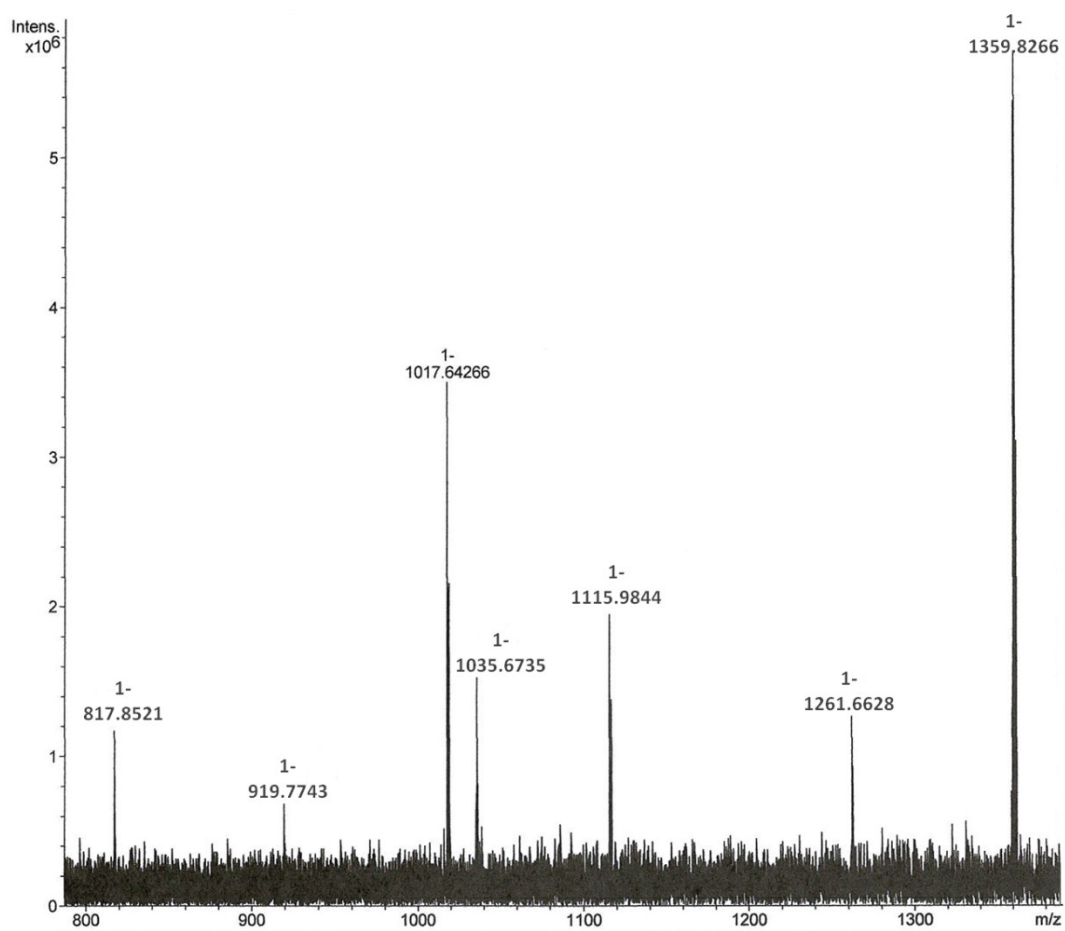


Figure 4.17: Negative ion CID MS/MS of the singly charged biphosphorylated Lipid A at m/z 1359.8266

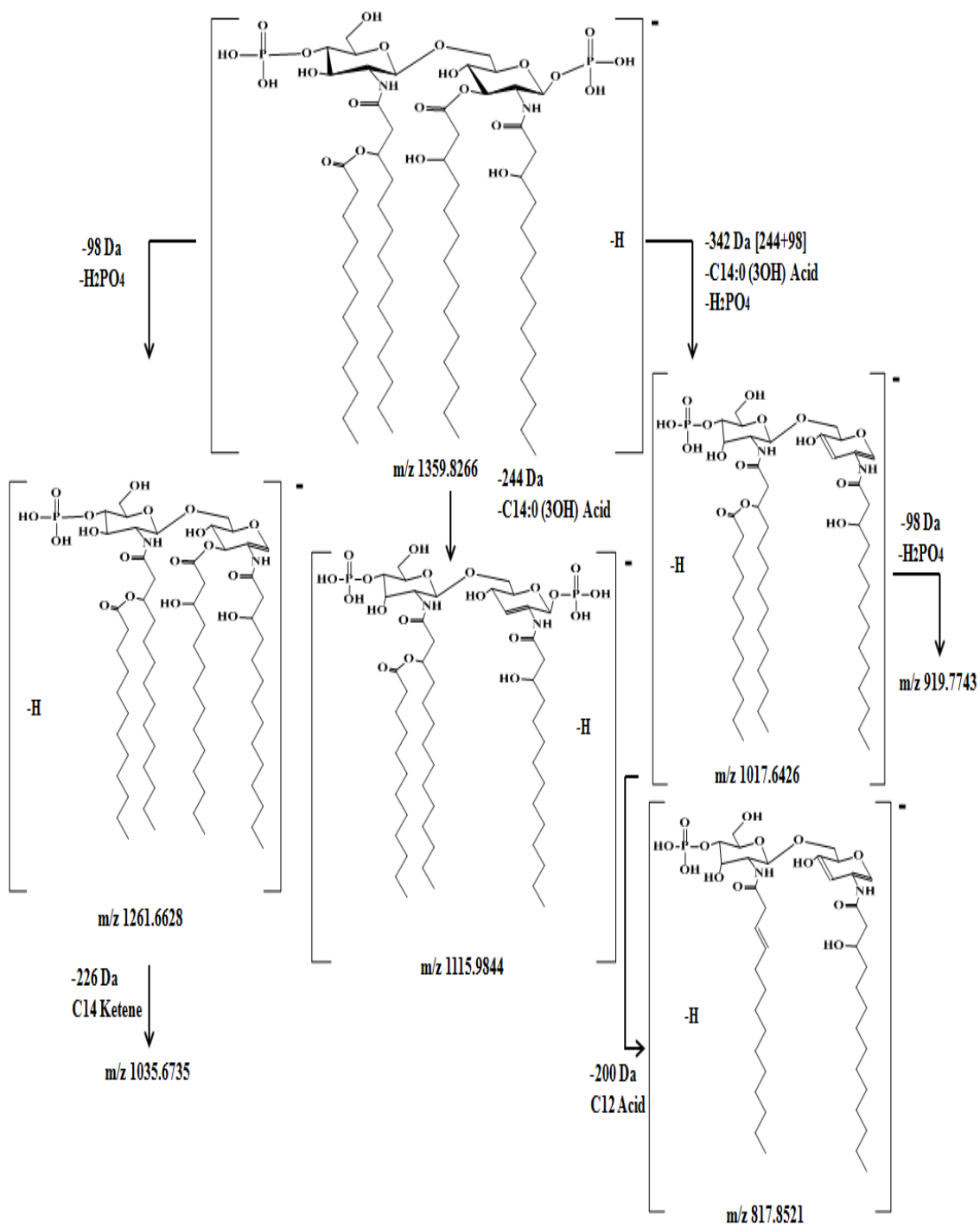


Figure 4.18: The proposed fragmentation pathway of the selected precursor ion at m/z 1359.8266

4.3.7 MS/MS of the abundant precursor ion at m/z 1279.867 isolated from LipA7

The CID analysis of the fort most abundant precursor ion at m/z 1279.8676 for LipA7 (Figure 4.19) showed product ions at m/z 1079.7355, 1053.7893, 1035.6529, 1017.6329, and 835.5964. The product ion of m/z 1079.7355 indicated elimination of the 12:0 fatty acid at the 14:0(3-(*R*)-*O*-12:0) group from the N-2' position (-200 Da). The mass difference between the ions at m/z 1279.8676 for LipA7 and at m/z 1053.7893 (-226 Da), indicated the elimination of a 14:0 ketene from the N-2' position from the precursor ion at m/z 1279.8676. The product ion at m/z 1035.6529, indicated the elimination of a 14:0 fatty acid from the 14:0(3-(*R*)-*O*-14:0) at the O-3 position from the precursor ion at 1279.8676. The loss of water from the product ion at m/z 1035.6529 gave the product ion at m/z 1017.6329. In addition, the elimination of a 14:0 fatty acid from the 14:0(3-(*R*)-*O*-14:0) at the O-3 position, a 14:0 ketene from the branched fatty acid at the N-2' position from the precursor ion at m/z 1279.8676 was appeared in the product ion at m/z 835.5964 (Figure 4.20). As a result of this elimination, 1279.8676 for LipA7 was assigned to the monophosphorylated, tetra-acylated lipid A form containing one phosphate group, three 14:0(3-OH) located at the N-2, O-3, and N-2' positions, one a 12:0 located on the 14:0(3-(*R*)-*O*-12:0) group at the N-2' position.

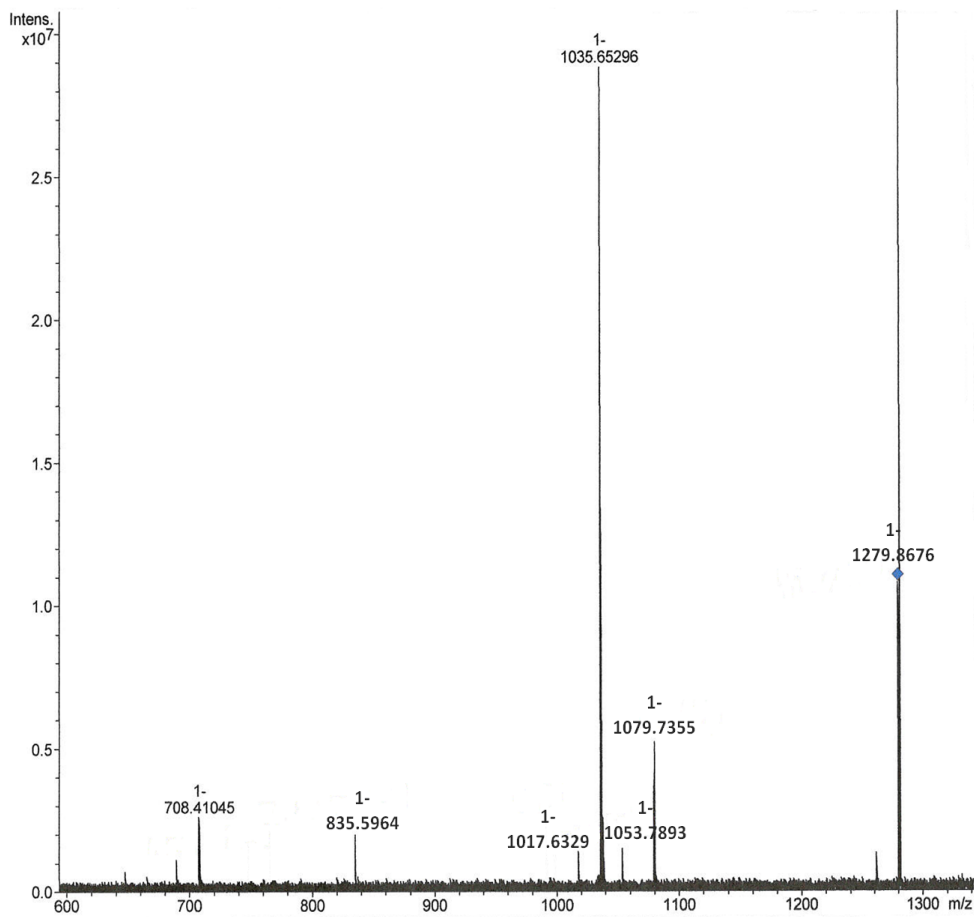


Figure 4.19: Negative ion CID MS/MS of the singly charged monophosphorylated Lipid A at m/z 1279.8676.

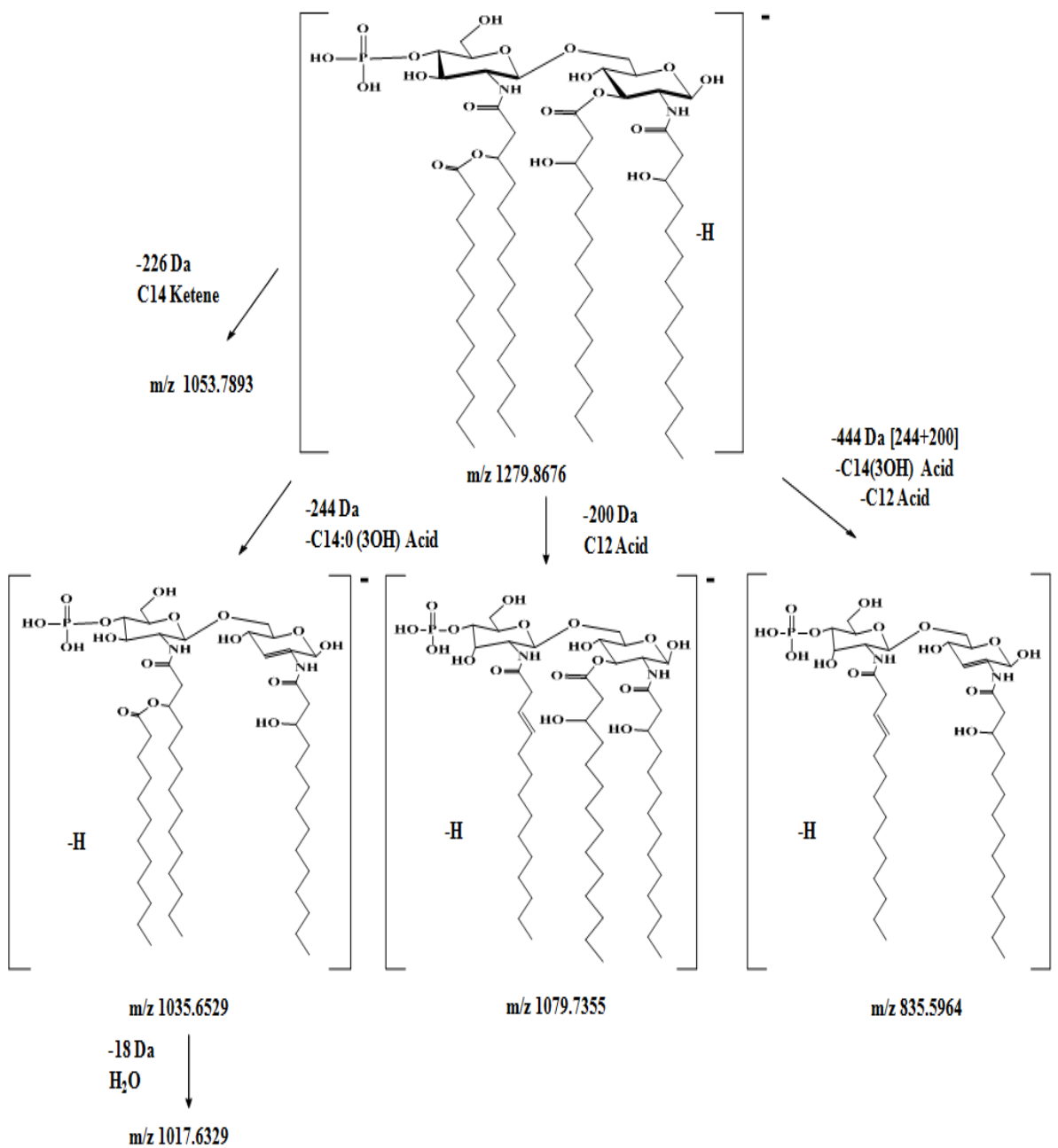


Figure 4.20: The proposed fragmentation pathway of the selected precursor ion at m/z 1279.8676.

To confirm the presence of the phosphate group position, the precursor ion at m/z 892.5778 was isolated and subjected to a CID analysis (Figure 4.21). The most abundant product ion at m/z 648.3460 was formed by loss of the 14:0 fatty acid on the 14:0(3-(*R*)-*O*-14:0) group at the O-3' position (-244 Da) of the disaccharide backbone of Lipid A. The suggested structure of the product ion at m/z 648.3460 appears to indicate that the position of the phosphate group could exist at either the C-1 position on the reducing end sugar, or on the O-4' of the non-reducing end sugar of the disaccharide backbone. The backbone is presumably acylated with the 14:0 fatty acid located at the branched fatty acid of N-2' and a 12:0 fatty acid from the 14:0(3-(*R*)-*O*-12:0) group at the N-2' position existed at either the reducing end or non-reducing end as shown in Figure 4.22.

Moreover, this CID of the precursor ions at m/z 448.1395 indicated the elimination of the 12:0 Acid (-200 Da) located at the 14:0(3-(*R*)-*O*-12:0) from N-2' position.

4.3.8 CID analysis of the [C-H]⁻ and [Y-H]⁻ ions

As mentioned earlier, one diagnostic ion which is formed during the biosynthesis of the complete Lipid A was assigned as the [C-H]⁻ ion at m/z 892.5932 which was observed in the conventional FT-ICR-MS scan (Figure 4.21). Ideally this ion would be produced by the glycosidic cleavages of the β -D-(1 \rightarrow 6) of the D-GlcN disaccharide during MS/MS of the complete lipid A. To confirm the proposed structure of this ion, MS/MS were acquired. The product ion scan of the selected [C-H]⁻ ion at m/z 892.5778 indicated a the loss of a 14:0 fatty acid chain from the C-3' to yield the product ion assigned as [C-(C14:0) (3-OH) acid-H]⁻ observed at m/z 648.3460 which can further

fragment by losing a 12:0 acid fragment located at the 14:0(3-(*R*)-*O*-12:0) at the N-2' position to afford the product ion observed at m/z 448.1395. This latter loss probably takes place from the labile *O*- linked fatty acid rather than the more stable amid *N*-linked one (Figures 4.22).

It is well-accepted that during CID analysis of the Lipid A moiety, the elimination of the fatty acid derivatives occurred mainly from the *O*- linked fatty acid esters. Therefore, it was projected that the major ion observed at m/z 648.3745 would be associated with the loss of the 14:0(3-OH) acid from the O-3' position, rather than a loss of 12:0 acid the 14:0(3-(*R*)-*O*-12:0) group at the N-2' position from the product ion observed at m/z 448.1395, it should be noted that it is very possible that these two processes occur simultaneously, as mentioned earlier. These product ions confirmed the proposed structure of Lipid A structures bearing two secondary ions and one phosphate group at the non-reducing end of the lipid A backbone.

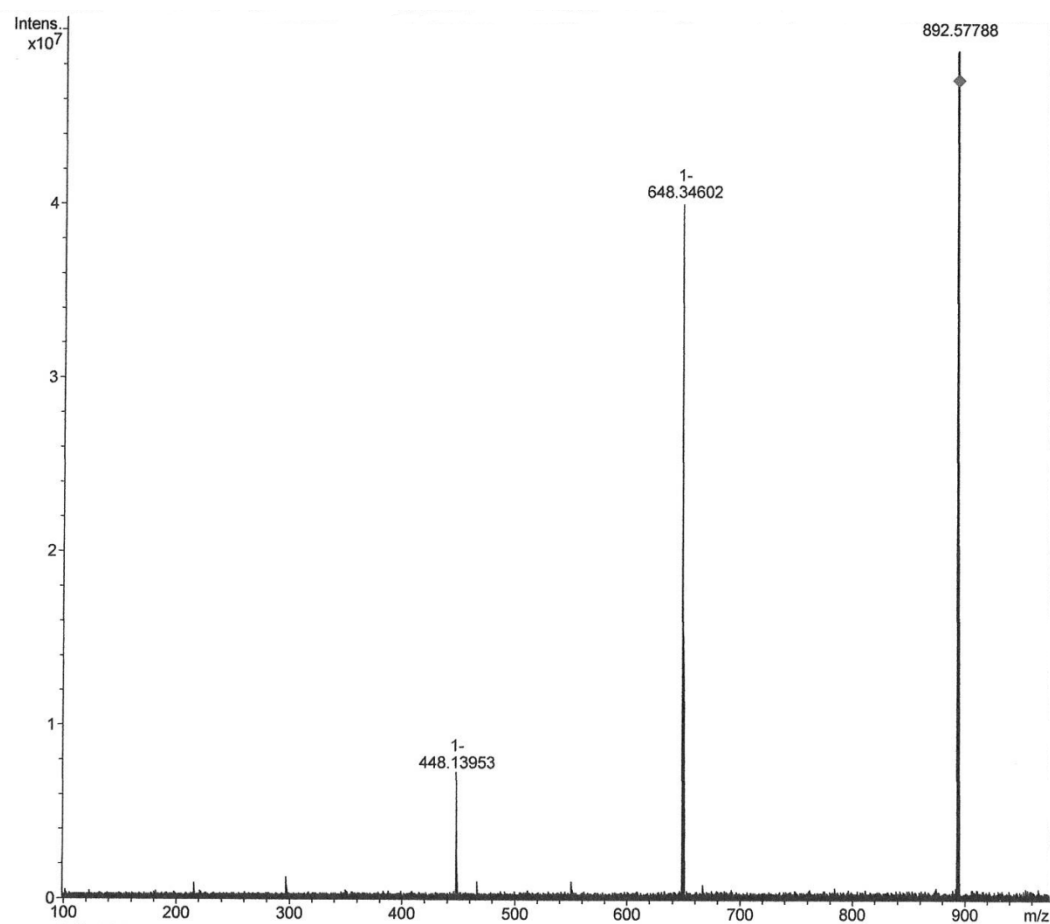


Figure 4.21: Negative ion CID MS/MS of the singly charged monophosphorylated lipid A [C-H]⁻ ion A at m/z 892.5778.

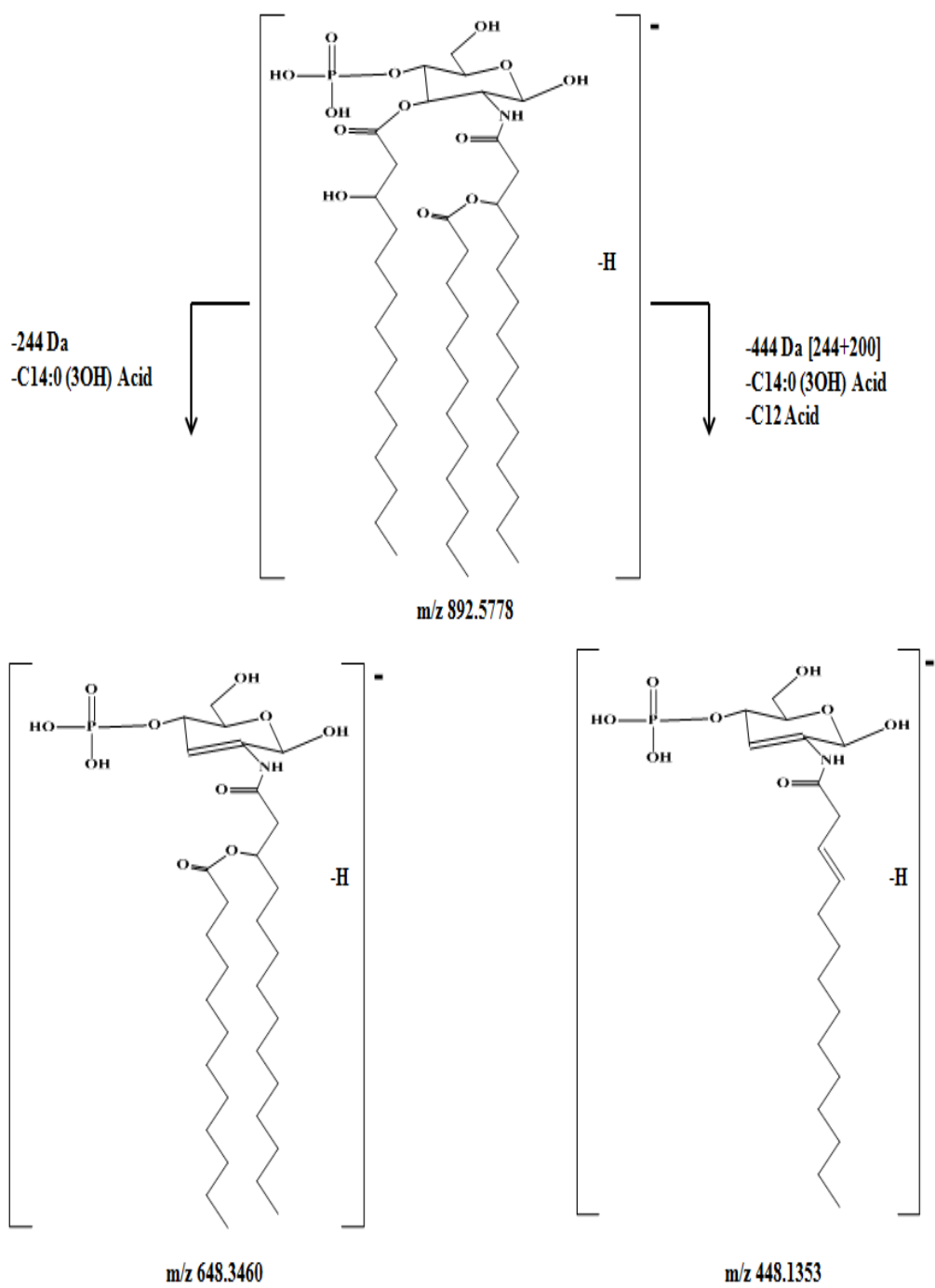


Figure 4.22: The proposed fragmentation pathway of the selected precursor ion at m/z 892.5778.

4.3.9 Summary

The chemical structure of Lipid A extract, isolated by mild acid hydrolysis from *Aeromonas Salmonicida* lipopolysaccharide, was investigated using electrospray ionization FTICR hybrid tandem in time mass spectrometry low collision-energy (CID), and illustrated a great degree of microheterogeneity. The chemical structure of the main constituent of this heterogeneous mixture was identified as a D-(1→6) linked glucosamine disaccharide substituted by two phosphates groups, being bound to the non-reducing end at position O-4' of the D-glucosamine disaccharide and being bound to the reducing end at position O-4 of the D-glucosamine disaccharide

The location of the fatty acids linked to the disaccharide backbone was established by identifying diagnostic ions in the conventional FT-ICR-MS scan. Low-energy collision (CID) tandem mass spectrometry analysis of the selected precursor diagnostic ions confirmed, unambiguously, their proposed molecular structures. It was established that a 14:0(3-(R)-O-12:0) acid residue was at the position O-3' linked to the non-reducing end of the D-GlcN residue with 3-hydroxy myristic (R)-14:0(3-OH) acid chains at the N-2' position, and also that a 14:0(3-(R)-O-12:0) acid residue was at the O-3 position linked to the reducing end of the D-GlcN residue with 3-hydroxy myristic (R)-14:0(3-OH) acid chains at the N-2 of the reducing end.

The MS and MS/MS data obtained allowed the determination of the complex molecular structure of Lipid A. In addition, the fragmentation patterns were clearly illustrated and established for this biologically-active compound.

Chapter 5 : Analysis of Lipid A Using MALDI-TOF-MS and High Energy CID-TOF/TOF-MS/MS

5.1 MALDI-TOF-MS analysis of the heterogeneous mixture of lipid As

MALDI-TOF-MS for the lipid A obtained from *Aeromonas salmonicida* SJ-112 were measured in the reflector mode with the TOF/TOF instrument and high laser power. It was again noticed that MALDI-MS showed similar spectra to those measured with the FT-ICR-MS instruments. This mainly displayed highly incomplete biosynthesis that mainly revealed multiple molecular ions as shown in Figure 5.1. Furthermore, the MALDI-TOF-MS revealed six unique deprotonated molecules *inter alia* that had similar structures to those of Lipid A at around m/z of 1768.2 for LipA1, and m/z 1688.0 for LipA2; and among these, four highly abundant ions at m/z 1585.6 for LipA3, at m/z 1505.7 for LipA4, at m/z 1359.5 for LipA5, and lastly, at m/z 1279.5 for LipA6.

Hence, the lower intensity ion mainly at m/z 1768.2 for LipA1 was further assigned to these already mentioned deprotonated fragments associated with the biphosphorylated Lipid A moiety that bears a phosphate group at each of the sugars.

In the case of the deprotonated fragments of the LipA1 at m/z 1768.2, it was postulated that most probably N-2' was specifically acylated with a fatty acid. For most of the deprotonated molecules such as LipA2 at around m/z 1688.2209 for LipA2, it was also proposed that the two 12:0 fatty acids specifically at position of

14:0(3-(*R*)-*O*-12:0) could be located at both N-2' as well as N-2 positions with one group of sugar at the non-reducing end (Figure 5.2).

In addition, two of the most abundant ions at around m/z 1585.7 for LipA3 and at m/z 1359.5 LipA5 were tentatively assigned to the biphosphorylated Lipid A forms for the deprotonated molecule LipA4 m/z 1585.7 carrying four (*R*)-14:0(OH) (primary fatty acid) possibly on the N-2, O-3, N-2' and O-3' positions of the Lipid A disaccharide, one 12:0 branched fatty acid at position of 14:0(3-(*R*)-*O*-12:0) at N-2' position at around m/z 1585.7. Similarly, the deprotonated molecule at around m/z 1359.5 LipA5 was also tentatively attributed to the biphosphorylated Lipid A forms carrying three (*R*)-14:0 (OH) (primary fatty acid) which most probably were located on the N-2, O-3 and N-2' positions of the Lipid A disaccharide; one 12:0 branched fatty acid on position 14:0(3-(*R*)-*O*-12:0) at the N-2' position, (Figure 5.2). It should be noted that the mass difference of 228 Da between the ions at m/z 1585.6 LipA3 and the ions at m/z 1359.8266 for LipA5 could indicate the elimination of a C14-acid at the O-3 position.

In addition to this, two of the most abundant ions at around m/z 1505.7 LipA4 along with at m/z 1279.5 for LipA6 were attributed tentatively to the mono-phosphorylated and penta-acylated different forms specifically for the deprotonated molecule LipA5 at around m/z 1505.7 that carries four (*R*)-14:0(OH) groups specifically on the N-2 as well as O-3, N-2' and also at O-3' of Lipid A disaccharide. In addition to this, the deprotonated molecule at m/z 1279.5 for LipA6 that is

attributed to the mono-phosphorylated tetra-acylated various forms carries around three (*R*)-14:0 (OH) groups on N-2, O-3 and N-2' positions in the overall structure of Lipid A disaccharide (Figure 5.2). It must also be noted that the overall mass difference of around 228 Da mainly between the ions at m/z 1505.7 for LipA5 along with the ions at m/z 1279.5 for LipA6 can possibly indicate the extent of elimination mainly of the C14-acid at around the O-3' position.

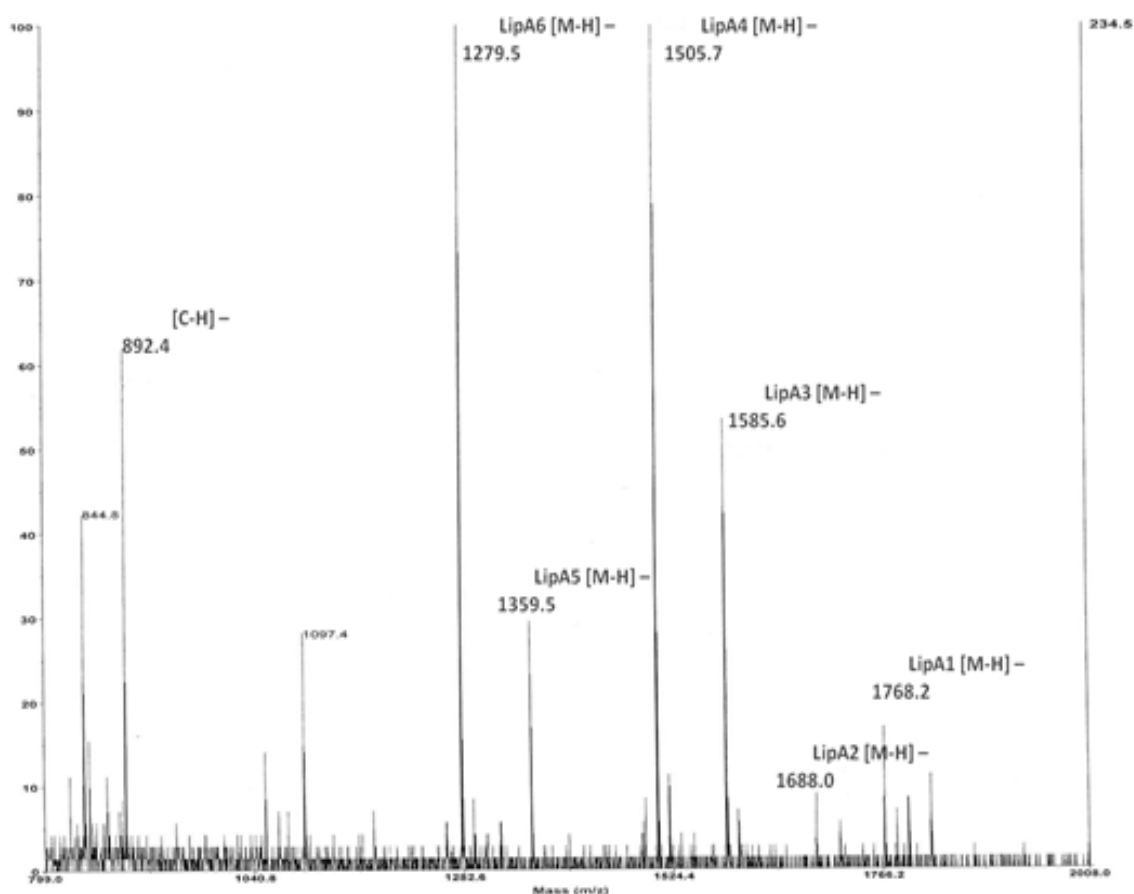


Figure 5.1: Negative ion MALDI-TOF-MS of the heterogeneous mixture of native Lipid A as extracted from *Aeromonas salmonicida* SJ-112.

The already proposed structures mainly of biphosphorylated as well as monophosphorylated Lipid A, along with its distinctive ions that were observed with the help of MALDI-TOF-MS, are diagrammatically illustrated in Figure 5.2. It must also be noted however, that at this specific stage of this entire study, the certain positions of fatty acids esterified were assigned tentatively and furthermore, there are many different possible structures that can be illustrated for this Lipid A. Hence, the postulated Lipid A extract structure that is shown in Figure 5.2 directly corresponds to a highly biphosphorylated lipid A having a postulated $[M-H]^-$ at m/z 1585.6 for LipA3 as well as at m/z 1359.5 for LipA5 respectively.

Moreover, the ions present at lower m/z values, as well as their intensities were assigned to different species of mono-phosphorylated that consisted of one D-GlcN that was devoid of a 14:0 acid as well as a 14:0(3-OH) fatty acid at m/z 892.4. Such lower m/z values of ions could be potentially explained with the help of a partial degradation specifically of Lipid A, during both the work-up as well as acid liability of most of the acyl chains as well as phosphate groups present at the O-1 position in the process of phenol extraction. Nevertheless, this is not the case. The presence of the single acylated glucosamine residues and underacylated Lipid As represent the incomplete biosynthesis, it is important to understand that the Gram negative bacteria used for this rationale, was infected by a phage (virus) and that the phage disrupted the biosynthesis of the LPS. Needless to say, the LPS extracted from conventional Gram negative bacteria by the phenol:water method of Westphal and Jann affords upon hydrolysis of LPS a unique sort of Lipid A.

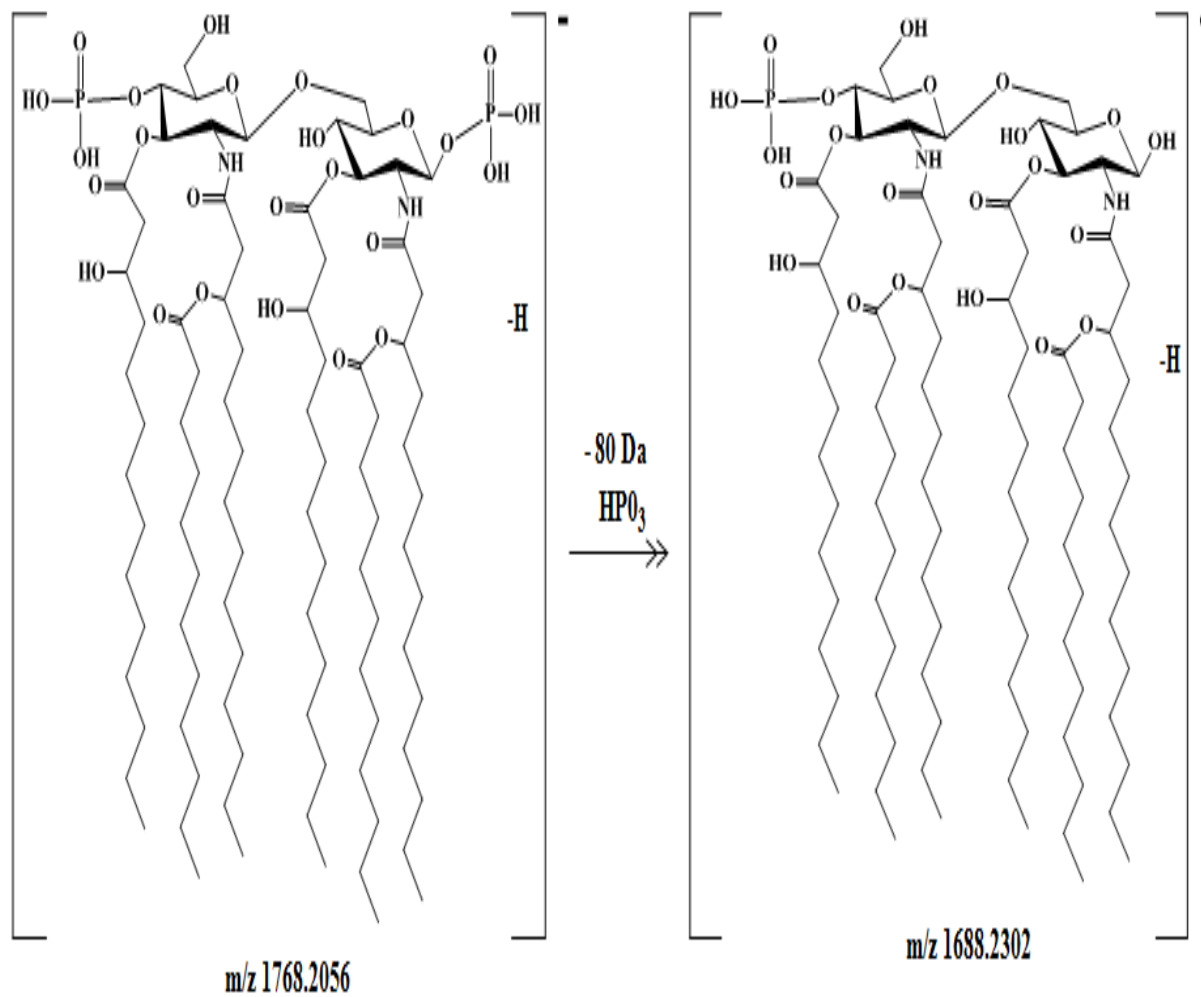


Figure 5.2: The six proposed structures of the native Lipid A extract from *Aeromonas salmonicida* SJ-112.

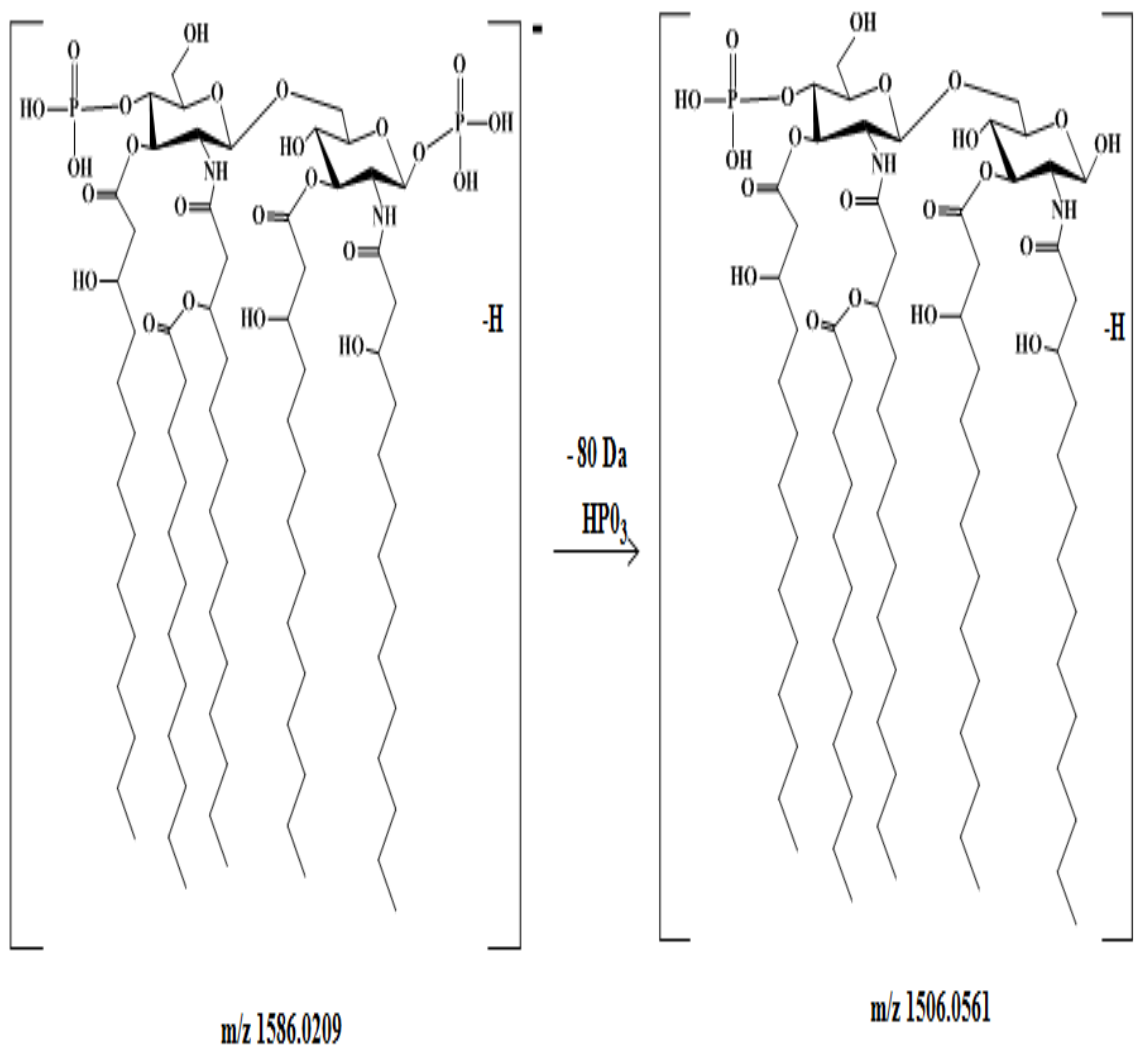


Figure 5.2, continued: The six proposed structures of the native Lipid A extract from *Aeromonas salmonicida* SJ-112.

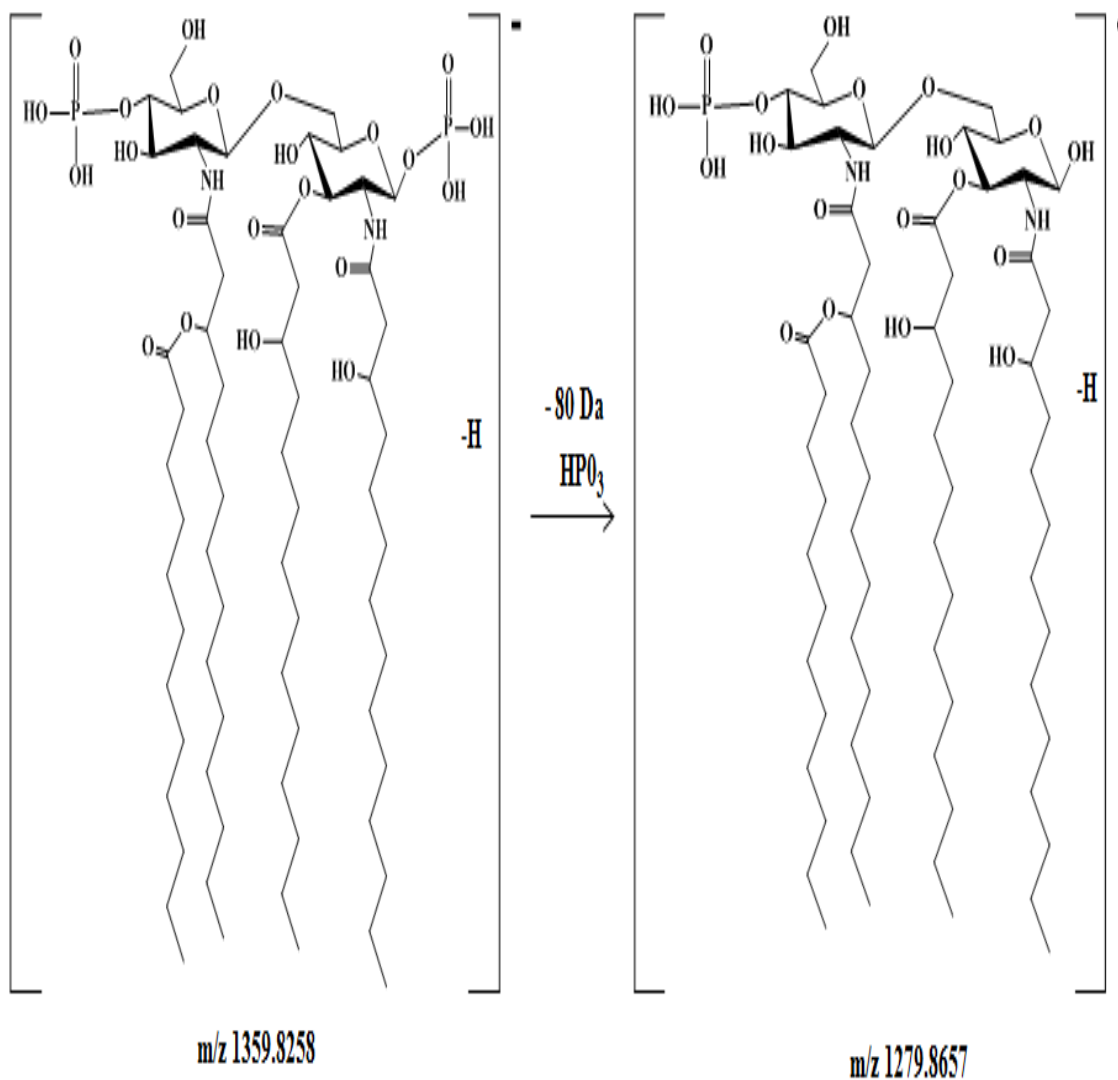


Figure 5.2, continued: The six proposed structures of the native Lipid A extract from *Aeromonas salmonicida* SJ-112.

It is important to note also that such lower values of m/z ions can be further explained by the nature of gas-phase fragmentation that can specifically in the traditional ESI-MS scan. On the basis of this, it was also noted that the prevalent glycosidic bond

cleavages can be further induced by the traditional ESI-MS cone fragmentation, thus, providing some useful structural information as well as sugar sequencing of some of the complex carbohydrates. Furthermore, in case of the medium m/z values from the MALDI-TOF-MS, a highly distinctive ion, at around m/z 892.4 was mainly observed and furthermore, it was also assigned the as $[C-H]^-$ ion, as shown in Figure 5.3. This major fragment ion significantly represented the GlcN residue that is mainly non-reducing and is also formed during the process of biosynthesis Lipid A.¹³¹

The assignment of those ions that were observed in the MS analysis which has much simpler one-stage high-resolution was basically based only on their molecular masses, but additional evidence is typically required for validating such assignments. Hence, without having further confirmation, it would be impossible to suggest different constitutional as well as isomer structures for this Lipid A mixture. For example, all the proposed ion structures shown in Figure 5.2 could also be correct if instead, the fatty acid acylation on the disaccharide backbone were reversed.

For this specific reason, employing tandem mass spectrometry greatly permitted the much needed identification of both the diagnostic ions product and additionally confirmed the initially proposed molecular structure. Thus, the structures that are shown in Figure 5.2 were mainly confirmed with the help of detailed MS/MS analysis of some of the selected molecular anions that are described in the up-coming sections. Consequently, some of the different proposed structures of the deprotonated molecules

that are attributed to LipA1 and eventually to LipA6, were obtained in the major conventional single stage, and has also been confirmed tentatively.

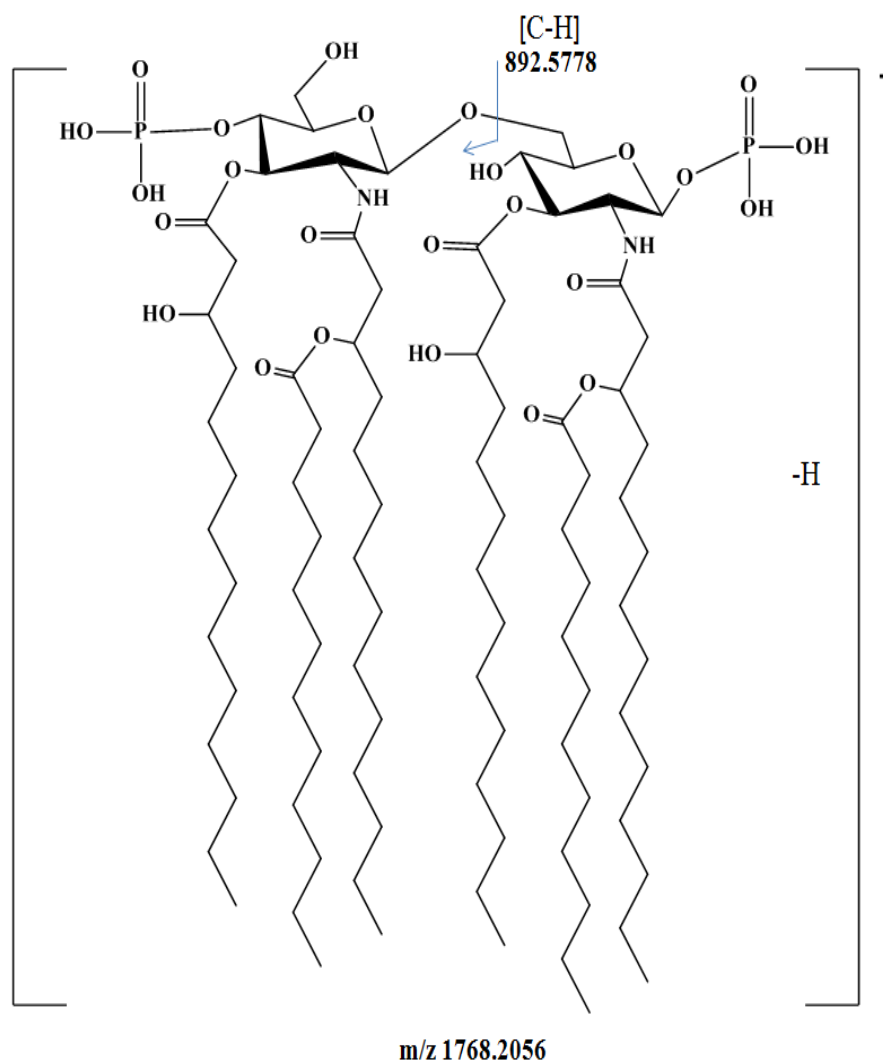


Figure 5.3: Schematic representation of the one of the common structure of Lipid A and the diagnostic ion of [C-H]⁻ observed in the MALDI-TOF-TOF-MS spectrum.

5.2 MALDI-CID-TOF/TOF-MS/MS analysis:

The overall distribution of the fatty acids for the initially discussed Lipid A that was isolated from the bacterial species *Aeromonas salmonicida* SJ-112 was determined with the help of high-energy collision disocation CID-TOF/TOF/-MS/MS. All the detected product ions were then interpreted on the basis of those rules that were described previously in Chapter 4 for the ESI-CID-MSⁿ analysis of lipid A.¹³⁸ The high-energy CID-TOF/TOF-MS/MS of the precursor ions at m/z 1768.2 for LipA1 (Figure 5.4), m/z 1688.0 for LipA2 (Figure 5.6), m/z 1585.6 for LipA3 (Figure 5.8), m/z 1505.7 for LipA4 (Figure 5.10), m/z 1359.5 for LipA5 (Figure 5.12), and m/z 1279.5 LipA6 (Figure 5.14) were performed for the determination of the distribution of the fatty acids on the Lipid A disaccharide backbone. Moreover, determining the precise location of the phosphate group mainly at m/z 892.4 was shown in Figure 5.6 and additionally, similar CID-MS² experiments are also performed.

5.2.1 MS/MS of the precursor ions at m/z 1768.2 isolated from LipA1

The location of the fatty acid acyl group distributions for LipA1 was performed with the help of MS/MS of the ion at m/z 1768.2 LipA1 observed in the MALDI-TOF-MS of Lipid A preparations from *Aeromonas salmonicida* SJ-112 (Figure 5.4). According to the proposed chemical structure for Lipid A constituents as well as after the MS/MS analysis, this specific ion was mainly assigned to the biphosphoylated along with the hexaacylated Lipid A form that consisted of two GlcN residues having two P groups at C-1 and C-4' of the GLcN disachharide backbone, as well as four (R)-14:0(3-OH)

mainly on the N-2 along with O-3, N-2', and on the O-3' positions, and also two 12:0 fatty acids present on the 14:0(3-(R)-O-12:0) fatty acid mainly at both the N-2 and N-2' positions.

In this regard, most of the abundant product ions at m/z 1488.2806 were basically formed from the precursor ion obtained at around m/z 1768.2 LipA1 and further indicated the eventually elimination of the 12:0 acid (-200 Da) from the branched fatty acid at the N-2 position, and the elimination of HPO_3 specifically from the reducing end (around -80 Da differences). The product ion at m/z 1244.0620 was formed by the consecutive elimination of the C14(3OH) acid from the C-3' of the non-reducing GlcN' residue (244 Da), the loss of C12:0 acid (200 Da) from the branched 14:0(3-(R)-O-14:0) present on the N-2 position, and elimination of HPO_3 (80 Da) from the reducing GlcN residue of the precursor ion at m/z 1768.2.

The product ion at m/z 1017.5594 was formed by the consecutive losses of two molecules of the 14:0 fatty acids (-488 Da) of the C-3 and C-3' position of both GlcN residues, followed by elimination of a C12:0 ketene from 14:0(3-(R)-O-14:0) branched fatty acid from the N-2 position and elimination of HPO_3 of the reducing GlcN, sugar group of the precursor ion at m/z 1768.8732 (Figure 5.5).

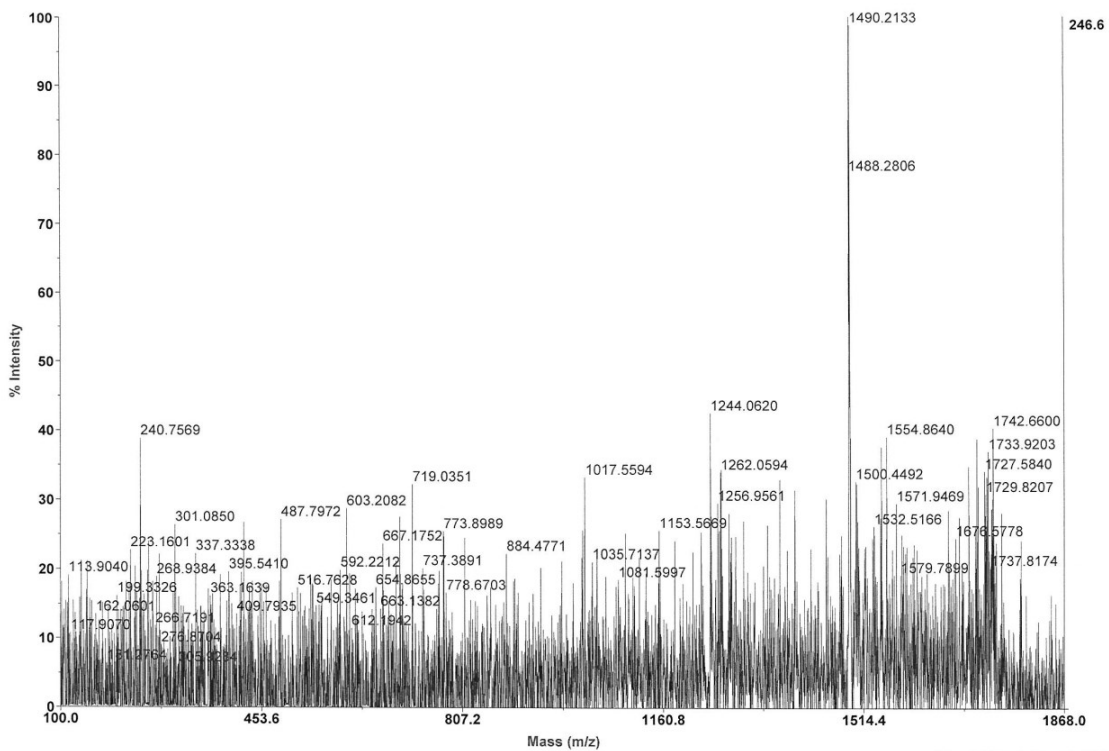


Figure 5.4: Negative ion CID MS/MS of the singly charged biphosphorylated lipid A [M-H]⁻ ion A at m/z 1768.2.

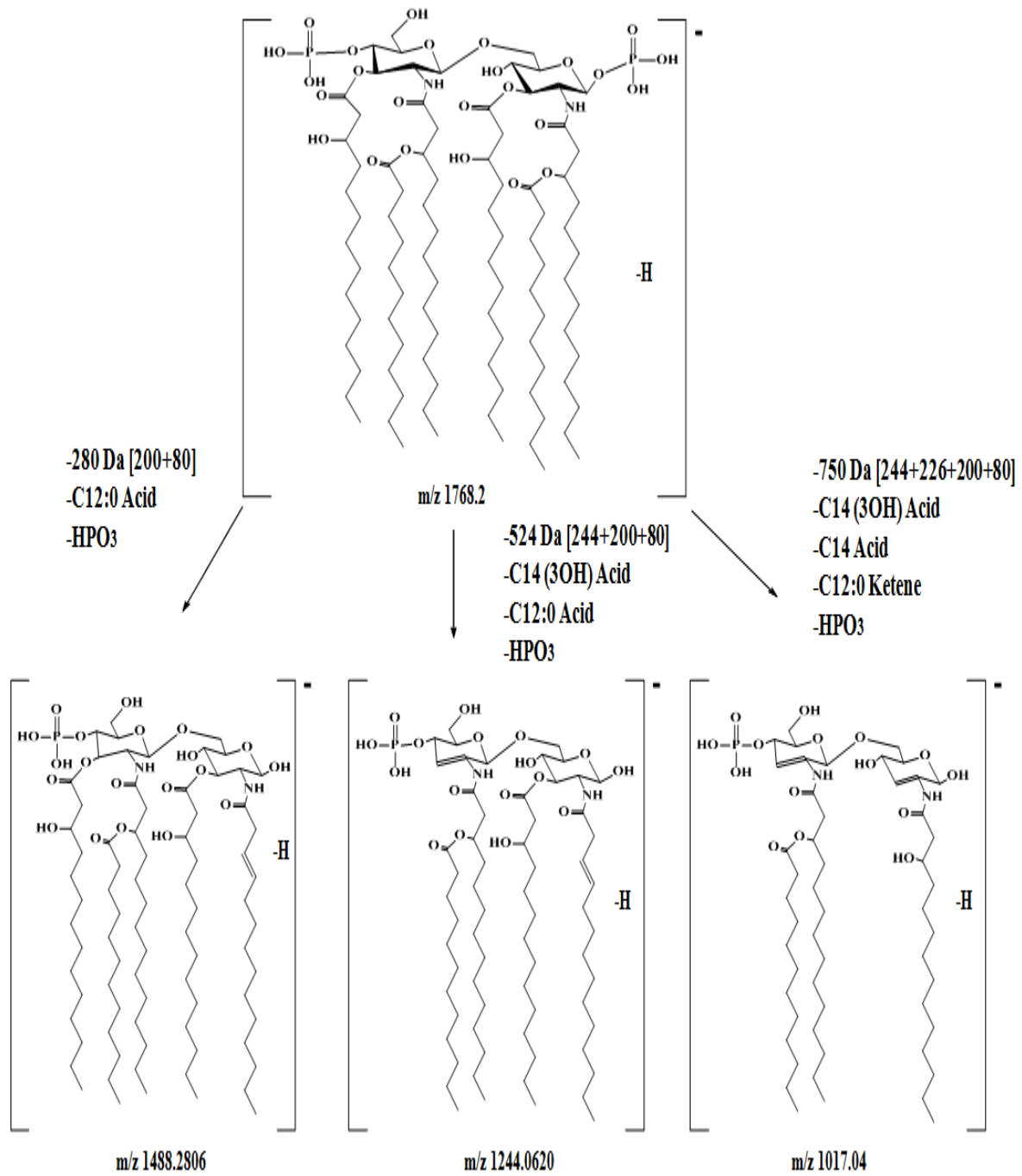


Figure 5.5: The proposed fragmentation pathway of the selected precursor ion at m/z 1768.2.

5.2.2 MS/MS of the precursor ions at m/z 1688.0 isolated from LipA2

The CID analysis of the precursor ion at m/z 1688.0 of LipA2 gave the product ions at m/z 1488.1086, and 1261.9907 as shown in Figure 5.6. It was observed that the main product ion at m/z 1488.1086, indicated the eventual elimination of the 12:0 acid (-200 Da) from the branched fatty acid at the N-2 position. The product ion of m/z 1261.9907 clearly indicated the eventual elimination of 14:0(3-OH) ketene from O-3' position (of around -226 Da difference) specifically from the precursor ion at m/z 1488.1086 as shown in Figure 5.7. Furthermore, these eliminations can in fact take place at N-2, at N-2' and even at O-3 and O-3' positions that is located respectively in the reducing end, or at the non-reducing end of the previously described disaccharide backbone of Lipid A.

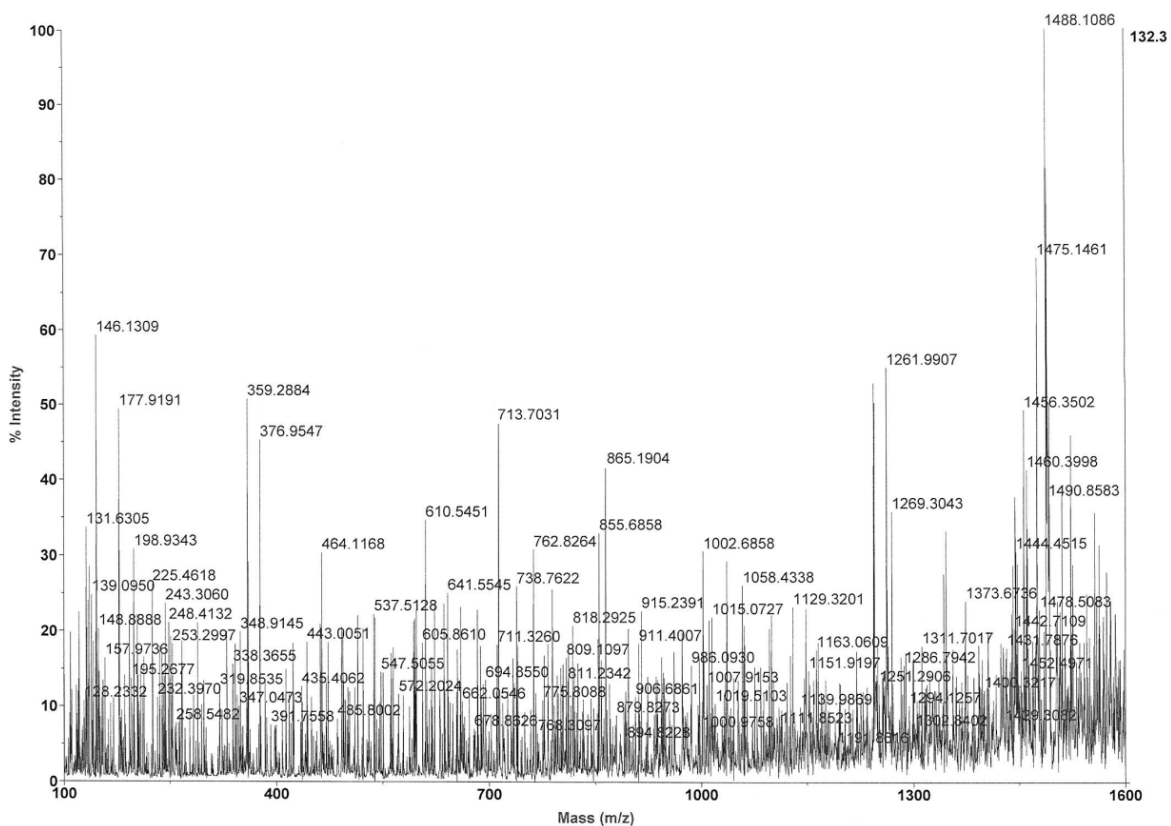


Figure 5.6: Negative ion CID MS/MS of the singly charged monophosphorylated Lipid A $[M-H]^-$ ion A at m/z 1688.2302

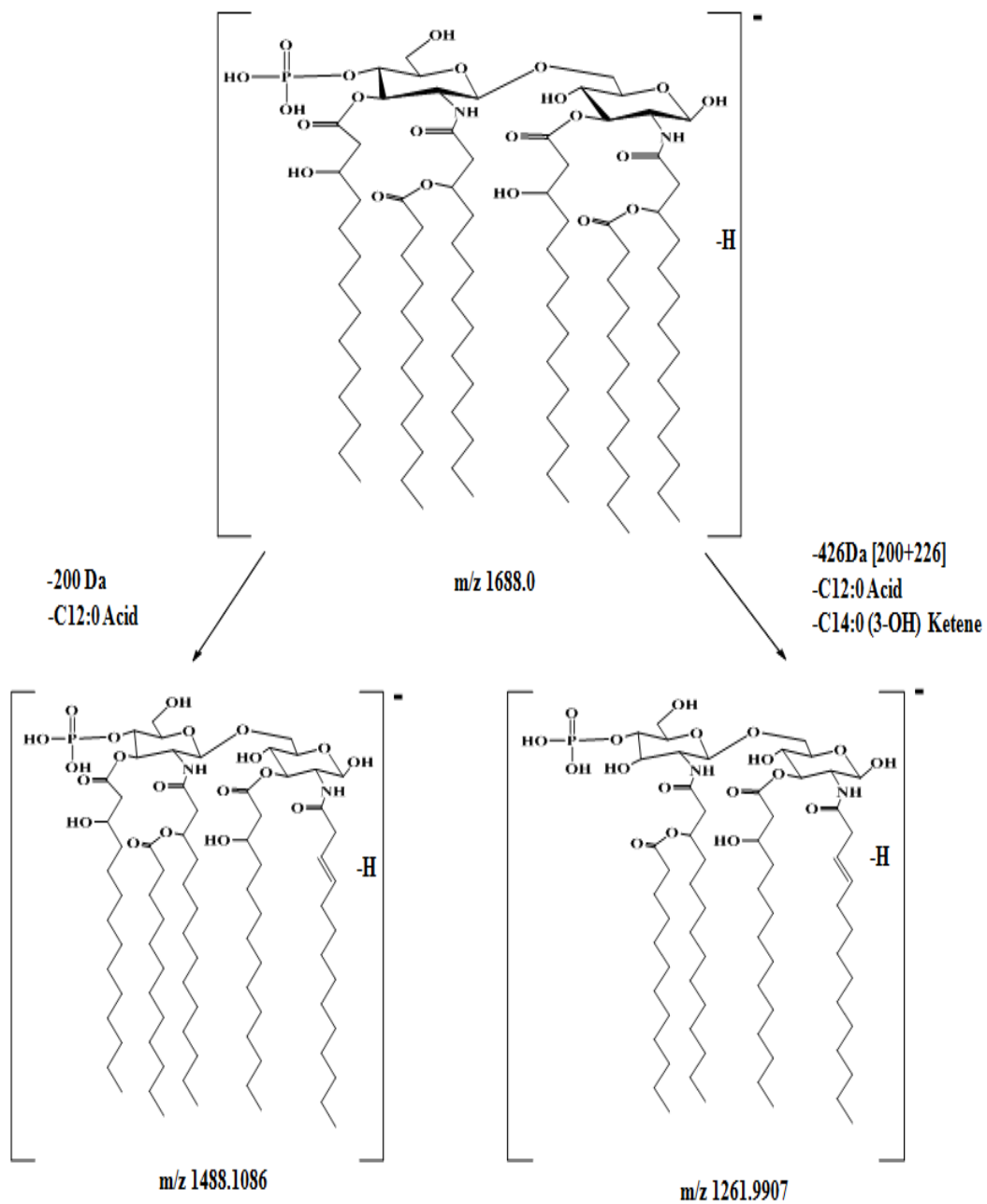


Figure 5.7: The proposed fragmentation pathway of the selected precursor ion at m/z 1688.0.

5.2.3 MS/MS of the abundant precursor ion at m/z 1585.6 LipA3

The precursor ion mainly at m/z 1585.6 of LipA3 was subjected to a MS² experiment, and is illustrated in Figure 5.8. The resulting product ions at m/z 1487.9103, 1341.7245, and 1243.7837 are shown in Figure 5.8. The main product ion at m/z 1487.9103 indicated the elimination of the H₂PO₄ from reducing sugar group and from the precursor ion of m/z 1585.6. The product ion at m/z 1341.7245 clearly showed the loss of a 14:0 fatty acid (of around -244 Da differences) from the 14:0(3-(*R*)-*O*-14:0) group from the O-3' position from the precursor ion at m/z 1585.6. Also, the elimination of a 14:0 fatty acid from the 14:0(3-(*R*)-*O*-14:0) at the O-3' position, and a H₂PO₄ from the reducing sugar group appeared in the product ion at m/z 1243.7837 (Figures 5.9).

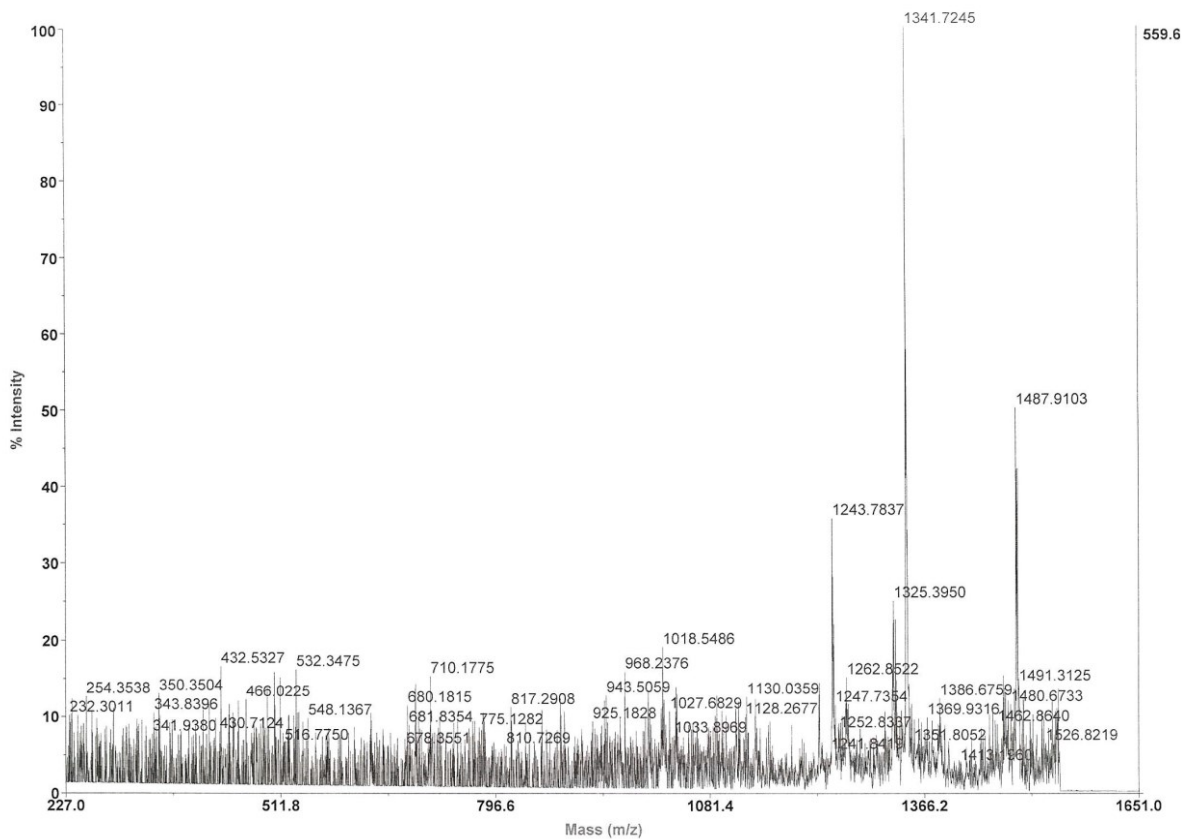


Figure 5.8: Negative ion CID MS/MS of the singly charged biphosphorylated Lipid A $[M-H]^-$ ion A at m/z 1585.6.

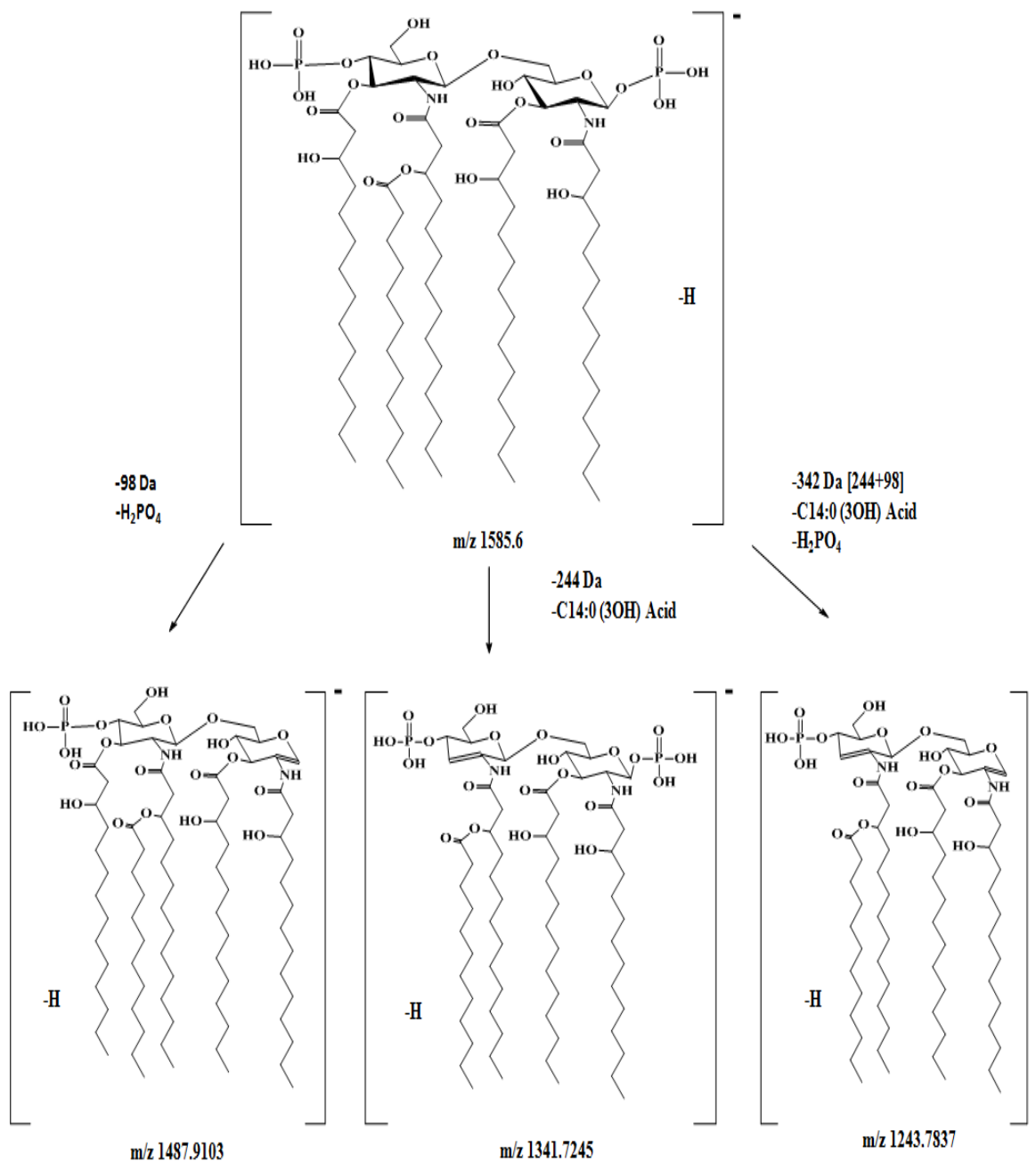


Figure 5.9: The proposed fragmentation pathway of the selected precursor ion at m/z 1585.6.

5.2.4 MS/MS of the abundant precursor ions at m/z 1505.7 isolated from LipA4

The CID analysis specifically of the second most highly abundant precursor ion at m/z 1505.7 of LipA4 shown in Figure 5.10 eventually afforded the product ions at m/z 1261.8335, 1243.8828, and 1017.5594, as shown in Figure 5.10. The main product ion of m/z 1261.8335 clearly indicated the eventual elimination of the 14:0(3-OH) acid from the O-3' position (of around -244 Da differences) specifically from the precursor ion at m/z 1505.7. Furthermore, this elimination can in fact take place at the O-3 and even at the O-3' positions that is located respectively in the reducing end, or in the non-reducing end of the previously described disaccharide backbone of lipid A. Moreover, from the product ions at m/z 1261.8335, the elimination of H₂O can occur to give the product ions at m/z 1243.8828. In addition to this, the eventual elimination of the 14:0(3-OH) acid at the exact O-3 position, appeared in the final product ion at around m/z 1017.5594 (Figure 5.11).

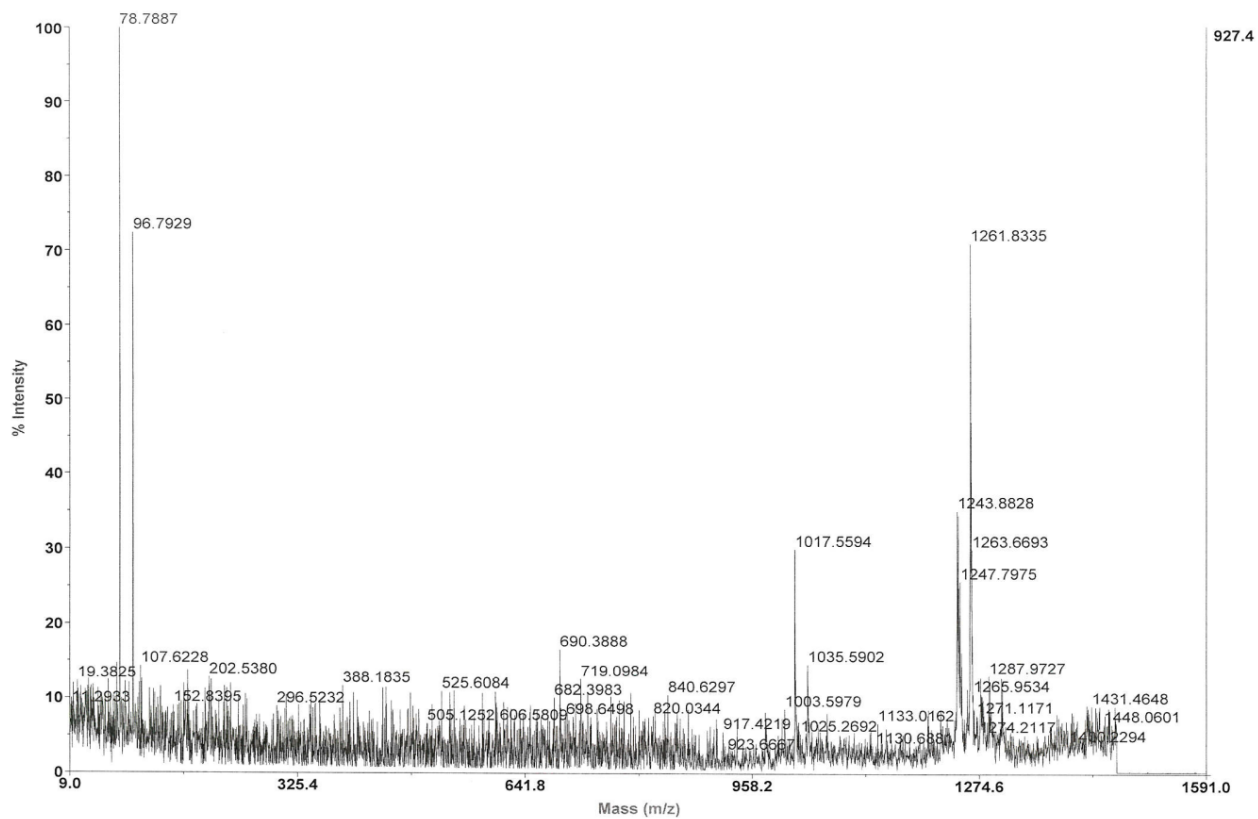


Figure 5.10: Negative ion CID MS/MS of the singly charged monophosphorylated Lipid A at m/z 1505.7.

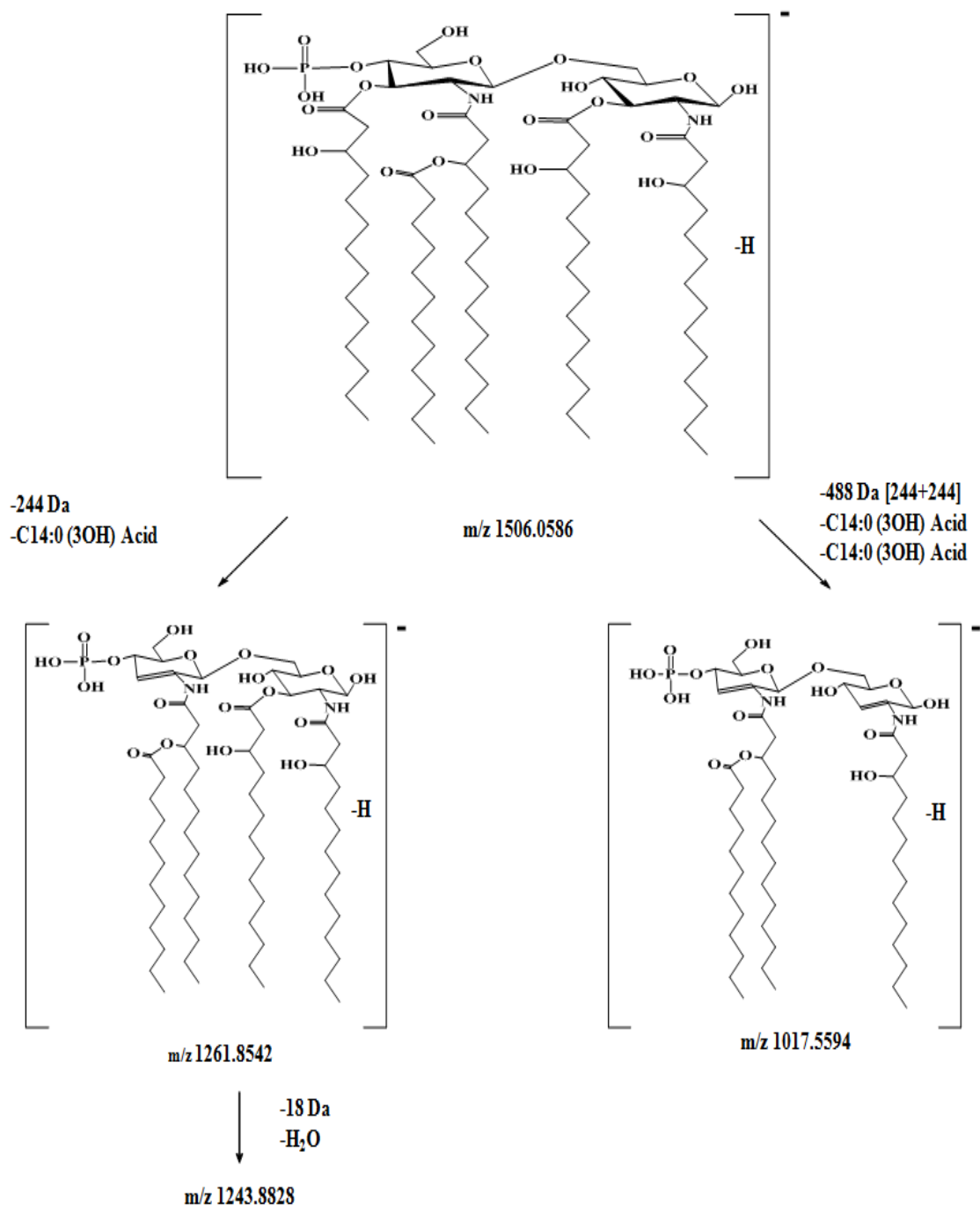


Figure 5.11: The proposed fragmentation pathway of the selected precursor ion at m/z 1506.0586.

5.2.5 MS/MS of the abundant precursor ion at m/z 1359.5 isolated from LipA5

The MS/MS CID analysis of the third abundant precursor ion mainly at m/z 1359.5 for LipA5 is shown in Figure 5.12, giving the product ions at m/z 1261.6610, 1115.4828, and 1017.4634. The product ion obtained from m/z 1261.6610 principally indicated the eventual elimination of H_2PO_4 specifically from reducing sugar group (around -98 Da differences) specifically from the precursor ion at m/z 1359.8266 LipA5. In addition to this, the mass difference (-244 Da) existing between the ions at m/z 1359.5 for LipA5 as well as at m/z 1115.4828 mainly indicated the eventual elimination of the 14:0(3-OH) acid mainly from the O-3 position. Furthermore, the elimination of H_2PO_4 from the reducing sugar group (-98 Da differences) specifically from the precursor ion at m/z 1115.4828 or the elimination of 14:0(3-OH) acid from the O-3 position (-244 Da difference) from the precursor ion at m/z 1261.6610, appeared in the final product ion at m/z 1017.4634, as shown in Figure 5.13.

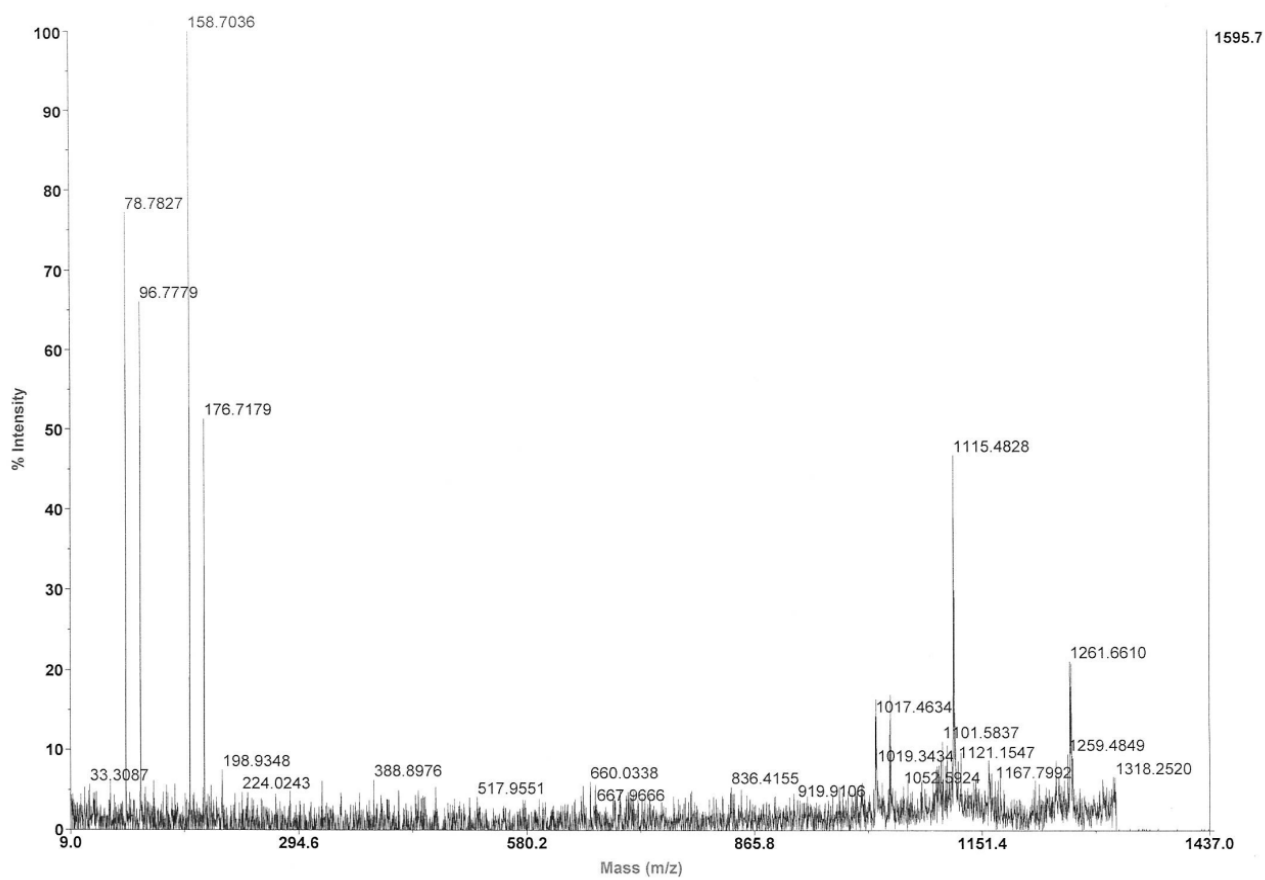


Figure 5.12: Negative ion CID MS/MS of the singly charged biphosphorylated lipid A at m/z 1359.5.

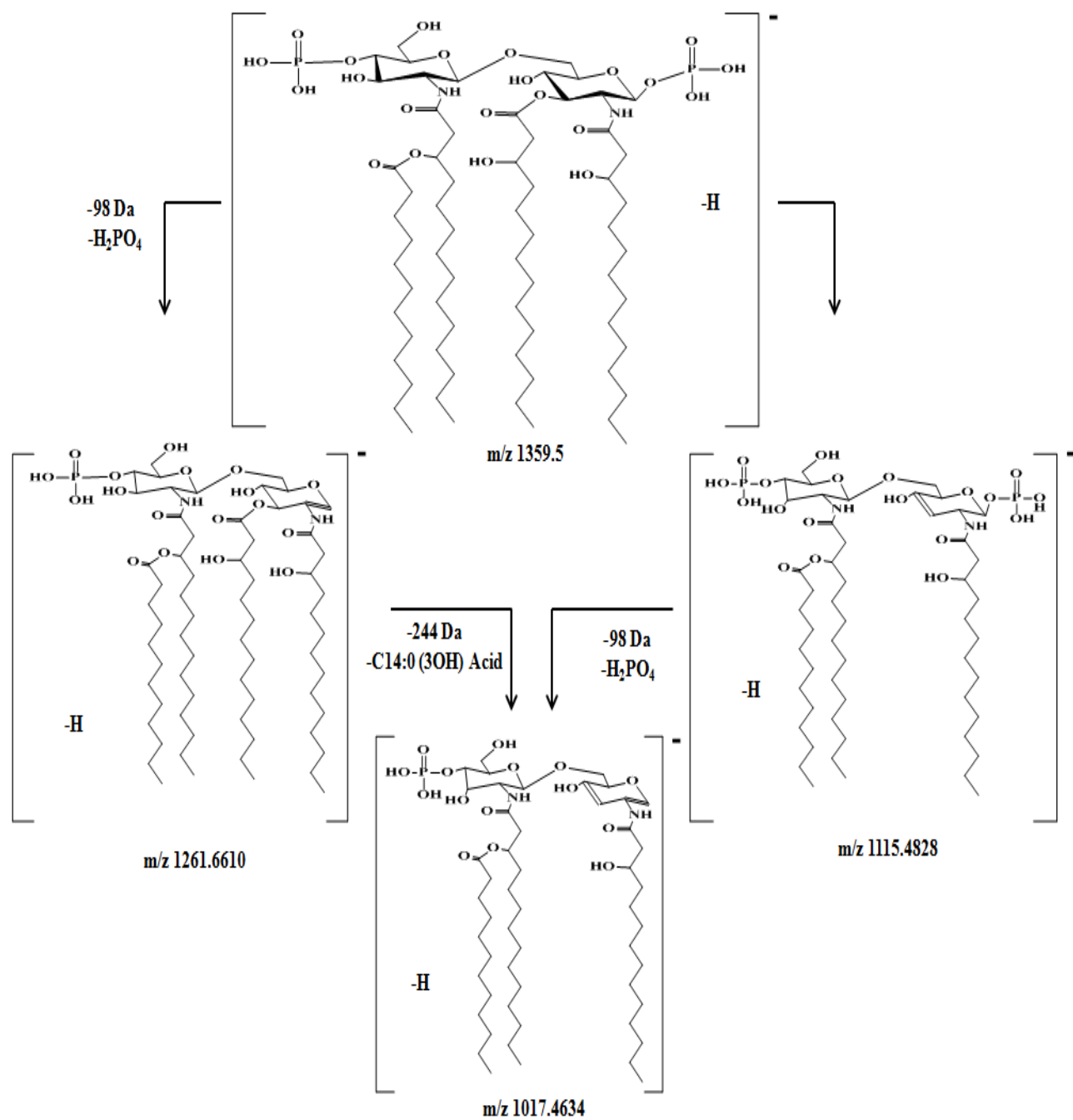


Figure 5.13: The proposed fragmentation pathway of the selected precursor ion at m/z 1359.5.

5.2.6 MS/MS of the abundant precursor ion at m/z 1279.5 isolated from LipA6

The CID analysis of the fourth most highly abundant precursor ion at m/z 1279.5 of LipA7 is shown in Figure 5.14 and gave the product ions at m/z 1079.4796, 1053.5066, 1035.4777, and 1017.5615. The obtained product ion from the m/z 1079.7355 ion typically was formed by the eventual elimination of the 12:0 fatty acid specifically at 14:0(3-(*R*)-*O*-12:0) group from the N-2' position (of around -200 Da). The existing mass difference specifically between the ions at m/z 1279.5 of LipA7 and 1053.5066 is -226 Da and it indicated the elimination of a 14:0 ketene obtained from the O-3 position of the precursor ion. The most abundant product ion at m/z 1035.4777 was formed by elimination of a 14:0 fatty acid from the 14:0(3-(*R*)-*O*-14:0) group at the O-3 position from the ion at m/z 1279.5.

Also, the loss of water from the product ion at m/z 1035.6529 gave the product ion at m/z 1017.5615 (Figure 5.15). As a result of this elimination, this latter ion was assigned to the monophosphorylated, tetra-acylated Lipid A form containing one phosphate group, three 14:0(3-OH) group located at the N-2, O-3, N-2' positions, and one 12:0 fatty acid located on the 14:0(3-(*R*)-*O*-12:0) group at the N-2' position.

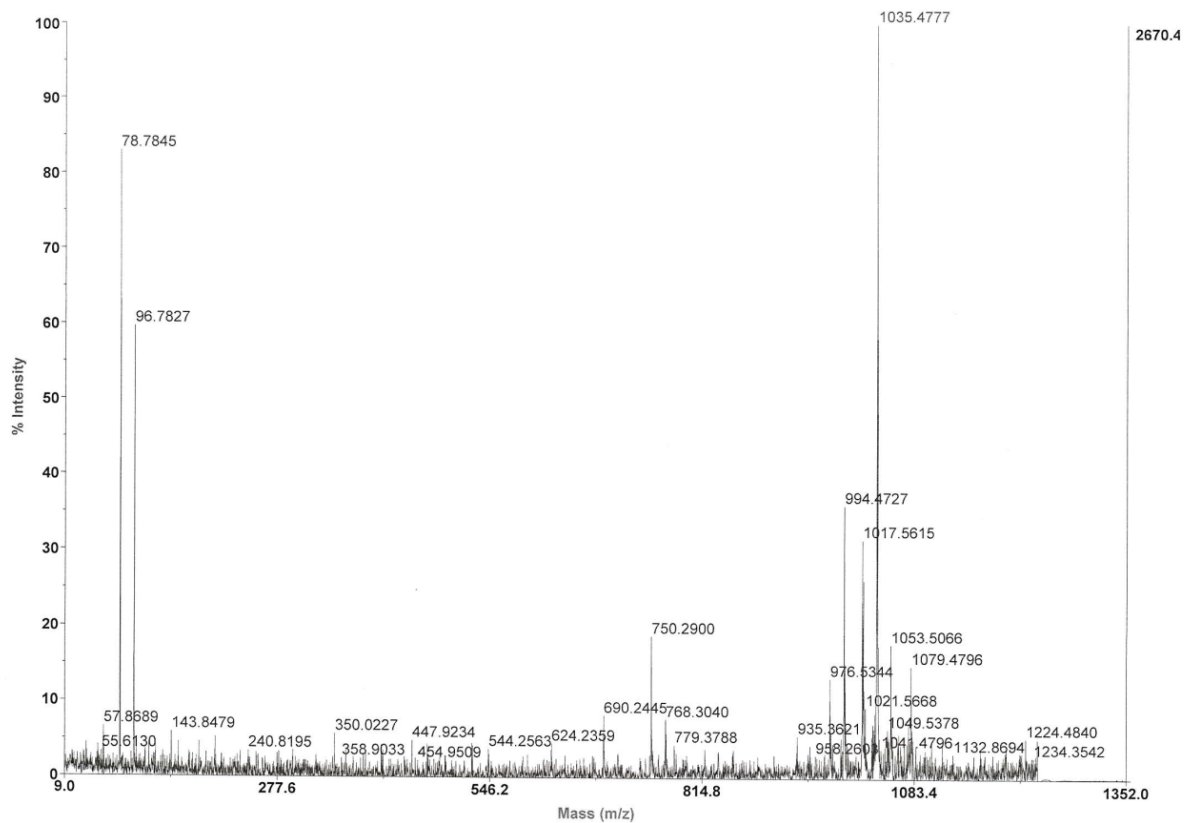


Figure 5.14: Negative ion CID MS/MS of the singly charged monophosphorylated Lipid A at m/z 1279.5.

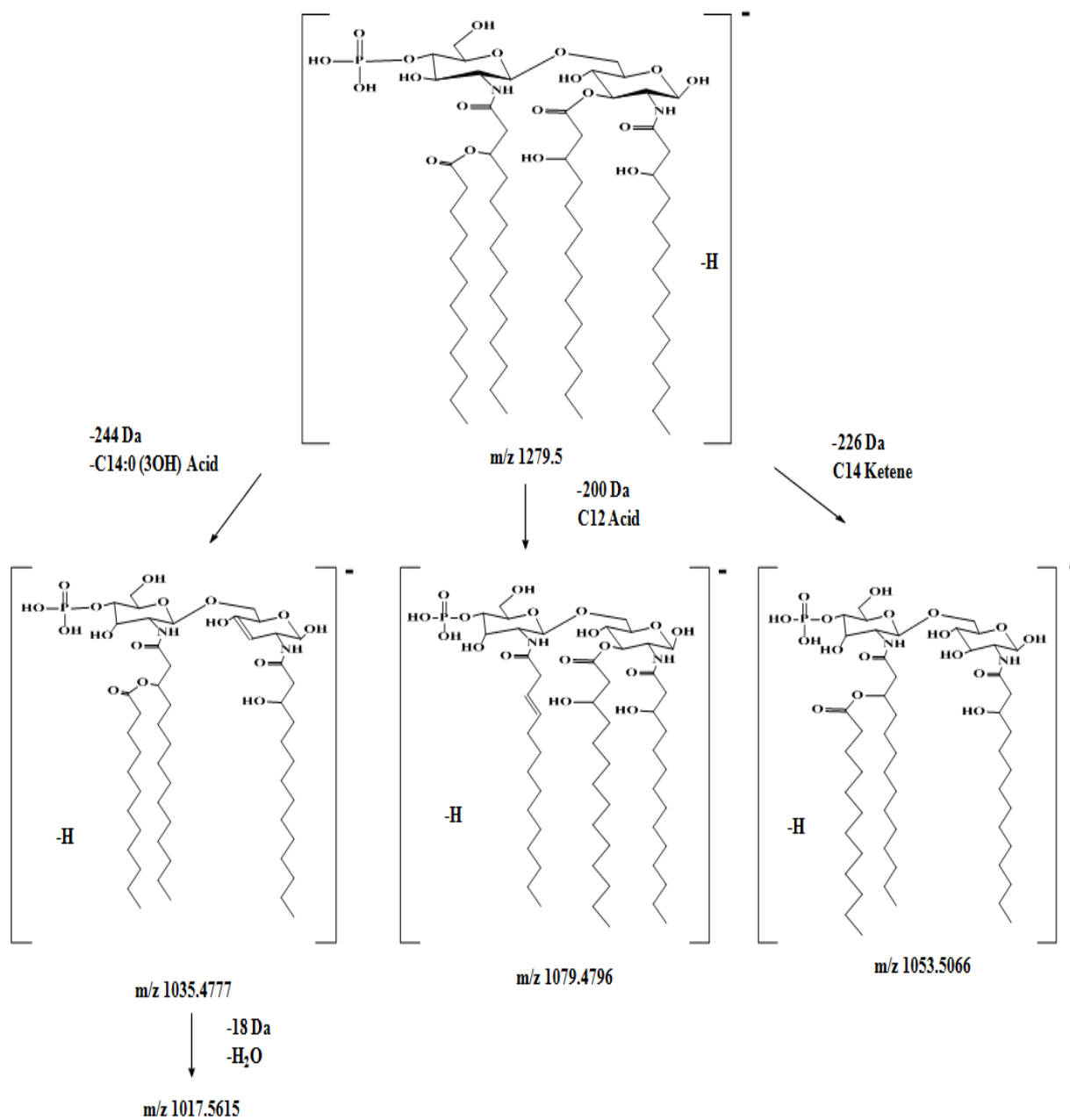


Figure 5.15: The proposed fragmentation pathway of the selected precursor ion at m/z 1279.5.

To confirm the phosphate group presence on that position, the precursor ion at m/z 892.4 was initially isolated and was later on subjected to a CID analysis as shown Figure 5.16. The most abundant product ion obtained at m/z 648.3460 was formed by a significant loss of the 14:0 fatty acid mainly on the 14:0(3-(*R*)-*O*-14:0) group located at the O-3' position (-244 Da) on Lipid A disaccharide backbone. Furthermore, the structure that was suggested for the product ion at m/z 648.3460 typically showed that the precise position of the phosphate group can also exist in either the C-1 position on the reducing sugar end or on the subsequent O-4' or the non-reducing sugar, which is acylated at N-2', with the 14:0 group situated at the fatty acid branch at N-2' as well as a 12:0 fatty acid obtained from the 14:0(3-(*R*)-*O*-12:0) group located on the N-2' position of the reducing sugar end or of the non-reducing end (Figure 5.20). Furthermore, the CID analysis of the precursor ions at m/z 666.3688 clearly indicated elimination of the C14:0 (3-OH) ketene (-226 Da) from the product ions at m/z 892.4.

5.3 CID analysis of the [C-H]⁻ and [Y-H]⁻ ions

As previously stated, one of the diagnostic ions, formed during the complete biosynthesis of Lipid A was assigned as the [C-H]⁻ ion at m/z 892.4 and it was later also observed in some of the traditional MALDI-TOF-MS reflect scanning analysis (as shown in Figure 5.16). This obtained ion can simply be produced by glycosidic cleavages mainly of the β-D-(1→6) in the D-GlcN disaccharide specifically during the MS/MS analysis of the complete Lipid A. To confirm the proposed structure of this obtained ion, MS/MS was conducted. Hence, the product ion scan of the ion [C-H]⁻ at m/z 892.4 clearly

showed the eventual loss of a 14:0 acid chain from position C-3' to yield the product ion at m/z 648.2242, assigned as the [C-(C14:0) (3-OH) acid-H] ion. Also, the elimination of C14:0 (3-OH) ketene located at position C-3', afforded the product ion at m/z 666.3688. This latter elimination is assumed to take place from the *O*-linked fatty acid located at position C-3' instead of the stable *N*-linked one located at position N-2' as shown in Figure 5.17.

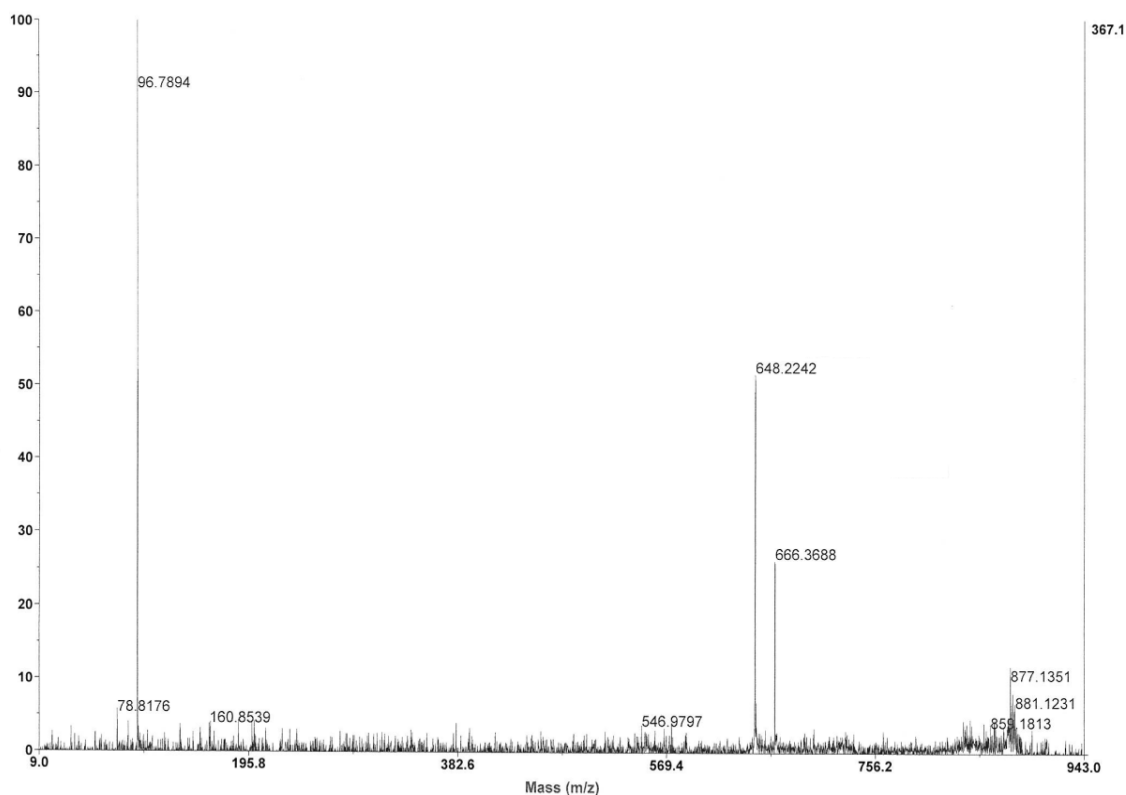


Figure 5.16: Negative ion CID MS/MS of the singly charged monophosphorylated Lipid A [C-H]- ion A at m/z 892.5778.

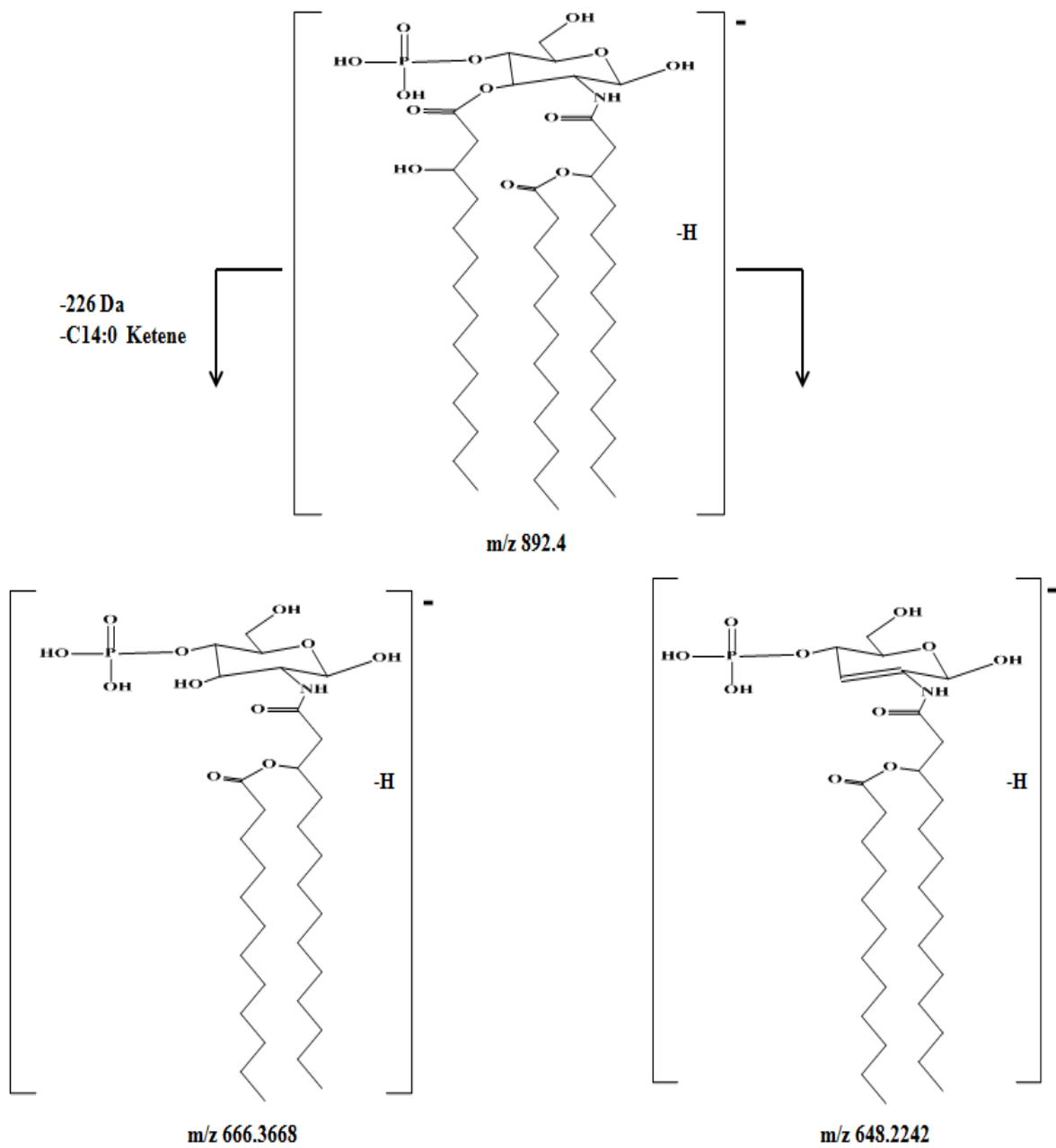


Figure 5.17: The proposed fragmentation pathway of the selected precursor ion at m/z 892.4.

5.4 Summary

The overall chemical structure mainly of Lipid A, when isolated after mild acid hydrolysis from the lipopolysaccharide fraction of the bacterial species *Aeromonas salmonicida* SJ-112 was elucidated using MALDI-TOF-TOF-MS hybrid tandem mass spectrometry with high-energy collision (CID) analysis. The data clearly illustrated a higher degree of microheterogeneity. In addition to this, the overall chemical structure for the major constituent of this specific heterogeneous mixture was later on in the study identified as being a D-(1→6) linked glucosamine disaccharide that was substituted by additional two phosphates groups that bonded to the main non-reducing end at C-4' position and also to the reducing end at C-1 of the D-glucosamine disaccharide.

The precise location specifically of the fatty acids that were linked to the disaccharide backbone was initially elucidated by careful identification of the diagnostic ions with the help of a MALDI-TOF/TOF-MS scan. Furthermore, high-energy collision (CID) mass spectrometry analysis specifically of already selected (diagnostic) precursor ions unambiguously confirmed their molecular structures. Moreover, it was also later on in the study established that the main 14:0(3-(*R*)-*O*-12:0) acid residue of it was on the O-3' position linked to the associated non-reducing sugar end of the D-GlcN residue having 3-hydroxymyristic (*R*)-14:0(3-OH) acid chains located at N-2', and additionally the 14:0(3-(*R*)-*O*-12:0) acidic residue was on the O-3 linkages to the main reducing end of the D-GlcN residue.

Lastly, the MS as well as the MS/MS data that were obtained, further allowed determination of Lipid A's complicated molecular structure.

Chapter 6 Conclusions

6.1 General Conclusion

The Lipid A extract of *Aeromonas Salmonicida* SJ-112 is not only composed of a single Lipid A entity but is a heterogeneous mixture of many structurally-related components produced by the incomplete biosynthesis of the Lipid.

Due to the complex nature of Lipid A, ESI-Mass spectrometry was used to tentatively propose the particular molecular structures within a biologically active extract. Tandem mass spectrometry using FT-ICR-MS² instruments were used to analyze the complex Lipid A mixture that is composed of various structurally related components, without the need for any tedious separation techniques. Similar structural results were obtained when the same heterogeneous mixture of structurally-related components was analyzed by MALDI-TOF-MS and high-energy CID-TOF/TOF-MS/MS.

It was shown that the major component of the Lipid A mixture contained two phosphate groups on both the reducing end (C-4) and non-reducing end (C-4') of the disaccharide Lipid A backbone. Additionally, several structures were identified containing both D-GlcN units of the β -D-(1 \rightarrow 6) disaccharides in which the *O*- and *N*-substituted with various fatty acids which were identified as 12:0 (3-OH), 14 (3-OH) and 16 (3-OH).

The distributions of these fatty acids on the individual Lipid A molecules were established by thoroughly analyzing the structures of the characteristic product ions

obtained in the FT-ICR-MS². In addition, the presence of the incomplete monosaccharide biosynthetic precursors were also established by revealing the structures of the [Y-H]⁻ and [C-H]⁻ derived product ions. Similar reasoning was applied for the case of the high-energy MALDI-TOF/TOF-MS/MS analyses. The presence of the diagnostic product [C-H]⁻ ion once more allowed to distinguish part of the monosaccharide biosynthetic precursor of the Lipid A backbone.

Moreover, product ions originating from inner sugar fragmentations were observed in the SORI-CID and CID-TOF/TOF-MSMS analysis. Furthermore, MS/MS analysis of the [Y]⁻ and [C]⁻ ions clearly confirmed the presence of two 14:0(3-OH) fatty acids on the reducing end group, and two 14:0(3-OH) on the non-reducing end group of the disaccharide. These were similarly evident by the generation of product ions that were associated with distinctive losses of these fatty chains, either as neutral ketene, or as a free fatty acid.

Lastly, mass spectrometric studies are now playing a leading role in the elucidation of lipopolysaccharide (LPS) structures through the characterization of antigenic polysaccharides, core oligosaccharides and lipid A components including LPS genetic modifications. The conventional MS and MS/MS analyses together with CID fragmentations can provide additional structural information complementary to the earlier analytical experiments. Thus, contributing to an integrated strategy for the simultaneous characterization and correct sequencing of the Lipid A moiety of this phage infected LPS.

Bibliography

1. Yates III, J. R. (2011). A century of mass spectrometry: from atoms to proteomes. *Nature methods*, 8(8), 633-637.
2. Sharma, K. S. (2013). Mass spectrometry—The early years. *International Journal of Mass Spectrometry*, 349, 3-8.
3. Brief obituary of Eugen Goldstein, *Nature*, 1931, volume 127, page 171.
4. Thomson, J. J. (1913). Bakerian lecture: Rays of positive electricity. *Proceedings of the Royal Society of London. Series A, Containing Papers of a Mathematical and Physical Character*, 1-20.
5. Dempster, A. J. (1918). A new method of positive ray analysis. *Physical Review*, 11(4), 316-325.
6. Downard, K. M. (2007). Francis William Aston: the man behind the mass spectrograph. *European Journal of Mass Spectrometry*, 13(3), 177-190.
7. Fenn, J. B., Mann, M., Meng, C. K., Wong, S. F., & Whitehouse, C. M. (1989). Electrospray ionization for mass spectrometry of large biomolecules. *Science*, 246(4926), 64-71.
8. "The Nobel Prize in Chemistry 2002". The Nobel Foundation. 9 October 2002. Retrieved 2013-01-31.
9. Kitson, F. G., Larsen, B. S., & McEwen, C. N. (1996). *Gas chromatography and mass spectrometry: a practical guide*. Academic Press. San Diego, pp. 381

10. Barber, M., Bordoli, R. S., Sedgwick, R. D., & Tyler, A. N. (1981). Fast atom bombardment of solids as an ion source in mass spectrometry. *Nature*, 293(5830), 270-275.
11. Morris, H. R., Panico, M., Barber, M., Bordoli, R. S., Sedgwick, R. D., & Tyler, A. (1981). Fast atom bombardment: a new mass spectrometric method for peptide sequence analysis. *Biochemical and biophysical research communications*, 101(2), 623-631.
12. Shackleton, C. H. L., & Straub, K. M. (1982). Direct analysis of steroid conjugates: the use of secondary ion mass spectrometry. *Steroids*, 40(1), 35-51.
13. Tanaka, K., Waki, H., Ido, Y., Akita, S., Yoshida, Y., Yoshida, T., & Matsuo, T. (1988). Protein and polymer analyses up to m/z 100 000 by laser ionization time of flight mass spectrometry. *Rapid Communications in Mass Spectrometry*, 2(8), 151-153.
14. Karas, M., Bahr, U., Ingendoh, A., Nordhoff, E., Stahl, B., Strupat, K., & Hillenkamp, F. (1990). Principles and applications of matrix-assisted UV-laser desorption/ionization mass spectrometry. *Analytica Chimica Acta*, 241(2), 175-185.
15. Yamashita, M., & Fenn, J. B. (1984). Electrospray ion source. Another variation on the free-jet theme. *The Journal of Physical Chemistry*, 88(20), 4451-4459.
16. Fenn, J. B., Mann, M., Meng, C. K., Wong, S. F., & Whitehouse, C. M. (1989). Electrospray ionization for mass spectrometry of large biomolecules. *Science*, 246(4926), 64-71.

17. Tanaka, K. (2003). The origin of macromolecule ionization by laser irradiation (Nobel lecture). *Angewandte Chemie International Edition*, 42(33), 3860-3870.
18. Louris, J. N., Brodbelt-Lustig, J. S., Cooks, R. G., Glish, G. L., van Berkel, G. J., & McLuckey, S. A. (1990). Ion isolation and sequential stages of mass spectrometry in a quadrupole ion trap mass spectrometer. *International journal of mass spectrometry and ion processes*, 96(2), 117-137.
19. Yost, R. A., & Enke, C. G. (1978). Selected ion fragmentation with a tandem quadrupole mass spectrometer. *Journal of the American Chemical Society*, 100(7), 2274-2275.
20. Cohen, A. M., Jahouh, F., Sioud, S., Rideout, R. M., Morgan, M. J., & Banoub, J. H. (2009). Quantification of Greenland halibut serum vitellogenin: a trip from the deep sea to the mass spectrometer. *Rapid Communications in Mass Spectrometry*, 23(7), 1049-1060.
21. Banoub, J., El Aneed, A., Cohen, A., & Martin, P. (2004). Characterization of the O-4 phosphorylated and O-5 substituted Kdo reducing end group and sequencing of the core oligosaccharide of *Aeromonas salmonicida* ssp *salmonicida* lipopolysaccharide using tandem mass spectrometry. *European Journal of Mass Spectrometry*, 10(5), 715-730.
22. Sinz, A., Kalkhof, S., & Ihling, C. (2005). Mapping protein interfaces by a trifunctional cross-linker combined with MALDI-TOF and ESI-FTICR mass spectrometry. *Journal of the American Society for Mass Spectrometry*, 16(12), 1921-1931.

23. Harrison, A. G., Mercer, R. S., Reiner, E. J., Young, A. B., Boyd, R. K., March, R. E., & Porter, C. J. (1986). A hybrid BEQQ mass spectrometer for studies in gaseous ion chemistry. *International journal of mass spectrometry and ion processes*, 74(1), 13-31.
24. Suckau, D., Resemann, A., Schuerenberg, M., Hufnagel, P., Franzen, J., & Holle, A. (2003). A novel MALDI LIFT-TOF/TOF mass spectrometer for proteomics. *Analytical and bioanalytical chemistry*, 376(7), 952-965.
25. Mechref, Y., Novotny, M. V., & Krishnan, C. (2003). Structural characterization of oligosaccharides using MALDI-TOF/TOF tandem mass spectrometry. *Analytical chemistry*, 75(18), 4895-4903.
26. Banoub J.H., Thibault, P., Mansour, A., Cohen, A., Heeley, D.H., Jackman, D. (2003). Characterisation of the intact rainbow trout vitellogenin protein and analysis of its derived tryptic and cyanogen bromide peptides by matrix-assisted laser desorption/ionisation time-of-flight-mass spectrometry and electrospray ionisation quadrupole/time-of-flight mass spectrometry. *Eur. J. Mass. Spectrom. (Chichester, Eng)*, 9(5):509-24.
27. Lewis, J. K., Wei, J., & Siuzdak, G. (2000). Matrix-assisted Laser Desorption/Ionization Mass Spectrometry in Peptide and Protein Analysis. *Encyclopaedia of Analytical Chemistry*, 1-14.
28. Cotter, R. J. (1992). Time-of-flight mass spectrometry for the structural analysis of biological molecules. *Analytical chemistry*, 64(21), 1027A-1039A.

29. Therisod, H., Labas, V., & Caroff, M. (2001). Direct microextraction and analysis of rough-type lipopolysaccharides by combined thin-layer chromatography and MALDI mass spectrometry. *Analytical chemistry*, 73(16), 3804-3807.
30. Hurst, G. B., Lankford, T. K., & Kennel, S. J. (2004). Mass spectrometric detection of affinity purified crosslinked peptides. *Journal of the American Society for Mass Spectrometry*, 15(6), 832-839.
31. Gut, I. G. (2004). DNA analysis by MALDI-TOF mass spectrometry. *Human mutation*, 23(5), 437-441.
32. Harvey, D. J. (2003). Matrix-assisted laser desorption/ionization mass spectrometry of carbohydrates and glycoconjugates. *International Journal of Mass Spectrometry*, 226(1), 1-35.
33. Balazy, M. (2004). Eicosanomics: targeted lipidomics of eicosanoids in biological systems. *Prostaglandins & other lipid mediators*, 73(3), 173-180.
34. Karas, M., Bahr, U., Ingendoh, A., Nordhoff, E., Stahl, B., Strupat, K., & Hillenkamp, F. (1990). Principles and applications of matrix-assisted UV-laser desorption/ionization mass spectrometry. *Analytica Chimica Acta*, 241(2), 175-185.
35. Beavis, R. C., Chait, B. T., & Fales, H. M. (1989). Cinnamic acid derivatives as matrices for ultraviolet laser desorption mass spectrometry of proteins. *Rapid Communications in Mass Spectrometry*, 3(12), 432-435.
36. Beavis, R. C., Chaudhary, T., & Chait, B. T. (1992). α -Cyano-4-hydroxycinnamic acid as a matrix for matrixassisted laser desorption mass spectrometry. *Organic Mass Spectrometry*, 27(2), 156-158.

37. Beavis, R. C., & Chait, B. T. (1991). Velocity distributions of intact high mass polypeptide molecule ions produced by matrix assisted laser desorption. *Chemical physics letters*, 181(5), 479-484.
38. Busch, K. L. (1995). Desorption ionization mass spectrometry. *Journal of Mass Spectrometry*, 30(2), 233-240.
39. Susnea, I., Bernevic, B., Wicke, M., Ma, L., Liu, S., Schellander, K., & Przybylski, M. (2013). Application of MALDI-TOF-mass spectrometry to proteome analysis using stain-free gel electrophoresis. In *Applications of MALDI-TOF Spectroscopy* (pp.37-54). Springer Berlin Heidelberg.
40. Ruprecht, B., & Lemeer, S. (2014). Proteomic analysis of phosphorylation in cancer. *Expert review of proteomics*, 11(3), 259-267.
41. Smith, J. S., Angel, T. E., Chavkin, C., Orton, D. J., Moore, R. J., & Smith, R. D. (2014). Characterization of individual mouse cerebrospinal fluid proteomes. *Proteomics*, 14(9), 1102-1106.
42. Bökman, C. F. (2002). Analytical aspects of atmospheric pressure ionisation in mass spectrometry.
43. Kebarle, P., & Tang, L. (1993). From ions in solution to ions in the gas phase-the mechanism of electrospray mass spectrometry. *Analytical Chemistry*, 65(22), 972A-986A.
44. Dawson, P. H. (1986). Quadrupole mass analyzers: performance, design and some recent applications. *Mass Spectrometry Reviews*, 5(1), 1-37.

45. El-Aneed, Anas. (2006). Mass Spectrometric Analysis and Fingerprint Identification of Natural Lipopolysaccharide Vaccine Candidates and Synthetic Liposomal Cholesteryl Neoglycolipids. *Phd. Thesis*, Memorial University of St John's Newfoundland; pp 15-16.
46. Goodley, P. (2007). Maximizing MS/MS fragmentation in the ion trap using CID voltage ramping. *Agilent Report*.
47. Fishbane, P. M., Gasiorowicz, S. G., & Thornton, S. T. (2005). *Physics*. Prentice-Hall.
48. Marshall, A. G., & Hendrickson, C. L. (2002). Fourier transform ion cyclotron resonance detection: principles and experimental configurations. *International Journal of Mass Spectrometry*, 215(1), 59-75.
49. Marshall, A. G., & Grosshans, P. B. (1991). Fourier transform ion cyclotron resonance mass spectrometry: the teenage years. *Analytical Chemistry*, 63(4), 215A-229A.
50. Pól, J., Vidová, V., Kruppa, G., Koblíha, V., Novák, P., Lemr, K., ... & Volný, M. (2009). Automated ambient desorption– ionization platform for surface imaging integrated with a commercial Fourier transform ion cyclotron resonance mass spectrometer. *Analytical chemistry*, 81(20), 8479-8487.
51. Yost, R. A., & Fetterolf, D. D. (1983). Tandem mass spectrometry (MS/MS) instrumentation. *Mass Spectrometry Reviews*, 2(1), 1-45.
52. Neubauer, G., & Mann, M. (1999). Mapping of phosphorylation sites of gel-isolated proteins by nanoelectrospray tandem mass spectrometry: potentials and limitations. *Analytical chemistry*, 71(1), 235-242.

53. De Hoffmann, E. (1996). Tandem mass spectrometry: a primer. *Journal of mass spectrometry*, 31(2), 129-137.
54. Dass, C. (1993). Dimerization of the ketene cation radical in the gas phase. *Rapid communications in mass spectrometry*, 7(1), 95-98.
55. Jennings, K. R. (1968). Collision-induced decompositions of aromatic molecular ions. *International Journal of Mass Spectrometry and Ion Physics*, 1(3), 227-235.
56. Zubarev, R. A., Kelleher, N. L., & McLafferty, F. W. (1998). Electron capture dissociation of multiply charged protein cations. A nonergodic process. *Journal of the American Chemical Society*, 120(13), 3265-3266.
57. Syka, J. E., Coon, J. J., Schroeder, M. J., Shabanowitz, J., & Hunt, D. F. (2004). Peptide and protein sequence analysis by electron transfer dissociation mass spectrometry. *Proceedings of the National Academy of Sciences of the United States of America*, 101(26), 9528-9533.
58. Mabud, M. A., Dekrey, M. J., & Cooks, R. G. (1985). Surface-induced dissociation of molecular ions. *International journal of mass spectrometry and ion processes*, 67(3), 285-294.
59. Håkansson, K., Chalmers, M. J., Quinn, J. P., McFarland, M. A., Hendrickson, C. L., & Marshall, A. G. (2003). Combined electron capture and infrared multiphoton dissociation for multistage MS/MS in a Fourier transform ion cyclotron resonance mass spectrometer. *Analytical chemistry*, 75(13), 3256-3262.
60. Rodriguez-Cruz, S. E., Jockusch, R. A., & Williams, E. R. (1998). Hydration Energies of Divalent Metal Ions, $\text{Ca}^{2+}(\text{H}_2\text{O})_n$ ($n= 5-7$) and $\text{Ni}^{2+}(\text{H}_2\text{O})_n$ ($n= 6-8$),

- Obtained by Blackbody Infrared Radiative Dissociation. *Journal of the American Chemical Society*, 120(23), 5842-5843.
61. Rodriguez-Cruz, S. E., Jockusch, R. A., & Williams, E. R. (1999). Hydration Energies and Structures of Alkaline Earth Metal Ions, $M^{2+} (H_2O)_n$, $n = 5-7$, $M = Mg, Ca, Sr, \text{ and } Ba$. *Journal of the American Chemical Society*, 121(38), 8898-8906.
62. Dunbar, R. C. (2004). BIRD (blackbody infrared radiative dissociation): evolution, principles, and applications. *Mass spectrometry reviews*, 23(2), 127-158.
63. Hofstadler, S. A., Wahl, J. H., Bakhtiar, R., Anderson, G. A., Bruce, J. E., & Smith, R. D. (1994). Capillary electrophoresis Fourier transform ion cyclotron resonance mass spectrometry with sustained off-resonance irradiation for the characterization of protein and peptide mixtures. *Journal of the American Society for Mass Spectrometry*, 5(10), 894-899.
64. Fridgen, T. D. (2009). Infrared consequence spectroscopy of gaseous protonated and metal ion cationized complexes. *Mass spectrometry reviews*, 28(4), 586-607.
65. Polfer, N. C., & Oomens, J. (2009). Vibrational spectroscopy of bare and solvated ionic complexes of biological relevance. *Mass spectrometry reviews*, 28(3), 468-494.
66. Polfer, N. C. (2011). Infrared multiple photon dissociation spectroscopy of trapped ions. *Chemical Society Reviews*, 40(5), 2211-2221.
67. Morris, H. R., Paxton, T., Dell, A., Langhorne, J., Berg, M., Bordoli, R. S., ... & Bateman, R. H. (1996). High sensitivity collisionally-activated decomposition tandem mass spectrometry on a novel quadrupole/orthogonal-acceleration time-of-flight mass spectrometer. *Rapid Communications in Mass Spectrometry*, 10(8), 889-896.

68. Krutchinsky, A. N., Chernushevich, I. V., Spicer, V. L., Ens, W., & Standing, K. G. (1998). Collisional damping interface for an electrospray ionization time-of-flight mass spectrometer. *Journal of the American Society for Mass Spectrometry*, 9(6), 569-579.
69. Ens, W., & Standing, K. G. (2005). Hybrid quadrupole/time-of-flight mass spectrometers for analysis of biomolecules. *Methods in enzymology*, 402, 49-78.
70. Stephens, W. E. (1946, January). A pulsed mass spectrometer with time dispersion. In *Physical Review* (Vol. 69, No. 11-1, pp. 691-691). ONE PHYSICS ELLIPSE, COLLEGE PK, MD 20740-3844 USA: AMERICAN PHYSICAL SOC.
71. Brown, R. S., & Lennon, J. J. (1995). Mass resolution improvement by incorporation of pulsed ion extraction in a matrix-assisted laser desorption/ionization linear time-of-flight mass spectrometer. *Analytical Chemistry*, 67(13), 1998-2003.
72. Mamyrin, B. A., & Shmikk, D. V. (1979). Linear mass reflectron. *Zh. Eksp. Teor. Fiz*, 76, 1500.
73. Verentchikov, A. N., Ens, W., & Standing, K. G. (1994). Reflecting time-of-flight mass spectrometer with an electrospray ion source and orthogonal extraction. *Analytical chemistry*, 66(1), 126-133.
74. Gram H. C. (1884). Uber die isolierte Farbung der Schizomyceten in Schnitt- und Trockenpreparaten. *Fortschritte derMedizin* 2: 185-189.
75. Seltmann, G., & Holst, O. (2002). *The bacterial cell wall*. Springer Science & Business Media.

76. Dijkstra, A. J., & Keck, W. (1996). Peptidoglycan as a barrier to transenvelope transport. *Journal of bacteriology*, 178(19), 5555.
77. Tipper, D. J., & Strominger, J. L. (1965). Mechanism of action of penicillins: a proposal based on their structural similarity to acyl-D-alanyl-D-alanine. *Proceedings of the National Academy of Sciences of the United States of America*, 54(4), 1133.
78. Wise Jr, E. M., & Park, J. T. (1965). Penicillin: its basic site of action as an inhibitor of a peptide cross-linking reaction in cell wall mucopeptide synthesis. *Proceedings of the National Academy of Sciences of the United States of America*, 54(1), 75.
79. Ward, J. B. (1981). Teichoic and teichuronic acids: biosynthesis, assembly, and location. *Microbiological reviews*, 45(2), 211.
80. Archibald, A. R., Baddiley, J., & Blumsom, N. L. (1968). The teichoic acids. *Advances in Enzymology and Related Areas of Molecular Biology, Volume 30*, 223-253.
81. Wicken, A. J., & Knox, K. W. (1975). Lipoteichoic acids: a new class of bacterial antigen. *Science*, 187(4182), 1161-1167.
82. Schäffer, C., & Messner, P. (2005). The structure of secondary cell wall polymers: how Gram-positive bacteria stick their cell walls together. *Microbiology*, 151(3), 643-651.
83. Wunschel, D. S., Fox, K. F., Fox, A., Nagpal, M. L., Kim, K., Stewart, G. C., & Shahgholi, M. (1997). Quantitative analysis of neutral and acidic sugars in whole bacterial cell hydrolysates using high-performance anion-exchange liquid

- chromatography–electrospray ionization tandem mass spectrometry. *Journal of Chromatography A*, 776(2), 205-219.
84. Kim, J. H., Seo, H., Han, S. H., Lin, J., Park, M. K., Sorensen, U. B., & Nahm, M. H. (2005). Monoacyl lipoteichoic acid from pneumococci stimulates human cells but not mouse cells. *Infection and immunity*, 73(2), 834-840.
85. Beveridge, T. J., & Davies, J. A. (1983). Cellular responses of *Bacillus subtilis* and *Escherichia coli* to the Gram stain. *Journal of bacteriology*, 156(2), 846-858.
86. Choma, A., Komaniecka, I., Turska-Szewczuk, A., Danikiewicz, W., & Spolnik, G. (2012). Structure of lipid A from a stem-nodulating bacterium *Azorhizobium caulinodans*. *Carbohydrate research*, 352, 126-136.
87. Matsuura, M. (2013). Structural modifications of bacterial lipopolysaccharide that facilitate Gram-negative bacteria evasion of host innate immunity. *Frontiers in immunology*, 4.
88. Sohlenkamp, C., Raetz, C. R., & Ingram, B. O. (2013). The calcium-stimulated lipid A 3-O deacylase from *Rhizobium etli* is not essential for plant nodulation. *Biochimica et Biophysica Acta (BBA)-Molecular and Cell Biology of Lipids*, 1831(7), 1250-1259.
89. Sforza, S., Silipo, A., Molinaro, A., Marchelli, R., Parrilli, M., & Lanzetta, R. (2004). Determination of fatty acid positions in native lipid A by positive and negative electrospray ionization mass spectrometry. *Journal of mass spectrometry*, 39(4), 378-383.

90. Banoub, J. H., Aneed, A. E., Cohen, A. M., & Joly, N. (2010). Structural investigation of bacterial lipopolysaccharides by mass spectrometry and tandem mass spectrometry. *Mass spectrometry reviews*, 29(4), 606-650.
91. MacLean, L. L., Perry, M. B., & Vinogradov, E. (2004). Characterization of the antigenic lipopolysaccharide O chain and the capsular polysaccharide produced by *Actinobacillus pleuropneumoniae* serotype 13. *Infection and immunity*, 72(10), 5925-5930.
92. Amor, K., Heinrichs, D. E., Fridrich, E., Ziebell, K., Johnson, R. P., & Whitfield, C. (2000). Distribution of core oligosaccharide types in lipopolysaccharides from *Escherichia coli*. *Infection and immunity*, 68(3), 1116-1124.
93. Kondakova, A. N., Toukach, F. V., Senchenkova, S. N., Arbatsky, N. P., Shashkov, A. S., Knirel, Y. A., ... & Sidorczyk, Z. (2003). New structures of the O-specific polysaccharides of *Proteus*. 3. Polysaccharides containing non-carbohydrate organic acids. *Biochemistry (Moscow)*, 68(4), 446-457.
94. Lukasiewicz, J., Niedziela, T., Jachymek, W., Kenne, L., & Lugowski, C. (2006). Structure of the lipid A-inner core region and biological activity of *Plesiomonas shigelloides* O54 (strain CNCTC 113/92) lipopolysaccharide. *Glycobiology*, 16(6), 538-550.
95. Sioud, S., Jahouh, F., Nashed, M., Joly, N., & Banoub, J. H. (2010). Determination of distinctive carbohydrate signatures obtained from the *Aeromonas hydrophila* (chemotype II) core oligosaccharide pinpointing the presence of the 4-O-phosphorylated 5-O-linked Kdo reducing end group using electrospray ionization

- quadrupole orthogonal time-of-flight mass spectrometry and tandem mass spectrometry. *Rapid Communications in Mass Spectrometry*, 24(17), 2475-2490.
96. Michaud, J. P., Hallé, M., Lampron, A., Thériault, P., Préfontaine, P., Filali, M., ... & Rivest, S. (2013). Toll-like receptor 4 stimulation with the detoxified ligand monophosphoryl lipid A improves Alzheimer's disease-related pathology. *Proceedings of the National Academy of Sciences*, 110(5), 1941-1946.
97. Caroff, M., & Karibian, D. (2003). Structure of bacterial lipopolysaccharides. *Carbohydrate research*, 338(23), 2431-2447.
98. Schwudke D., Linscheid M., Strauch E., Appel B., Zahringer U., Moll H., Muller M., Brecker L., Gronow S., and Lindner B. (2003). The obligate predatory *Bdellovibrio bacteriovorus* possesses a neutral lipid A containing alpha-D-Mannoses that replace phosphate residues: similarities and differences between the lipid As and the lipopolysaccharides of the wild type strain B. bacteriovorus HD 100 and its host-independent derivative HI100. *JB iol Chem* 278: 27502-12.
99. Zdrovenko, G. M., Shashkov, A. S., Zdrovenko, E. L., Kocharova, N. A., Yakovleva, L. M., Knirel, Y. A., & Rudolph, K. (2001). Characterization of the lipopolysaccharide and structure of the O-specific polysaccharide of the bacterium *Pseudomonas syringae* pv. *atofaciens* IMV 948. *Biochemistry (Moscow)*, 66(4), 369-377.
100. Mikhail, I., Yildirim, H. H., Lindahl, E. C., & Schweda, E. K. (2005). Structural characterization of lipid A from nontypeable and type f *Haemophilus influenzae*: variability of fatty acid substitution. *Analytical biochemistry*, 340(2), 303-316.

101. Corsaro, M. M., Lanzetta, R., Parrilli, E., Parrilli, M., Tutino, M. L., & Ummarino, S. (2004). Influence of growth temperature on lipid and phosphate contents of surface polysaccharides from the Antarctic bacterium *Pseudoalteromonas haloplanktis* TAC 125. *Journal of bacteriology*, *186*(1), 29-34.
102. Li, J., Martin, A., Cox, A. D., Moxon, E. R., Richards, J. C., & Thibault, P. (2005). Mapping bacterial glycolipid complexity using capillary electrophoresis and electrospray mass spectrometry. *Methods in enzymology*, *405*, 369-397.
103. Rund, S., Lindner, B., Brade, H., & Holst, O. (2000). Structural analysis of the lipopolysaccharide from *Chlamydophila psittaci* strain 6BC. *European Journal of Biochemistry*, *267*(18), 5717-5726.
104. Kelly, J., Masoud, H., Perry, M. B., Richards, J. C., & Thibault, P. (1996). Separation and Characterization of O-Deacylated Lipooligosaccharides and Glycans Derived from *Moraxella catarrhalis* Using Capillary Electrophoresis–Electrospray Mass Spectrometry and Tandem Mass Spectrometry. *Analytical biochemistry*, *233*(1), 15-30.
105. Silipo, A., Molinaro, A., Cescutti, P., Bedini, E., Rizzo, R., Parrilli, M., & Lanzetta, R. (2005). Complete structural characterization of the lipid A fraction of a clinical strain of *B. cepacia* genomovar I lipopolysaccharide. *Glycobiology*, *15*(5), 561-570.
106. Peri, F., Marinzi, C., Barath, M., Granucci, F., Urbano, M., & Nicotra, F. (2006). Synthesis and biological evaluation of novel lipid A antagonists. *Bioorganic & medicinal chemistry*, *14*(1), 190-199.

107. Li, B., An, H. J., Hedrick, J. L., & Lebrilla, C. B. (2009). Collision-induced dissociation tandem mass spectrometry for structural elucidation of glycans. In *Glycomics* (pp. 133-145). Humana Press.
108. Zhang, J., Schubothe, K., Li, B., Russell, S., & Lebrilla, C. B. (2005). Infrared multiphoton dissociation of O-linked mucin-type oligosaccharides. *Analytical chemistry*, 77(1), 208-214.
109. Domon, B., & Costello, C. E. (1988). A systematic nomenclature for carbohydrate fragmentations in FAB-MS/MS spectra of glycoconjugates. *Glycoconjugate Journal*, 5(4), 397-409.
110. Erridge, C., Stewart, J., Bennett-Guerrero, E., McIntosh, T. J., & Poxton, I. R. (2002). The biological activity of a liposomal complete core lipopolysaccharide vaccine. *Journal of endotoxin research*, 8(1), 39-46.
111. Kawai, Y., Watanabe, M., Matsuura, M., Nishijima, M., & Kawahara, K. (2002). The partially degraded lipopolysaccharide of *Burkholderia cepacia* and ornithine-containing lipids derived from some Gram-negative bacteria are useful complex lipid adjuvants. *FEMS Immunology & Medical Microbiology*, 34(3), 173-179.
112. Baldrige, J. R., Yorgensen, Y., Ward, J. R., & Ulrich, J. T. (2000). Monophosphoryl lipid A enhances mucosal and systemic immunity to vaccine antigens following intranasal administration. *Vaccine*, 18(22), 2416-2425.
113. Persing, D. H., Coler, R. N., Lacy, M. J., Johnson, D. A., Baldrige, J. R., Hershberg, R. M., & Reed, S. G. (2002). Taking toll: lipid A mimetics as adjuvants and immunomodulators. *Trends in microbiology*, 10(10), s32-s37.

114. Prince, G. A., Denamur, F., Deschamps, M., Garçon, N., Prieels, J. P., Slaoui, M., & Porter, D. D. (2001). Monophosphoryl lipid A adjuvant reverses a principal histologic parameter of formalin-inactivated respiratory syncytial virus vaccine-induced disease. *Vaccine*, *19*(15), 2048-2054.
115. Larmonier, C. B., Arnould, L., Larmonier, N., Baumann, S., Moutet, M., Saint-Giorgio, V., ... & Jeannin, J. F. (2004). Kinetics of tumor cell apoptosis and immune cell activation during the regression of tumors induced by lipid A in a rat model of colon cancer. *International journal of molecular medicine*, *13*(3), 355-361.
116. Reisser, D., Pance, A., & Jeannin, J. F. (2002). Mechanisms of the antitumoral effect of lipid A. *Bioessays*, *24*(3), 284-289.
117. Won, E. K., Zahner, M. C., Grant, E. A., Gore, P., & Chicoine, M. R. (2003). Analysis of the antitumoral mechanisms of lipopolysaccharide against glioblastoma multiforme. *Anti-cancer drugs*, *14*(6), 457-466.
118. Brandenburg, K., Matsuura, M., Heine, H., Müller, M., Kiso, M., Ishida, H., ... & Seydel, U. (2002). Biophysical characterization of triacyl monosaccharide lipid A partial structures in relation to bioactivity. *Biophysical journal*, *83*(1), 322-333.
119. Brandenburg, K., Richter, W., Koch, M. H. J., Meyer, H. W., & Seydel, U. (1998). Characterization of the nonlamellar cubic and H II structures of lipid A from *Salmonella enterica* serovar Minnesota by X-ray diffraction and freeze-fracture electron microscopy. *Chemistry and physics of lipids*, *91*(1), 53-69.

120. Fukuoka, S., Brandenburg, K., Müller, M., Lindner, B., Koch, M. H., & Seydel, U. (2001). Physico-chemical analysis of lipid A fractions of lipopolysaccharide from *Erwinia carotovora* in relation to bioactivity. *Biochimica et Biophysica Acta (BBA)-Biomembranes*, 1510(1), 185-197.
121. Brecker, L. (2003). Nuclear magnetic resonance of lipid A—the influence of solvents on spin relaxation and spectral quality. *Chemistry and physics of lipids*, 125(1), 27-39.
122. Hashimoto, M., Asai, Y., Tamai, R., Jinno, T., Umatani, K., & Ogawa, T. (2003). Chemical structure and immunobiological activity of lipid A from *Prevotella intermedia* ATCC 25611 lipopolysaccharide. *FEBS letters*, 543(1), 98-102.
123. Johnson, R. S., Her, G. R., Grabarek, J., Hawiger, J., & Reinhold, V. N. (1990). Structural characterization of monophosphoryl lipid A homologs obtained from *Salmonella minnesota* Re595 lipopolysaccharide. *Journal of Biological Chemistry*, 265(14), 8108-8116.
124. Qureshi, N., Takayama, K., Mascagni, P., Honovich, J., Wong, R. O. N. G., & Cotter, R. J. (1988). Complete structural determination of lipopolysaccharide obtained from deep rough mutant of *Escherichia coli*. Purification by high performance liquid chromatography and direct analysis by plasma desorption mass spectrometry. *Journal of Biological Chemistry*, 263(24), 11971-11976.
125. SEYDEL, U., LINDNER, B., WOLLENWEBER, H. W., & RIETSCHER, E. T. (1984). Structural studies on the lipid A component of enterobacterial

- lipopolysaccharides by laser desorption mass spectrometry. *European Journal of Biochemistry*, 145(3), 505-509.
126. Boué, S. M., & Cole, R. B. (2000). Confirmation of the structure of lipid A from *Enterobacter agglomerans* by electrospray ionization tandem mass spectrometry. *Journal of mass spectrometry*, 35(3), 361-368.
127. Chan, S., & Reinhold, V. N. (1994). Detailed structural characterization of lipid A: electrospray ionization coupled with tandem mass-spectrometry. *Analytical biochemistry*, 218(1), 63-73.
128. Corsaro, M. M., Piaz, F. D., Lanzetta, R., & Parrilli, M. (2002). Lipid A structure of *Pseudoalteromonas haloplanktis* TAC 125: use of electrospray ionization tandem mass spectrometry for the determination of fatty acid distribution. *Journal of mass spectrometry*, 37(5), 481-488.
129. Krasikova, I. N., Kapustina, N. V., Svetashev, V. I., Gorshkova, R. P., Tomshich, S. V., Nazarenko, E. L., & Solov'eva, T. F. (2001). Chemical characterization of lipid A from some marine proteobacteria. *Biochemistry (Moscow)*, 66(9), 1047-1054.
130. Zarrouk, H., Karibian, D., Bodie, S., Perry, M. B., Richards, J. C., & Caroff, M. (1997). Structural characterization of the lipids A of three *Bordetella bronchiseptica* strains: variability of fatty acid substitution. *Journal of bacteriology*, 179(11), 3756-3760.

131. Domon, B., & Costello, C. E. (1988). A systematic nomenclature for carbohydrate fragmentations in FAB-MS/MS spectra of glycoconjugates. *Glycoconjugate Journal*, 5(4), 397-409.
132. Lukasiewicz, J., Jachymek, W., Niedziela, T., Kenne, L., & Lugowski, C. (2010). Structural analysis of the lipid A isolated from *Hafnia alvei* 32 and PCM 1192 lipopolysaccharides. *Journal of lipid research*, 51(3), 564-574.
133. Gunn, J. S., Lim, K. B., Krueger, J., Kim, K., Guo, L., Hackett, M., & Miller, S. I. (1998). PmrA–PmrB-regulated genes necessary for 4- aminoarabinose lipid A modification and polymyxin resistance. *Molecular microbiology*, 27(6), 1171-1182.
134. Raetz, C. R., Guan, Z., Ingram, B. O., Six, D. A., Song, F., Wang, X., & Zhao, J. (2009). Discovery of new biosynthetic pathways: the lipid A story. *Journal of lipid research*, 50(Supplement), S103-S108.
135. Visintin, A., Halmen, K. A., Latz, E., Monks, B. G., & Golenbock, D. T. (2005). Pharmacological inhibition of endotoxin responses is achieved by targeting the TLR4 coreceptor, MD-2. *The Journal of Immunology*, 175(10), 6465-6472.
136. Van Duin, D., Medzhitov, R., & Shaw, A. C. (2006). Triggering TLR signaling in vaccination. *Trends in immunology*, 27(1), 49-55.
137. Krziwon C, Zähringer U, Kawahara K, Weidemann B, Kusumoto S, Rietschel ET. (1995). Glycosphingolipids from *Sphingomonas paucimobilis* induce monokine production in human mononuclear cells. *Infect Immun*, 63(8), 2899-905.

138. Babinski, K. J., Ribeiro, A. A., & Raetz, C. R. (2002). The Escherichia coli gene encoding the UDP-2, 3-diacylglucosamine pyrophosphatase of lipid A biosynthesis. *Journal of Biological Chemistry*, 277(29), 25937-25946.
139. Williamson, J. M., Anderson, M. S., & Raetz, C. R. (1991). Acyl-acyl carrier protein specificity of UDP-GlcNAc acyltransferases from gram-negative bacteria: relationship to lipid A structure. *Journal of bacteriology*, 173(11), 3591-3596.
140. Wyckoff, T. J., Lin, S., Cotter, R. J., Dotson, G. D., & Raetz, C. R. (1998). Hydrocarbon rulers in UDP-N-acetylglucosamine acyltransferases. *Journal of Biological Chemistry*, 273(49), 32369-32372.
141. Jackman, J. E., Raetz, C. R., & Fierke, C. A. (2001). Site-directed mutagenesis of the bacterial metalloamidase UDP-(3-O-acyl)-N-acetylglucosamine deacetylase (LpxC). Identification of the zinc binding site. *Biochemistry*, 40(2), 514-523.
142. Vorachek-Warren, M. K., Ramirez, S., Cotter, R. J., & Raetz, C. R. (2002). A triple mutant of Escherichia coli lacking secondary acyl chains on lipid A. *Journal of Biological Chemistry*, 277(16), 14194-14205.
143. Saitoh, S. I., Akashi, S., Yamada, T., Tanimura, N., Kobayashi, M., Konno, K., ... & Miyake, K. (2004). Lipid A antagonist, lipid IVa, is distinct from lipid A in interaction with Toll-like receptor 4 (TLR4)-MD-2 and ligand-induced TLR4 oligomerization. *International immunology*, 16(7), 961-969.
144. Belunis, C. J., & Raetz, C. R. (1992). Biosynthesis of endotoxins. Purification and catalytic properties of 3-deoxy-D-manno-octulosonic acid transferase from Escherichia coli. *Journal of Biological Chemistry*, 267(14), 9988-9997.

145. Brozek, K. A., & Raetz, C. R. (1990). Biosynthesis of lipid A in *Escherichia coli*. Acyl carrier protein-dependent incorporation of laurate and myristate. *Journal of Biological Chemistry*, 265(26), 15410-15417.
146. Reynolds, C. M., Kalb, S. R., Cotter, R. J., & Raetz, C. R. (2005). A Phosphoethanolamine Transferase Specific for the Outer 3-Deoxy-D-mannooctulosonic Acid Residue of *Escherichia coli* Lipopolysaccharide IDENTIFICATION OF THE *eptB* GENE AND Ca^{2+} HYPERSENSITIVITY OF AN *eptB* DELETION MUTANT. *Journal of Biological Chemistry*, 280(22), 21202-21211.
147. Trent, M. S., & Raetz, C. R. H. (2002). Cloning of *EptA*, the lipid A phosphoethanolamine transferase associated with polymyxin resistance. *J Endotoxin Res*, 8, 159.
148. Babinski, K. J., Kanjilal, S. J., & Raetz, C. R. (2002). Accumulation of the lipid A precursor UDP-2, 3-diacetylglucosamine in an *Escherichia coli* mutant lacking the *lpxH* gene. *Journal of Biological Chemistry*, 277(29), 25947-25956.
149. Wang, X., & Quinn, P. J. (2010). Lipopolysaccharide: Biosynthetic pathway and structure modification. *Progress in lipid research*, 49(2), 97-107.